이학박사학위논문

파이로포스페이트 분자 인식

Molecular Recognition of Pyrophosphate

2020 년 2 월

서울대학교 대학원

화학부 유기화학 전공

오 진 록

파이로포스페이트 분자 인식

Molecular Recognition of Pyrophosphate

지도교수 홍 종 인

이 논문을 이학박사학위 논문으로 제출함.

2020 년 2 월

서울대학교 대학원 화학부

유기화학전공

오 진 록

오진록의 이학박사 학위논문을 인준함.

2020 년 2 월

위 원 장 이 동 환 (인)

부 위 원 장 홍 종 인 (인)

위 원 김 병 문 (인)

위 원 이 현 우 (인)

위 원 김 해 조 (인)

Abstract

Molecular Recognition of Pyrophosphate

Jinrok Oh

Major in Organic Chemistry

Department of Chemistry

Graduate School

Seoul National University

Molecular recognition of anions has drawn considerable attention in recent decades. At the center are the anions of great importance in biological systems, such as fluoride (F^-), cyanide (CN^-), sulfate (SO_4^{2-}), phosphate (Pi, PO_4^{3-}), and pyrophosphate (PPi, $P_2O_7^{4-}$). Pyrophosphate (PPi) especially appears as a unique byproduct of several enzymes, such as nucleic acid polymerases, aminoacyl-tRNA synthetases, and adenylyl cyclase, all of which are crucial for sustaining life.

Therefore, measuring the concentration of PPi precisely in a complex mixture would help with not only understanding physiological phenomena but also diagnosing diseases related to the enzymes. Since it was discovered that PPi fit the cavity of bis(Zn-DPA) structure, so far are developed many molecular probes for PPi based on bis(Zn-DPA) moiety. However, only a few of them are useful in measuring an enzyme activity accurately.

Part I describes our recent effort to expand the ability of bis(Zn-DPA) to detect phosphate-containing biomolecules. It includes a discrimination of four redox-responsible biomolecules NAD^+, $NADP^+$, FAD, and FMN by a single molecular probe, as well as detection of a bacterial signaling molecule cyclic-di-GMP, with probes and receptors based on excimer–monomer strategy or biomimetic molecular design.

Part II focuses on improving selectivity of PPi receptors by studying structure–function relationship of bis(Zn-DPA) derivatives. We synthesized extended bis(Zn-DPA), chiral bis(Zn-DPA), as well as homo- and heterodinuclear complexes. We effectively controlled the exchange kinetics and selectivity by varying number and shape of the substituents. We also observed a relationship, as we termed *diastereoselectivity–sensitivity compensation*, for a series of chiral bis(Zn-DPA) derivatives. Indium(III) was chelated instead of zinc(II) to control physical features of the cavity, we were able to control both stoichiometry and selectivity of the receptor.

Part III presents a development of molecular probes for PPi. Inspired by the previous studies, we developed a number of molecular probes based on the FRET and PeT mechanisms. Throughout the developmental process, we demonstrated the importance of choosing an appropriate fluorophore and controlling the distance between fluorophore and quencher, depending on which mechanism is involved in. As a result, we successfully synthesized a fluorescent probe that exhibits different responses toward various nucleotides and PPi. Especially, this probe is expected to detect a consumption of GTP and ATP by choosing appropriate sensing media. Finally, we quantitatively analyzed the effect of metal cations (Na^+, Mg^{2+} and Ca^{2+}), which are frequently included in biological buffers, on selectivity and sensitivity.

Keywords: molecular recognition, indicator displacement assay, pyrophosphate, bis(Zn-DPA), thermodynamics, kinetics, compensation

Student Number: 2010 – 20284

Contents

Part I.

Fluorescent Sensing of Phosphate-Containing Biomolecules

Section 1. Background

1. Designing molecular receptors

1.1. Principle of complementarity

The concept of molecular recognition originated from the direct observations of which superstructures occurs in nature.[1] All enzymes and ribozymes recognize their own substrates and (allosteric) effectors with exceptional selectivity to transform substrates into the corresponding products or to regulate the reaction rates. For example, phosphofructokinase I (PFK) recognizes fructose-6-phosphate (F6P) and adenosine 5'-triphosphate (ATP) as the substrates and phosphate-containing anions as allosteric effectors.[2] A recent crystal structure of PFK unambiguously reveals two proximal binding sites for substrates F6P and ATP nearby the catalytic domain and another binding site for phosphate, an allosteric effector, that is spatially separated from the active site.[3] If we look at the structure more closely, we can find a large number of possible contacts between enzyme and substrates by the help of various noncovalent interactions including hydrogen bond, ion-ion, ion-dipole, dipole-dipole, and π-π (Figure 1–1). The picture of natural molecular recognition perhaps implies that the geometrically well-aligned set of interactive components is an essence of nature's high specificity.

Inspired by the marvels of nature, many scientists have attempted to imitate the molecular recognition of nature. For designing a proper host molecule, it has

been a reasonable starting point to compare the Corey-Pauling-Koltun (CPK) molecular models and the crystal structures of the artificial receptors (i.e., hosts) in the presence of or absence of the substrates (i.e., guests). From the extensive studies on the molecular structures of complexes, Cram derived a self-evident *principle of complementarity*: "to complex, hosts must have binding sites which cooperatively contact and attract binding sites of guests without generating strong non-bonded repulsions."[4]

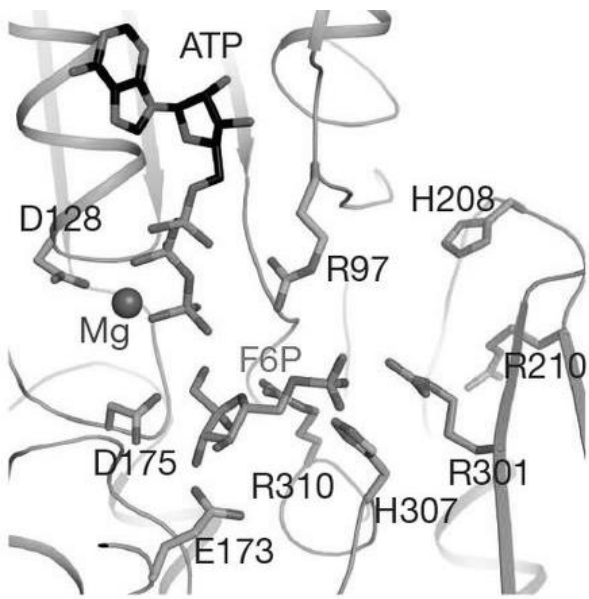

Figure 1–1. The ribbon diagram of PFKP with ATP, magnesium, and F6P. Reprinted by permission from reference 3, copyright 2015 Macmillan Publishers Ltd.

1.2. Principle of preorganization

In a study on the association between alkali metal ion and a series of spherands (receptor molecules of spherical shape) including **1** and its acyclic analogue **2**, Cram

and colleagues found that **1** can bind to lithium ion at least 17 kcal mol^{-1} more strongly than **2**.[5] Because **1** and **2** have identical number and kind of functional groups for the interaction with alkali metal ion, they concluded that the presence of functional group for complexation is not the only determining factor of binding strength.

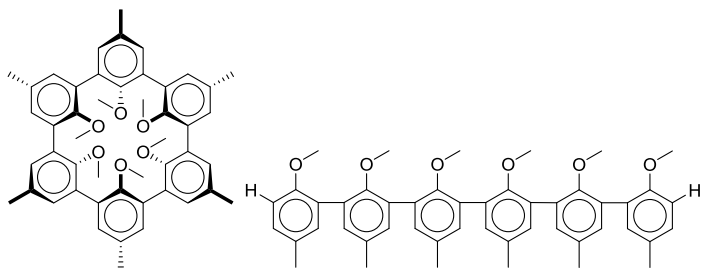

1 **2**

Scheme 1–1. The molecular structure of a spherand **1** and its acyclic analog **2**. Reprinted with permission from reference 5. Copyright 1984 American Chemical Society.

In other words, while the *principle of complementarity* dictates structural prerequisites for a molecule to be a suitable receptor, the comparison between **1** and **2** suggests a necessity of another principle that governs the thermodynamics of complexation. Within the consideration that **2** can have more than 1000 possible conformation (while only one possible conformation for **1**), Cram derived another *principle of preorganization*: "the more highly hosts and guests are organized for binding and low solvation prior to their complexation, the more stable will be their complexes."[6]

According to the principles devised by Cram, one can imagine that a rigid and preorganized receptor is the best receptor for a given guest molecule, but in many times, such receptor has troubles in exchange reaction, allosteric regulation, and

cooperativity.[7] Interestingly however, these concepts are believed to be the most important keys to understand the chemistry of nature at molecular level.[8] Therefore, a sufficiently preorganized yet flexible receptor molecule is highly desirable in order to understand and to mimic nature. In this regard, a report by Shinkai and colleagues is of high interest because it shows how important the flexibility is for creating a cooperativity.[9] The molecular receptor **3**, which comprises two porphyrin rings sandwiching a cerium(IV) ion, seems highly preorganized but it is still flexible in which two porphyrin rings can freely rotate against each other. **3** shows unfavorable binding to the first diacid because the binding event through a two-point contact with each porphyrin ring necessarily restrict the free rotation of **3**. However, once a diacid binds to **3**, the complex much more favorably binds to additional diacids because subsequent binding events do not need to sacrifice any more rotational freedom.

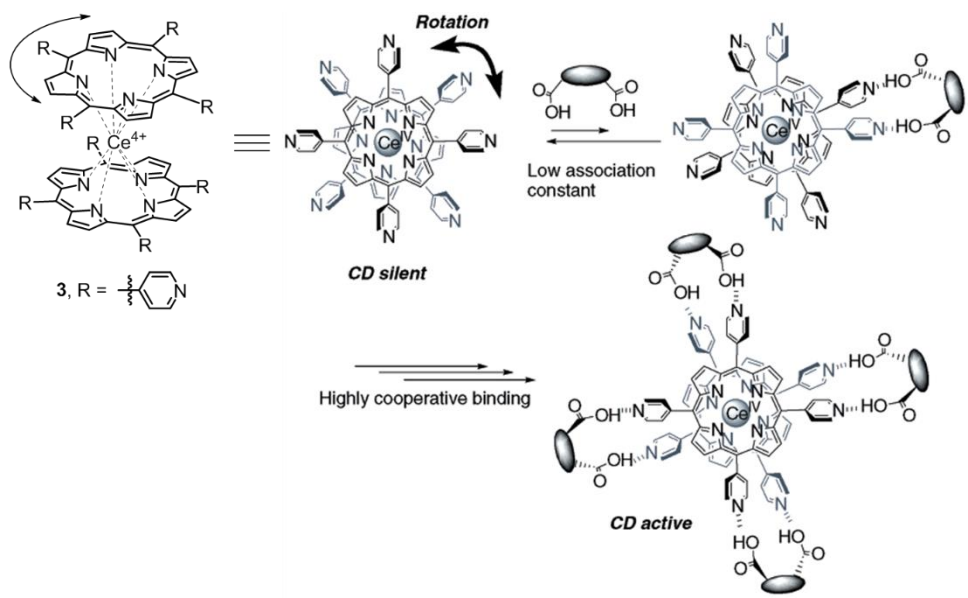

Scheme 1–2. A cooperative recognition of four diacid molecules by **3**.

1.3. Attractive forces in molecular recognition

To design a molecular receptor, choosing appropriate functional groups that can attract a guest molecule is the first inevitable task. Therefore, a knowledge on attractive intermolecular forces must be as important as the principles dealt before. There are a number of important and famous intermolecular attractive forces that are frequently employed in designing a molecular receptor, including hydrogen bond, electrostatic attraction, and London dispersion force. Throughout this chapter will be introduced some of the most important ones.

Before we start, it is worth noting how strong the intermolecular interactions are. A binding strength of a conventional hydrogen bond, a representative intermolecular interaction, is about 3 kcal mol^{-1}, while a covalent carbon-hydrogen bond strength is about 100 kcal mol^{-1}. Therefore, a covalent bond is about 30 times stronger than single hydrogen bond.[10] For another example, one of the strongest molecular recognition in nature, the binding between avidin and biotin, reaches the binding strength of 21 kcal mol^{-1},[11] which is one-fifth of a covalent single bond. However, the *weakness* of the intermolecular interactions is indeed the quintessence of the supramolecular chemistry. It enables a simultaneous creation and destruction of a superstructure at which temperature most of the covalent bond remains intact, as well as precise control of binding strength by varying number of interactions or by modifying the functional groups involved in the interactions.

There is an extraordinary example of controlling binding strength and selectivity. In a nucleic acid duplex, cytidine, and guanine are held together by three hydrogen bond contacts. Matteucci and colleagues attempted to enhance binding strength of the cytidine-guanine natural pair by adding more hydrogen bonds.[12] They designed **4a** to involve additional hydrogen bond donor in cytidine structure. An

incorporation of **4a** into a DNA duplex in place of a cytidine remarkably raised the melting temperature, which manifests a stronger binding of **4a** to guanine than cytidine. Sasaki and colleagues synthesized **4b** by changing ammonium to carbamate, and this small difference resulted in dramatic change in selectivity, in which **4b** exclusively binds to 8-oxoguanosine while **4a** can bind both guanosine and 8-oxoguanosine without any significant selectivity.[13]

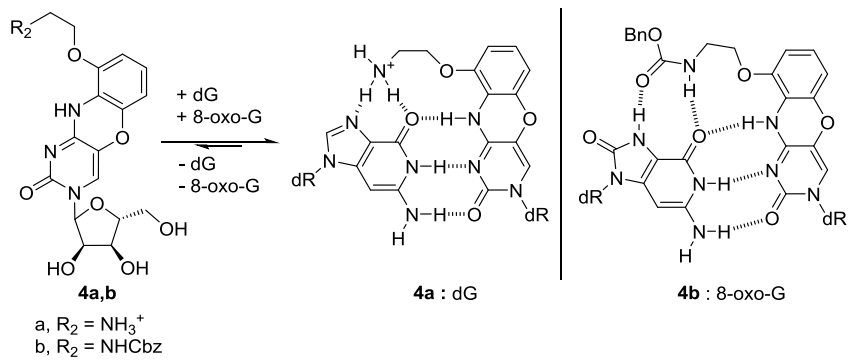

Scheme 1–3. Molecular recognition of **4a** and **4b**. Reprinted by permission from reference 12 and 13. Copyright 1998 American Chemical Society. Copyright 2007 John Wiley & Sons, Inc.

The very first attractive force introduced is hydrogen bond. It is obviously the most famous intermolecular interaction and is defined by an interaction between highly polarized proton (hydrogen bond donor) and a Lewis base (hydrogen bond acceptor).[10] The strength of hydrogen bond ranges 0 ~ 5 kcal mol^{-1} depending on the structure of the donor and acceptor involved in. In designing a synthetic receptor, a hydrogen bond donor frequently employs flat and acidic amines (amide, urea, imide, carbamate, and others) and a hydrogen bond acceptor generally utilizes ether, amine, and carbonyls. A molecular receptor using multiple hydrogen bonds is particularly useful in nonpolar organic media such as chloroform or acetonitrile. However, it can

barely form complexes with guest molecules in aqueous media because water molecules are both strong hydrogen bond donor and acceptor.

Scheme 1–4. The general structure of hydrogen bond. D and A represents donor and acceptor, respectively.

A halogen bond is an interesting interaction in that it has an analogous structure with a hydrogen bond.[14,15] A halogen bond refers to an interaction between highly polarized halogen atom (halogen bond donor) and an electronegative functional group through the σ-hole present at halogen atom. The strength of a halogen bond also ranges from 0 to 5 kcal mol^{-1}. One very interesting feature of halogen bond is the orientation. A highly polarized halogen atom always have both electropositive σ-hole and electronegative equatorial band, thus it can recognize two electrically opposite acceptor simultaneously.

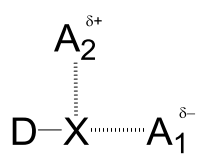

Scheme 1–5. The general structure of halogen bond. D, A, and δ represent donor, acceptor and partial charge, respectively.

Electrostatic attraction is also one of great importance. It includes any attractive force between charges, dipoles, and quadrupoles. A charge-charge interaction is the strongest among a number of electrostatic attractions, and it appears

as salt bridge form in the nonpolar environment, which is of paramount importance especially in a biological system. However, everything changes in a polar medium such as water. A polar medium diminishes long-range charge-charge interaction by effective screening of charges. Therefore, the interactions between charge and dipole or quadrupole, such as cation-π[16] and anion-π[17,18] interactions become significant. A representative is the molecular recognition of phosphocholine by McPC603,[19] which persuaded Dougherty to develop an artificial acetylcholine receptor through multiple cation-π interactions (Figure 1–2).[20]

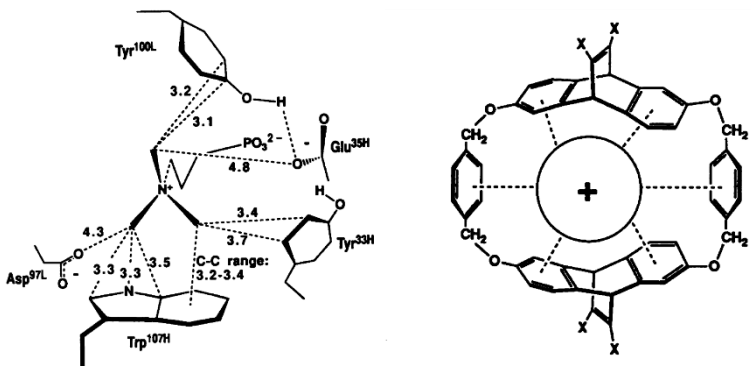

Figure 1–2. (Left) A partial crystal structure of McPC603 with a bound phosphocholine. Some distances are shown in Å. (Right) A schematic illustration of the acetylcholine recognition by a synthetic receptor. Reprinted by permission from reference 20. Copyright 1990 American Association for the Advancement of Science.

London dispersion force is another of great importance.[21] As an attractive part of van der Waals interaction, it forms a basis for hydrophobic interaction. Therefore, it became a powerful tool in not only designing a molecular receptor for hydrocarbon compounds but also predicting the structure of hydrophobic molecular complexes in aqueous environment.[22]

2. Designing molecular probes

2.1. General strategy

After learning the fundamentals of designing an artificial receptor, the focus of the supramolecular chemistry spontaneously moved into the *functions*. Chemists started to develop molecular catalysts, machines, devices, and probes and explored the underlying yet uncovered principles.

Among various subjects derived from molecular recognition, the term *molecular probe* could be defined by a molecular entity that converts the extent of its own molecular recognition into signals. Therefore, a molecular probe requires both a receptor part and a functional part (or a reporter part) that exhibit a signal that is dependent to the complexation state of the molecular receptor. (Figure 1–3)

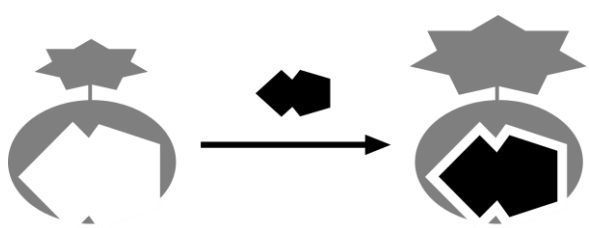

Figure 1–3. A general scheme of the molecular recognition by a molecular probe. Grey and black represent molecular probe and guest, respectively.

Since it is the only condition for the reporter part to exhibit a signal according to the state of the host, there must be numerous potent reporter groups. For example, a proton of a molecule can be the simplest reporter group because its ^{1}H NMR signal

shall be shifted downfield or upfield according to the receptor's molecular structure and corresponding microenvironment. Radioisotope also can be a reporter group, because the radiation from such element serves as a unique and traceable marker and the amount of radiation is proportional to the concentration of the chemical species. However, detection of such signals requires highly complicated instrumentation or protective equipment. In addition, scientists always are interested in finding an easier way to detect a change, thus the signal of which we can perceive through our sensory organs are highly desirable. Among various sensory stimuli, a visual one is the most prominent signal we can perceive, therefore the majority of signaling strategies relies on the optics.

2.2. Optical signaling strategies

Many chemicals, called *chromophores*, can absorb a light and some of them, called *luminophores*, can emit light as well. One particularly interesting thing is that they, chromophores and luminophores, change absorption and emission spectra according to the environmental conditions.[23] These dependencies on conditions of these photophysically active chemicals led scientists to utilize these chemicals as reporter groups. There are many excellent reviews dealing with the strategies using optical reporter groups[24-28] and this thesis will cover some of the relevant topics.

The first topic covered is an *intrinsic* fluorescent/colorimetric strategy. The term intrinsic dictates a direct perception of the chemical information at the receptor part by the reporter. Therefore, most of the intrinsic probes have somehow similar structure in which (1) the receptor part imposes a part of the reporter and (2) they have small side rams for a cooperative coordination to given guest molecules.

Scheme 1–6 shows two of the most representative intrinsic fluorescent/colorimetric probes, **5**[29] and **6**[30] for zinc (II) ion and fluoride ion, respectively. In both cases, two phenols of the reporter groups (fluorescein and azophenol) participate in recognizing guest molecule. The direct contact of the reporter to a guest molecule perturbs the electronic state of the reporter, thus this type of the probes generally show a significant spectral change in wavelength as well as in intensity.

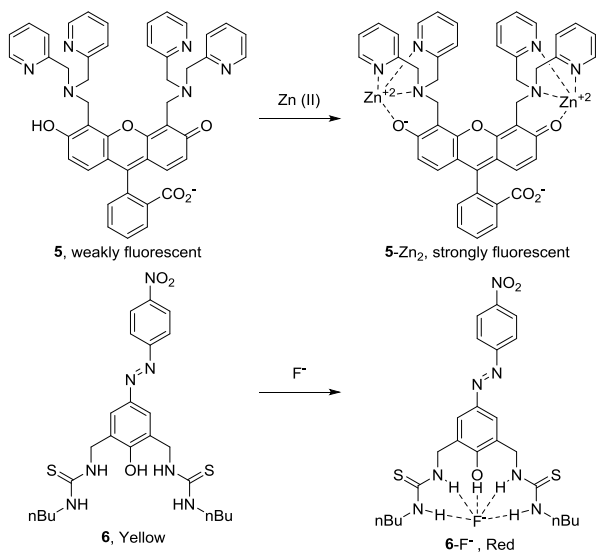

Scheme 1–6. Molecular structures of colorimetric probes for zinc (II) ion, **5** and fluoride, **6**. Reprinted by permission from reference 29 and 30. Copyright 2002 American Chemical Society. Copyright 2001 American Chemical Society.

Excited state intramolecular proton transfer (ESIPT) is a special proton transfer reaction in which it is observed only for the molecules that possess a hydrogen bond within the skeleton of the fluorophore. A general photophysical scheme for the ESIPT process is depicted in Figure 1–4.[31] Briefly, when ESIPT fluorophore absorbs light, the fluorophore efficiently tautomerizes from enol form

to keto form by the help of the electronic redistribution. In many cases, the tautomerization occurs so fast that the majority of the emission comes from keto form. The necessity of hydrogen atom to establish ESIPT process persuaded scientists to design intrinsic fluorescent probes using ESIPT fluorophore, and Scheme 1–7 shows one of the successful examples.[32] Probe **7**, which has an intramolecular hydrogen bond between sulfonamide and benzimidazole, emits sky blue fluorescence by ESIPT mechanism, while **7**-Zn emits blue fluorescence because of no available hydrogen atom for ESIPT.

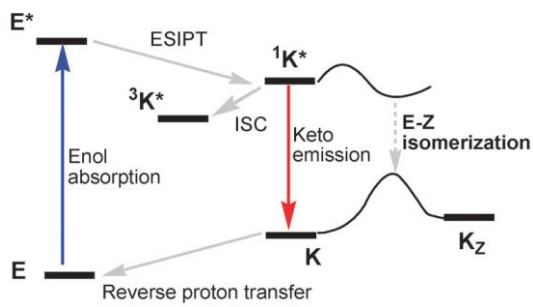

Figure 1–4. The general scheme for the ESIPT process. E and K denote enol- and keto-form of tautomers. Reproduced from reference 31 with permission of The Royal Society of Chemistry.

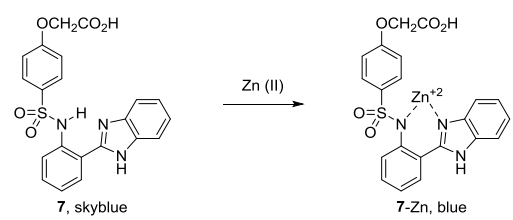

Scheme 1–7. A molecular probe for zinc (II) ion using ESIPT mechanism. Reprinted by permission from reference 32. Copyright 2004 John Wiley & Sons, Inc.

Since we dealt with intrinsic strategy, it is logical to step into *extrinsic* strategy. The term extrinsic denotes an indirect perception of the chemical information at the receptor part by the reporter. The definition implies that the reporter and the receptor of a probe are electronically separated, and communicate through space. This strategy is especially useful when a probe employs fluorescent reporter rather than chromogenic reporter, because of a lot more strategies disturbing or modulating a fluorescence emission compared to colorimetric response. The strategies include photoinduced electron transfer (PeT), monomer–excimer, conformational restriction, resonant energy transfer (RET) and displacement of an indicator.

Photoinduced electron transfer (PeT) is the most extensively studied and widely used mechanism for modulating the luminescent signal.[25] Ever since Weller proposed a feasibility of PeT mechanism, numerous researchers including Czarnik, Tsien, Shinkai, and de Silva have demonstrated how powerful PeT mechanism is in modulating a fluorescence response.[24] The mechanism of PeT starts from a consideration of an excited state. For an excited state of a fluorophore, an external electron of high enough energy can spontaneously occupy lower singly occupied molecular orbital (lower SOMO), or an excited electron in higher singly occupied molecular orbital (higher SOMO) can spontaneously move into an empty external orbital of suitable energy. These two schemes describe donor-PeT (d-PeT, excited state is an electron donor) and acceptor-PeT (a-PeT, excited state is an electron acceptor), respectively (Figure 1–5). It is noticeable that two distinct PeT mechanisms commonly result in the quenching of the luminophores, and therefore we term the functional groups that induce PeT as PeT quenchers. In addition, tertiary amines and phenols are famous quenchers inducing a-PeT and nitroarenes are representatives for a-PeT.

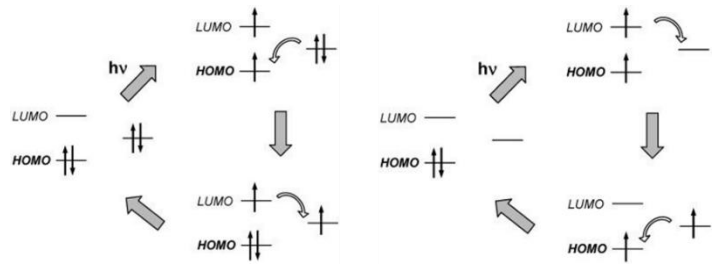

Figure 1–5. A schematic illustration for donor-PeT (left) and acceptor-PeT (right). Reprinted by permission from reference 25. Copyright 2003 American Chemical Society.

An excimer is a homodimer complex of which one of them is in an excited state. Anthracene and pyrene are renowned for emitting excimer emission. Because an emission from an excimer typically appears in the longer wavelength region, the monomer–excimer strategy often involves a large spectral change. Figure 1–6 shows a straightforward molecular design using monomer–excimer strategy. The design may require a flexible linker that enables efficient folding of the entire molecule into a "tweezer" structure only in the presence of guest molecule.

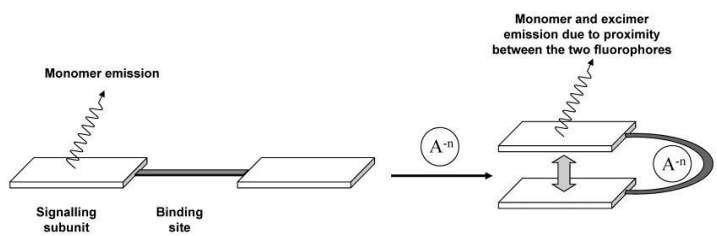

Figure 1–6. A design strategy using monomer–excimer strategy and a flexible linker. Reprinted by permission from reference 25. Copyright 2003 American Chemical Society.

Resonant energy transfer is another very famous strategy in modulating luminescence signal. There are several kinds of resonant energy transfer, for example,

Förster resonance energy transfer (FRET), bioluminescence resonance energy transfer (BRET) and chemiluminescence resonance energy transfer (CRET), depending on the type of energy donor. The common term *resonant* describes the requirement for efficient energy transfer, that is, an adequate spectral overlap between the emission of the donor and the absorption of the acceptor. In addition, this nonradiative energy transfer occurs through a dipole-dipole coupling, the energy transfer process is largely dependent on both distance and relative orientation of the corresponding luminophores.

In many cases, it is hard to design a highly specific molecular receptor to a guest molecule. In other words, several physically analogous molecules to a given guest molecule can competitively bind to the designed receptor molecule. If one of the competent changes its physical property by binding to the receptor, it is possible to analyze the binding event of the target guest and receptor indirectly by measuring a physical property of it. This strategy, called indicator displacement assay (IDA), is particularly useful when no signal modulation strategy is available or embedding a signal modulator into the receptor is an arduous task.

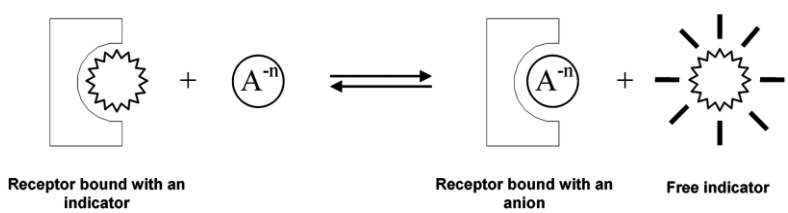

Figure 1–7. A design strategy using indicator displacement. Reprinted by permission from reference 25. Copyright 2003 American Chemical Society.

3. Molecular probes for phosphate-containing anions

3.1. Pyrophosphate probes

Pyrophosphate ($P_2O_7^{4-}$, PPi) is one of the most important biological anions in which it is generated as a necessary side product of numerous coupled enzymatic reactions.[2] The reactions involve aminoacyl-tRNA synthesis, polymerization of nucleic acids and biosynthesis of signaling molecules (e.g. cAMP, cGMP, and steroids), all of which requires high energy to the transformation. Some enzymes such as pyrophosphatase (PPase) hydrolyze PPi for regulating biological PPi concentration,[33] and dysfunction of these enzymes or accumulation of PPi are proven to induce several diseases including pseudogout and osteoarthritis.[34,35] A clinical and biochemical importance of PPi has attracted scientists to develop molecular probes and receptors that are useful for bioanalytical applications.[36,37]

The design of molecular probes for PPi started from a pioneering work by Czarnik and colleagues (Scheme 1–8).[38] The molecular recognition of PPi by **8** purely relies on the charge-charge interaction, and the increased fluorescence emission is likely due to the combination of PeT and chelation-enhanced fluorescence mechanism. The matchless dissociation constant (K_d) of 2.9 μM with PPi enabled the detection of PPi presented in micromolar concentration and monitoring of PPase activity. It is noticeable that the proposed molecular recognition pattern and high selectivity to PPi over phosphate (PO_4^{3-}, Pi) undoubtedly manifest the principle of complementarity.

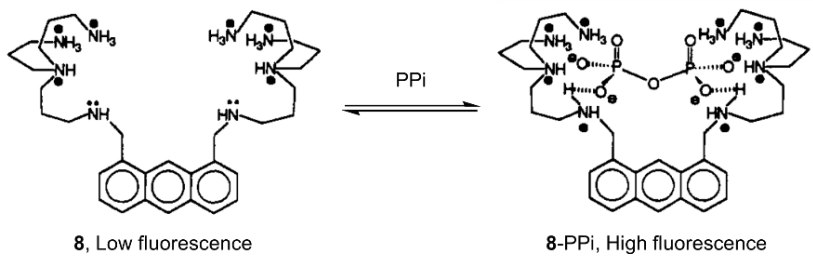

Scheme 1–8. A molecular probe for pyrophosphate by Czarnik. Reprinted by permission from reference 38. Copyright 1994 American Chemical Society.

In 2003, Hong and colleagues reported a colorimetric probe **9** for PPi bearing bis(Zn-DPA) unit (Figure 1–8).[39] The binding of PPi to **9** induced bathochromic shift in absorption spectrum while the binding of other anions did not. The dissociation constant was determined as 12 nM, therefore they almost completely quantified a submicromolar concentration of PPi. The crystal structure of **9**-PPi unambiguously revealed the perfect connectivity between **9** and PPi, which resembles the adamantane structure. In 2004, they reported a fluorescent PPi probe[40] **10** by introducing fluorescent naphthyl moiety instead of azophenol moiety. The probe analogously showed bathochromic shift in both absorption and emission spectra. By discussing the relative association constants of **10** with PPi and ATP (i.e. selectivity against ATP), they started a long journey of research to develop a highly selective PPi probe against ATP and to utilize such probes in monitoring enzyme activities that converts ATP into PPi.

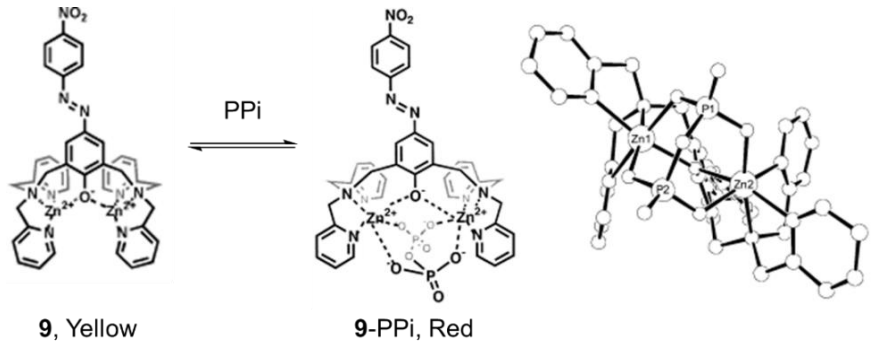

Figure 1–8. The molecular structure of probe **9** and the crystal structure **9**–PPi. Reprinted by permission from reference 39. Copyright 2003 American Chemical Society.

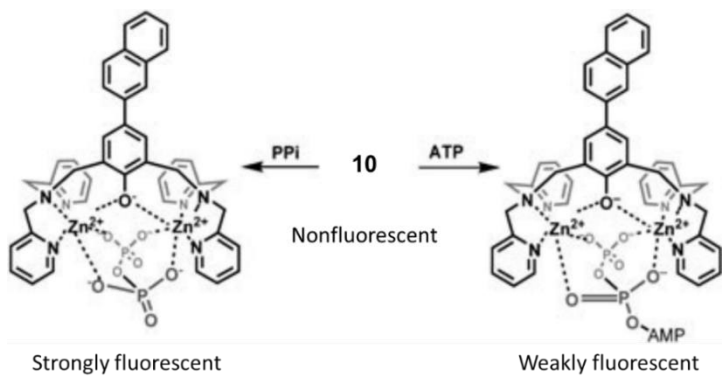

Scheme 1–9. The molecular structure of probe **10** and its molecular recognition. Reprinted by permission from reference 40. Copyright 2004 John Wiley & Sons, Inc.

After the discovery of the potential of bis(Zn-DPA), numerous PPi probes based on Zn-DPA has been developed.[36,37,41] The probes utilized various strategies including PeT,[42] colorimetric,[43] fluorogenic,[44] aggregation-induced emission (AIE),[45] monomer–excimer,[46-48] ESIPT[49] and indicator displacement.[50] Scheme 1–10 shows selected PPi probes.

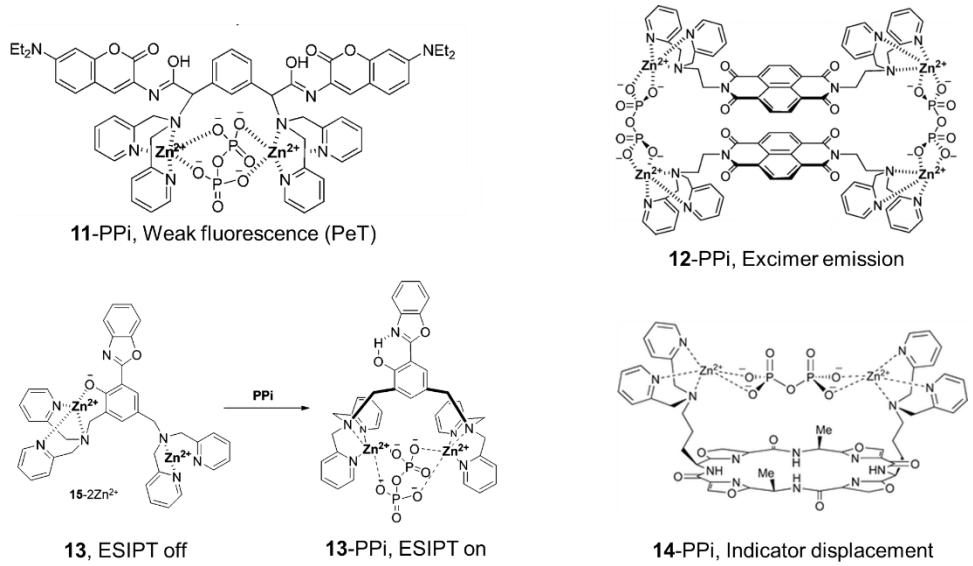

Scheme 1–10. Representative probes for the detection of PPi. Reprinted by permission from reference 42, 48, 49 and 50. Copyright 2011 Elsevier. Copyright 2005, 2011 American Chemical Society. Copyright 2013 The Royal Society of Chemistry.

3.2. Nucleotide and nucleoside probes[51]

Nucleotide describes a common molecular structure consisting of three parts: nucleobase, sugars, and phosphates, while nucleosides are without phosphate. Scheme 1–11 shows the general molecular structure of nucleosides and nucleotides. Nucleotides are involved in numerous enzymatic reactions and cellular signaling pathways. In addition, they serve as the major components of nucleic acids and energy carrier as well. The biological importance of nucleotides, as well as the structural features, have led organic chemists to develop molecular receptors and probes for nucleotides. Although there are millions of molecular receptors and probes for nucleotides, only selected ones of great significance will be introduced.

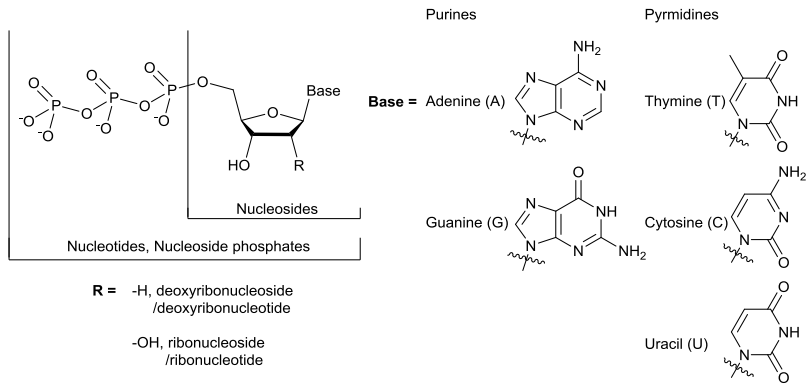

Scheme 1–11. General structures of nucleosides and nucleotides.

Hamachi and colleagues developed a molecular probe **15** bearing bis(Zn-DPA) complex and xanthene that exhibit bright fluorescence in the presence of ATP.[52] The fluorescence enhancing mechanism is unique, in which the binding event reversibly switches the π-conjugation over the fluorophore (Scheme 1–12). The *in situ creation of fluorophore* mechanism enabled the development of FRET-based molecular probe that is capable of ratiometric visualization of intracellular ATP concentration.[53]

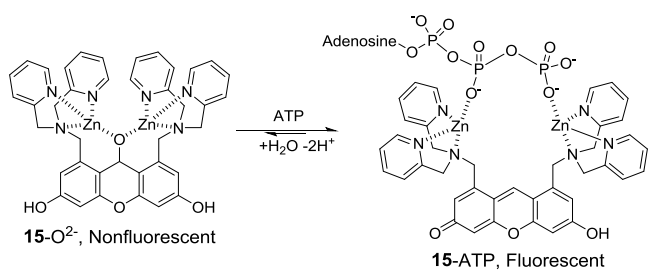

Scheme 1–12. Molecular recognition and detection mechanism of **15** with ATP. Reprinted by permission from reference 52. Copyright 2008 American Chemical Society.

Hong[54] and Spiccia[55] independently developed probes for the detection of thymidine 5'-triphosphate (TTP). Although the strategies differed from each other, they are common in which they utilized molecular recognition of both thymidine and phosphate. The main strategy of Hong's is to create a termolecular complex to enable efficient energy transfer within the complex. On the other hand, as depicted in scheme 1–13, the strategy of Spiccia seems very close to the ideal design using monomer–excimer strategy. They connected two pyrenes by a flexible linker that folds into the hairpin structure by interacting with thymidine and triphosphate.

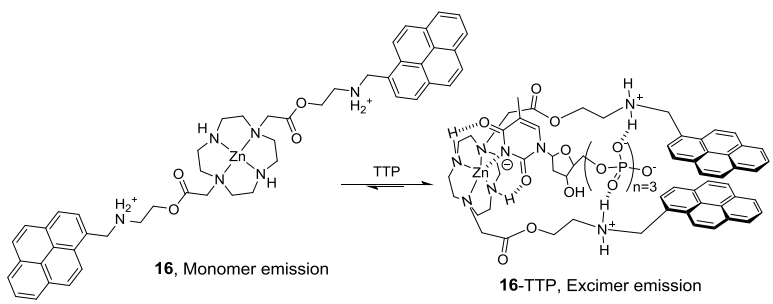

Scheme 1–13. Molecular recognition of **16** with TTP. Reprinted by permission from reference 55. Copyright 2009 The Royal Society of Chemistry.

Guanosine 3'-diphosphate-5'-diphosphate (ppGpp) is a bacterial signaling molecule that generates a stringent response under harsh conditions. It has two pyrophosphate units within the molecule, therefore, Hong and colleagues developed a molecular probe **17** for the detection of ppGpp.[56] The probe design employed monomer–excimer emission strategy, by making termolecular complex. In this regard, it merged two independent strategies to create a unique detection mechanism. As shown in Scheme 1–14, only the simultaneous recognition of both pyrophosphate of ppGpp can generate excimer emission. Other possible competitors, such as PPi,

ATP and guanosine 5'-triphosphate (GTP) did not induce any spectral change in excimer emission region.

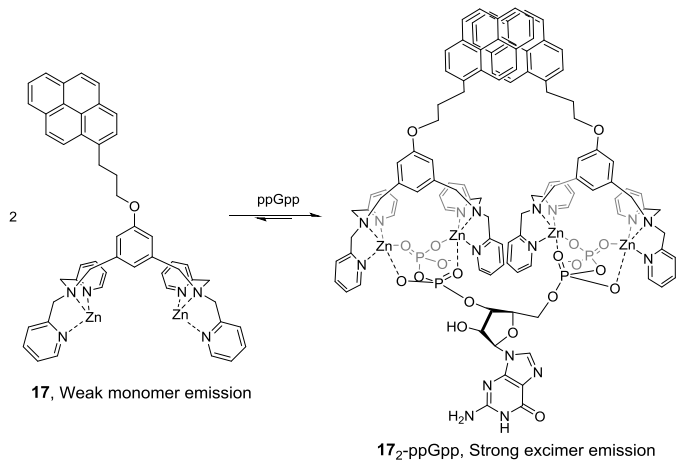

Scheme 1–14. Molecular recognition and detection mechanism of **17** with ppGpp. Reprinted by permission from reference 56. Copyright 2008 American Chemical Society.

Flavins are important nucleosides/nucleotides in biological systems because of their numerous roles in redox reactions of metabolic processes. They exist in three major forms as coenzymes in nature, flavin adenine dinucleotide (FAD), flavin mononucleotide (FMN) and riboflavin (vitamin B_2). With different molecular structures, they have different roles in biological systems. Therefore, the differentiation among them is of great interest. Hong and colleagues developed an extremely simple method to discriminate FAD from FMN.[57] The addition of a simple molecular receptor, FAD and FMN reacted differently. In the presence of the receptor, FAD enhanced its intrinsic fluorescence while the fluorescence of FMN was greatly diminished. The reason for the different behavior was illustrated in

Scheme 1–15. The molecular receptor **18** is not only bound to guest molecules but also either catalyzes self-lysis reaction or effectively quenches the fluorescence.

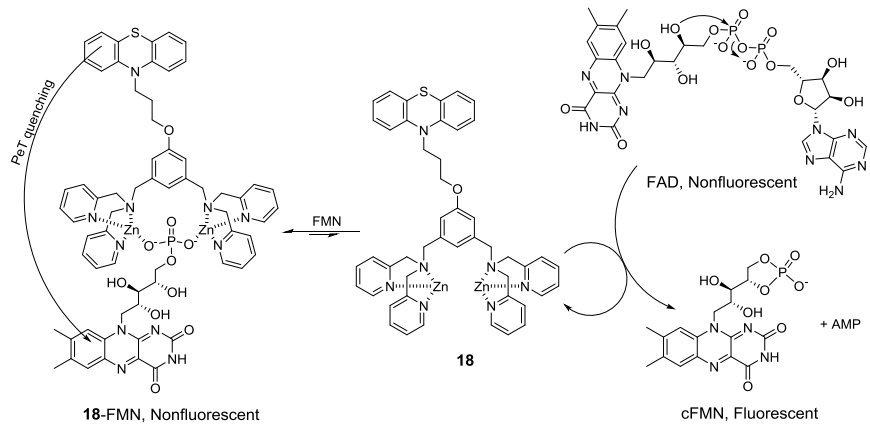

Scheme 1–15. Differential recognition mechanism of **18** with FAD and FMN. Reprinted by permission from reference 57. Copyright 2009 American Chemical Society.

Lehn and colleagues reported a molecular probe **19** for nicotinamide nucleotides, based on oxazacrown ethers and acridines (Scheme 1–16).[58] Azacrown ethers are positively charged at neutral conditions and interact electrostatically with phosphates, while appended acridines are expected to change their intrinsic fluorescence *via* interactions with the aromatic components of analytes. Interestingly, reduced nicotinamide adenine dinucleotide phosphate (NADPH) showed a three-order higher association constant than nicotinamide adenine dinucleotide phosphate ($NADP^+$). The large difference in two association constants was rationalized by the degree of electrostatic interactions depending on the charges of guest molecule.

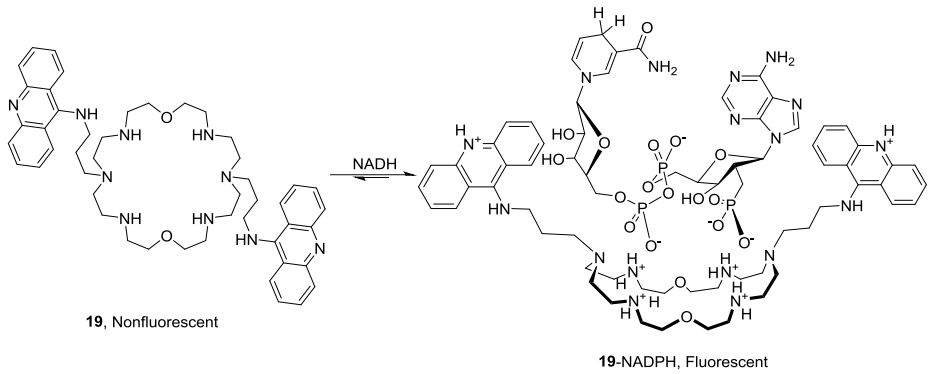

Scheme 1–16. Molecular recognition of NADPH by **19**. Reprinted by permission from reference 58. Copyright 1997 John Wiley & Sons Inc.

Section 2. Discrimination of Redox-Responsible Biomolecules

A part of this section was published in *Organic Letters*.[59]

1. Introduction

Redox reactions are ubiquitous in biological systems in which they are involved in protein regulation, oxidative phosphorylation, and metabolic reactions.[2] Redox-responsible functional groups, such as N-alkyl-β-nicotinamide and the isoalloxazine moiety, are involved in biological redox reactions. Nicotinamide adenine dinucleotide (NAD^+) and $NADP^+$ contain β-nicotinamide, which is responsible for hydride transfer reactions. In particular, NAD^+ and $NADP^+$ are known to be extensively involved in oxidative reactions and reductive reactions, respectively. FMN, FAD, and riboflavin (RF) have the isoalloxazine moiety in common, and they serve either as electron acceptors in the oxidized form or as electron donors in the reduced form. As a prosthetic group in flavoproteins, they are involved in metabolic reactions and the redox reactions of electron transport chains.[60-62] The most intriguing feature about these molecules is the relationship between their structures and their roles. For example, $NADP^+$ has the same structure as that of NAD^+ except for an additional phosphate group at the 2′ position of the ribose ring connected to the adenine moiety. The slight structural difference between NAD^+ and $NADP^+$ leads to a significant difference in their roles: NAD^+ for oxidative and $NADP^+$ for reductive reactions.

Capillary electrophoresis (CE) techniques have been developed for the detection of nicotinamides[63] and flavins[64]. However, CE is not suitable for the real-time or *in vivo* detection of those redox-responsible biomolecules. In addition, it is known that the adenine unit of FAD significantly decreases the fluorescence of isoalloxazine by an intramolecular PeT quenching mechanism,[65] which has attracted considerable attention in the detection and discrimination of flavins using fluorescence methods. A recent result by Hong and colleagues (see page 21~23), the study on the molecular recognition of ppGpp and the differential recognition of flavin species inspired us to study further the ability of **17** to discriminate between redox-responsible molecules.

2. Result and discussion

2.1. New synthesis of 17

The previously reported synthetic route to the synthesis of **17** employed two inefficient bimolecular nucleophilic substitution (S_N2) reactions using aryl lithium reagent and less-nucleophilic phenol as the nucleophiles. The two steps gave desired products only in less than 15 % and the overall yield after three more steps recorded below 1 %. Therefore, another synthetic route to **17** with an improved synthetic efficiency is highly desired.

The new synthesis replaced these two low-yield steps by four sequential steps of Knoevenagel condensation, catalytic hydrogenation, reduction, and Mitsunobu reaction. Although the number of steps was increased, the yield was 33-fold improved. Since the latter steps of previous report showed moderate yields, we

completed our new synthesis of **17** by adapting the procedures. And notably, single chromatographic separation at the final stage was sufficient to afford pure free ligand **25** (for a detailed procedure and characterization, see Experimental section).

2.2. Discrimination of NAD^+ and $NADP^+$

We conducted fluorescence titration experiments to investigate the possibility of discrimination between NAD^+ and $NADP^+$ using **17**. Because $NADP^+$ has an additional phosphate group, we expected that only $NADP^+$ could induce pyrene excimer emission. As expected, only $NADP^+$ increased excimer emission of pyrene centered at 470 nm, while both NAD^+ and $NADP^+$ decreased monomer emission of pyrene (Figure 1–9). This result indicates that it is possible to discriminate $NADP^+$ from NAD^+ by the fluorometric method.

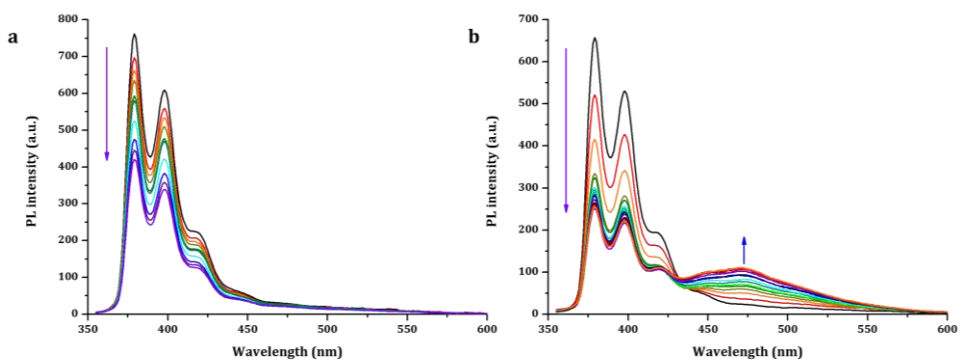

Figure 1–9. Fluorescence spectral change of 20 μM **17** upon addition of either (a) NAD^+ or (b) $NADP^+$ in 1 mM HEPES buffer solution (pH 7.40).

What would cause the decrease in the monomeric pyrene emission upon the addition of either NAD^+ or $NADP^+$? In a previously reported screening test, binding of ATP to **17** resulted in enhancement of the monomeric pyrene emission;[56] thus, it is likely that the nicotinamide moiety is responsible for emission quenching of pyrene. In order to determine the underlying quenching mechanism, we performed electrochemical studies using **20** and **21** (Scheme 1–17 and 1–18, see Experimental section) as model compounds of pyrene and nicotinamide ($NAD(P)^+$), respectively. As depicted in Figure 1–10, the reduction potentials of **20** and **21** were estimated to be −3.52 eV and −3.75 eV from the vacuum level. This slightly higher lowest unoccupied molecular orbital (LUMO) level of pyrene (~0.2 eV) suggests that oxidative PeT quenching from the excited pyrene to NAD^+ is possible. On the other hand, the highest occupied molecular orbitals (HOMOs) of **20** and **21** were estimated to be −6.87 eV and −5.53 eV respectively. However, the calculated HOMO level of NAD^+ is not expected to be in the nicotinamide core and the large energy level difference (>1.3 eV) is undesirable for electron transfer.[66] Therefore, the d-PeT (electron transfer from excited pyrene to nicotinamide species) seems to be the most plausible for quenching mechanism.

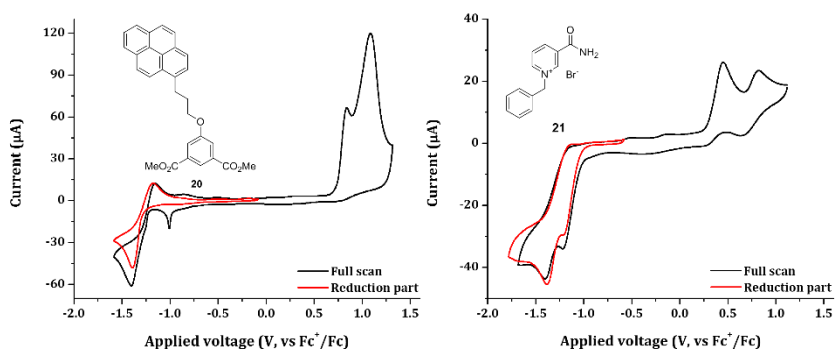

Figure 1–10. Molecular structure and cyclic voltammogram of **20** and **21**.

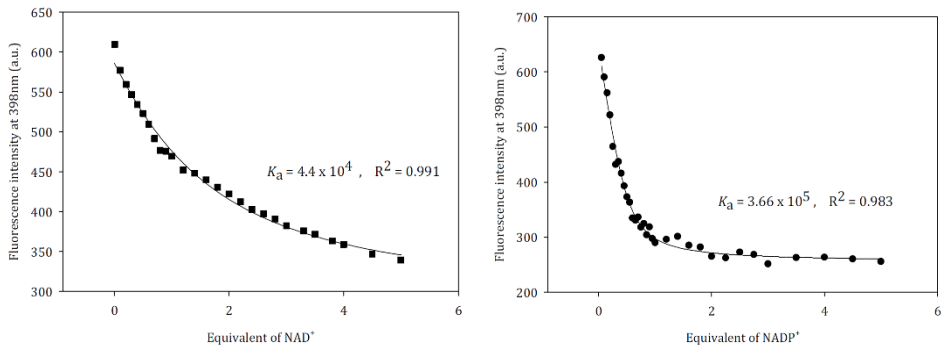

Figure 1–11. Fluorescence spectral change of **17** upon addition of either NAD^+ (left) or $NADP^+$ (right) was fitted with a one to one binding equilibrium isotherm. (See text)

Further study on the binding between **17** and $NAD(P)^+$ was performed. In the case of NAD^+, the fluorescence spectral changes at 398 nm fitted well with a one to one binding equilibrium, and its association constant (K_a) was estimated to be 4.4×10^4 M^{-1}, which is similar to the binding affinity toward monohydrogen phosphate. $NADP^+$ showed more efficient quenching of the emission of monomeric pyrene than did NAD^+, and it does not follow a one to one binding equilibrium. Interestingly, the emission changes of **17** when a twofold concentration of $NADP^+$ ($R^2 = 0.983$) is used indicates that **17** interacts with $NADP^+$ with a 2:1 binding stoichiometry via coordination with diphosphate and phosphate moieties of which the two corresponding binding constants are very similar. Job's plot analysis also supports a 2:1 binding stoichiometry. The apparent K_a of $NADP^+$ was estimated to be 3.7×10^5 M^{-1}, which is about 8 times larger than that of NAD^+. One intriguing observation is that the pyrene dimer formed in the 2:1 complex remains intact upon addition of even large amounts of $NADP^+$. This is completely different from the binding of **17** to ppGpp, in which the excimer emission decreased at a high level of ppGpp. This

saturation behavior and ratiometric property toward $NADP^+$ would be advantageous in the selective sensing of $NADP^+$, while ppGpp shows concentration-dependent pyrene excimer emission, showing the highest excimer emission at optimal guest concentration. The fact that **17**–$NADP^+$ complexation exhibits an increased K_a compared to that of **17** binding with NAD^+ and maintains the pyrene dimeric structure even at high concentrations of $NADP^+$ can be understood in terms of the cooperative effect of the aromatic groups involved in the complexation.[67]

2.3. Discrimination of flavin species

Next, we wondered if **17** could discriminate flavin species by taking advantage of isoalloxazine's fluorescence. A fluorescence titration experiment for FMN revealed that the monomeric emission of **17** was greatly decreased, while FMN emission was enhanced, which may indicate that FRET between the two fluorophores (pyrene and isoalloxazine) occurs (Figure 1–12a). However, the normalized excitation spectra of FMN did not differ, regardless of the presence of **17**, which implies that no efficient FRET between **17** and FMN takes place (data not shown). In addition, the addition of pyrophosphate resulted in a great enhancement in the emission intensity of both **17** and FMN. These results suggest that there is an extensive mutual quenching between **17** and FMN. Interestingly, however, we were able to detect green fluorescence from isoalloxazine in a 1:1 mixture of **17** and FMN under 365 nm UV irradiation.

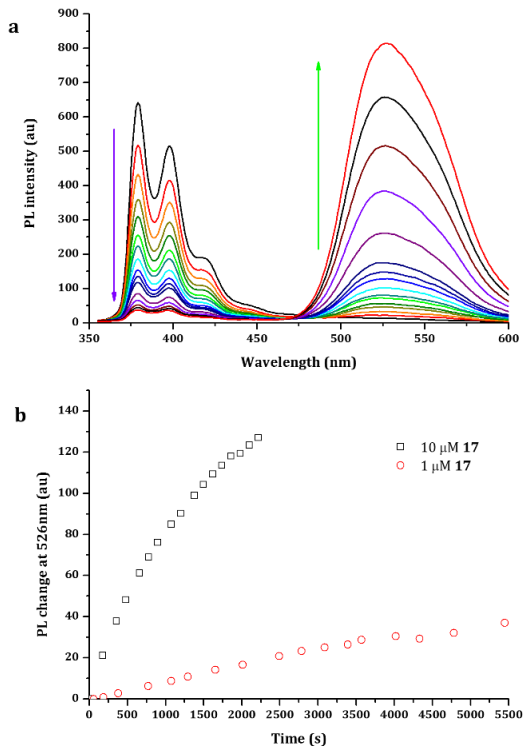

Figure 1–12. (a) Fluorescence spectral change upon addition of FMN in the presence of 20 μM **17**. (b) Fluorescence intensity change at 526 nm with time in the presence of 15 μM FAD and either 1 μM (red circle) or 10 μM (black square) of **17**. In both cases, experiments were performed in 1 mM HEPES buffer solution (pH 7.40).

The quenching mechanism of **17** by FMN (and *vice versa*) was also studied by the electrochemical method. Reduction potentials of both pyrene and **22** (a model compound for isoalloxazine moiety) were measured to be −3.52 eV, indicating that reversible electron transfer between the two LUMOs of the fluorophores is possible. On the other hand, we estimated HOMOs of pyrene and FMN as −6.87 eV and −5.92 eV, respectively. These data suggest that efficient a-PeT quenching of **17** by FMN

could occur. From the relative energy level distribution, it is expected that **17** is extensively quenched by FMN, while FMN itself is partially quenched, which is exactly what is observed.

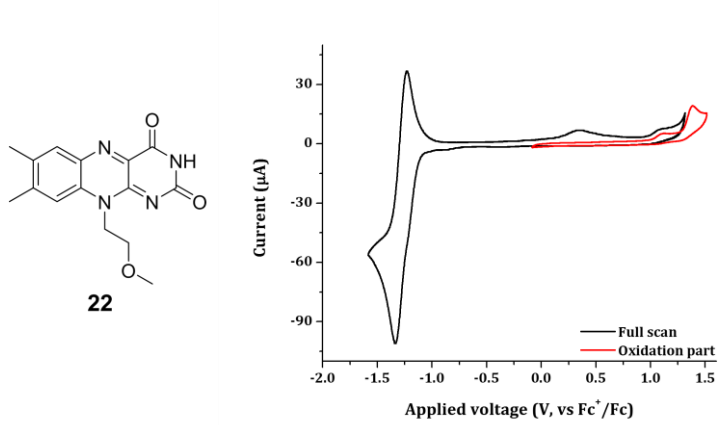

Figure 1–13. Molecular structure and cyclic voltammogram of **22**.

Our first attempt to rationalize the fluorescence changes of **17** with respect to FMN concentration failed under the assumption of a 1:1 binding mode. There are two possible explanations for this: (1) more than one quenching pathway is involved and (2) multiple binding modes are involved. A Stern-Volmer plot of **17** (Figure 1–14), in the presence of FMN as a quencher, showed two distinguishable and proportional coefficients. This implies that there are two major quenching pathways: PeT quenching between flavin and pyrene, which is supported by the electrochemical data; and absorption sharing of **17** and FMN. In addition, Job's plot reveals 2:1 binding stoichiometry between **17** and FMN, presumably through coordination with phosphate and imide moieties. Based on these results, the fluorescence intensity change of **17** with respect to FMN concentration was

successfully rationalized. The apparent association constant was estimated to be 1.93 × 10^5 M^{-1} and FMN was expected to completely quench the fluorescence of **17** (Figure 1–15, R_Q = 1.0). This estimation of quenching efficiency is consistent with the results of other experiments, such as a simultaneous increase in the fluorescence intensity of **17**–FMN ensemble upon pyrophosphate addition.

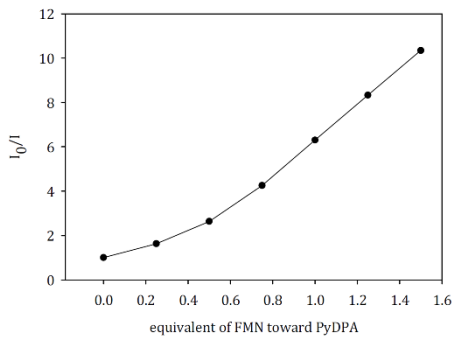

Figure 1–14. Stern-Volmer plot of **17** with respect to FMN concentration

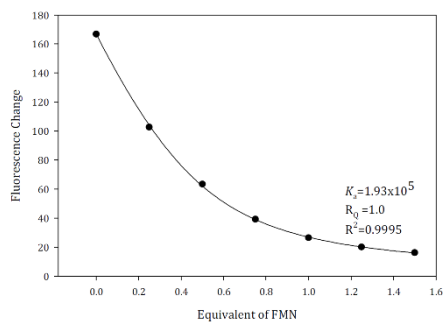

Figure 1–15. Fluorescence spectral change of **17** upon addition of FMN and its fitting result with respect to a twofold concentration of added FMN.

The catalytic group for the self-lysis of FAD is the same in **17** as in **18**. Therefore, **17** is also expected to catalyze the lysis of FAD into cFMN and AMP. As

depicted in Figure 1–16, **17** showed a similar fluorescence enhancing behavior with time as **18** did (Figure 1–16). This fluorescence change also agrees well with pseudo-first-order kinetics, with an apparent rate constant of 70 s^{-1}. These results indicate that **17** can discriminate between riboflavin, FMN, and FAD with respect to (time-course) fluorescence spectral change. FMN is significantly quenched by the addition of a large amount of **17** while FAD is detected by a gradual increase in the fluorescence intensity of isoalloxazine with time upon addition of **17**. Finally, the fluorescence of riboflavin is not altered by **17**.

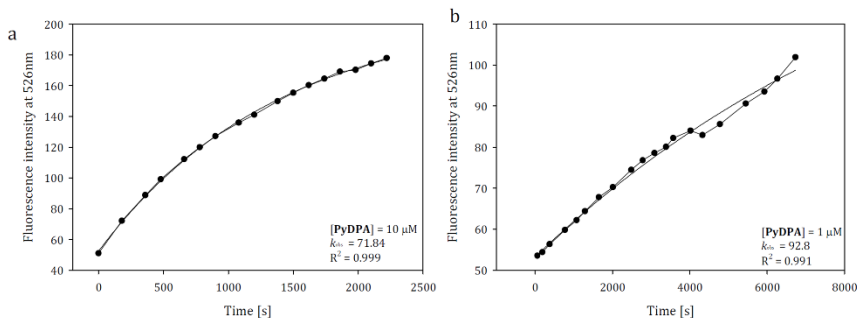

Figure 1–16. Pseudo-first-order kinetics of FAD self-lysis at different concentrations of **17**.

3. Conclusion

In conclusion, we developed a new synthetic strategy for the large-scale production of **17** and investigated its use in the discrimination of redox-related biomolecules. NAD^+ and $NADP^+$ were distinguished by the presence or absence of excimer emission of **17**. FMN and FAD were differentiated by means of the quenching of FMN emission and the time-dependent fluorescence enhancement, respectively.

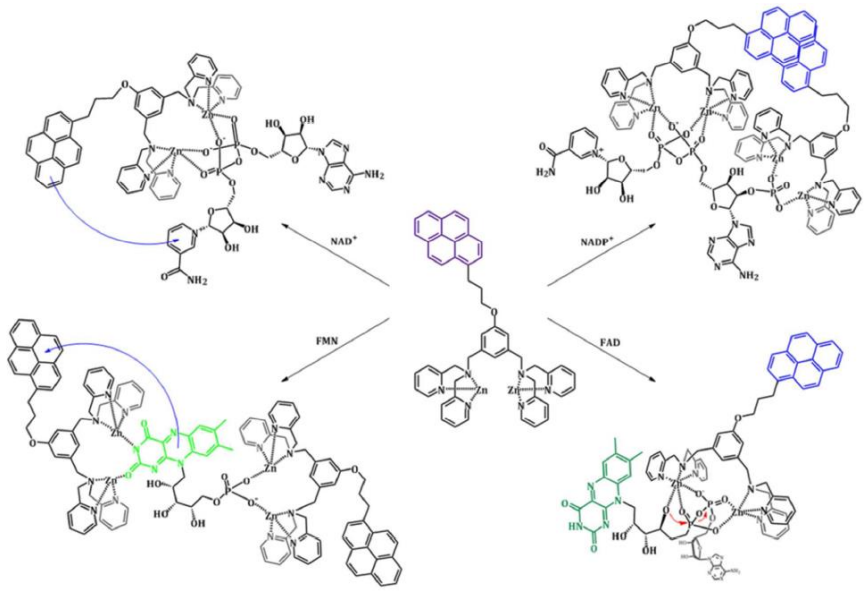

Figure 1–17. Plausible binding modes and signal modulation mechanisms of **17**.

4. Experimental section

4.1. General information

All chemicals were purchased from either Sigma-Aldrich or Tokyo Chemical Industry (TCI) and were used as received except anhydrous solvents. Thin layer chromatography was performed over Merck silica gel 60 F254 on aluminum foil. Merck silica gel 60 was used for the stationary phase in chromatographic separation or silica pad filtration. Celite® 545 was used for celite filtration. All ^{1}H and ^{13}C NMR spectra were obtained from Bruker DRX 300 NMR spectrometer. Fluorescence emission spectra were recorded on a JASCO FP-6500 spectrometer and the slit width was 3 or 5 nm for excitation and 5nm for emission. HRMS were taken by Agilent

6890 Series, with FAB-positive mode. The solution of **17** for all photophysical experiments was prepared from 20 mM stock solution in DMSO.

4.2. Synthesis of the compounds

Dichloromethane and tetrahydrofuran were distilled over calcium hydride and sodium/benzophenone ketyl, respectively. NMR samples were prepared by dissolving in DMSO-d_6, $CDCl_3$ or acetone-d_6. Multiplicities: s, singlet; d, doublet; t, triplet; m, multiplet; br, broad.

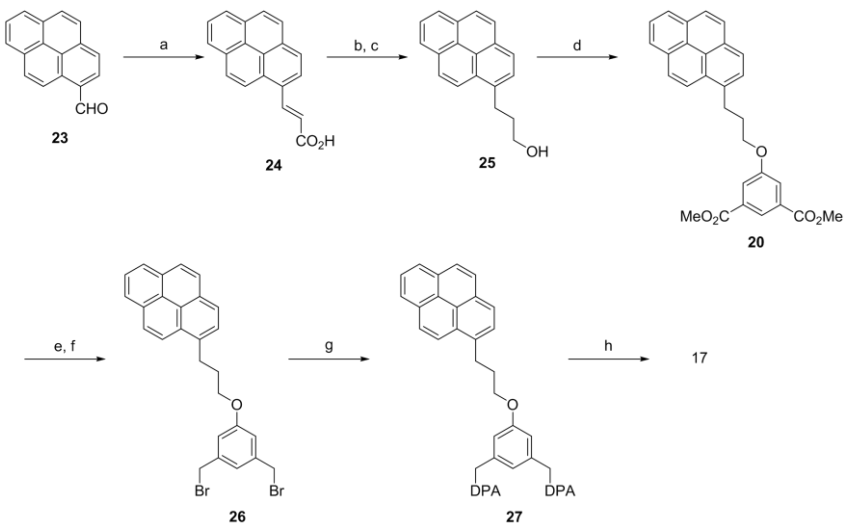

Scheme 1–17. Synthesis of 17. a) malonic acid, cat. piperidine, Pyridine, reflux; b) Pd/C, H_2(1atm), THF/*i*PrOH; c) $LiAlH_4$, THF; d) dimethyl 5-hydroxyisophthalate, DIAD, PPh_3, THF, –78°C then reflux; e) $LiAlH_4$, THF; f) PBr_3, DCM; g) di(2-picolyl)amine, K_2CO_3, KI, Acetonitrile, reflux; h) $Zn(NO_3)_2 \cdot 6H_2O$, Acetonitrile. THF = tetrahydrofuran, *i*PrOH = 2-propanol, DIAD = diisopropyl azodicarboxylate, DCM = dichloromethane.

Synthesis of **24**: To a stirred solid mixture of 1-pyrenecarboxaldehyde (**23**, 1100 mg, 4.78 mmol, 1.0 equiv.), and malonic acid (920 mg, 8.8 mmol, 1.8 equiv.),

6 mL of pyridine, and a catalytic amount of piperidine (8 drops) were successively added, and then refluxed for 3 hours. The mixture was poured into 3 M HCl solution cooled to 0 ^{o}C. The resulting solid was filtered, washed with cold water and recrystallized from $CHCl_3$–MeOH to give 1.1g (84%) of pure yellow solid product of **24**: ^{1}H NMR (300 MHz, DMSO-d_6) δ 6.79 (1H, d, *J*=15.8Hz), 8.08 (1H, t, *J* = 7.6 Hz), 8.16–8.34 (6H, m), 8.46 (1H, d, *J*=4.4Hz), 8.49 (1H, *J*=5.7Hz), 8.66 (1H, d, *J*=15.7Hz), 12.6 (1H, br s). ^{13}C NMR (75 MHz, DMSO-d_6) δ 122.050, 122.649, 124.193, 124.433, 124.978, 125.696, 126.237, 126.502, 126.986, 127.735, 128.266, 128.846, 129.050, 129.313, 130.588, 131.252, 132.493, 140.335, 168.095. HRMS (FAB^{+}) [M = $C_{19}H_{12}O_2$]$^{+}$, calculated 272.0837, found 272.0837.

Synthesis of **25**: To a stirred solution of **24** (1.0 g, 4.04 mmol, 1.0 equiv.) in tetrahydrofuran/2-propanol mixture (40/20 mL) was added a suspension of 10 wt% Pd/C (20 mg in 10 mL 2-propanol). The mixture was stirred under hydrogen atmosphere (1 atm) for 3 hours until the characteristic ^{1}H NMR signal at δ 6.8 (olefinic proton) were completely disappeared. Solution was filtered through celite pad and evaporated under reduced pressure. Trace of solvents was azeotropically removed with hexanes. The resulting material dissolved in 40 mL of anhydrous tetrahydrofuran was added via cannula to the pre-chilled suspension of $LiAlH_4$ (600 mg, 15.8 mmol, 3.6 equiv.) in anhydrous tetrahydrofuran. The mixture was stirred overnight at room temperature. Excessive hydride was destroyed by successive addition of 1 mL water, 2 mL 15% $NaOH_{(aq)}$, and 3 mL water. The mixture was filtered through celite pad and concentrated under reduced pressure to give 880 mg (84% over two steps) of semi-solid product, **25**: ^{1}H NMR (300 MHz, $CDCl_3$) δ 2.10 (2H, m, *J*=7.4Hz), 2.97 (1H, br s), 3.38 (2H, t, *J*=8.0Hz), 3.76 (2H, t, *J*=6.4Hz), 7.80 (1H, d, *J=7.*8Hz), 7.9–8.08 (5H, m), 8.16 (2H, t, *J*=7.9Hz), 8.23 (1H, d, *J*=9.2Hz).

^{13}C NMR (75 MHz, $CDCl_3$) δ 29.655, 34.511, 62.293, 123.357, 124.801, 124.897, 124.941, 125.059, 125.120, 125.871, 126.669, 127.194, 127.315, 127.574, 128.692, 129.884, 130.962, 131.489, 136.227. HRMS (FAB^+) [M = $C_{19}H_{16}O]^+$, calculated 260.1201, found 260.1201.

Synthesis of **20**: To a pre-chilled, stirred solution of **4** (781 mg, 3.0 mmol, 1.0 equiv.), dimethyl 5-hydroxyisophthalate (945 mg, 4.5 mmol, 1.5 equiv.), and triphenylphosphine (944 mg, 3.6 mmol, 1.2 equiv.) in anhydrous tetrahydrofuran (50 mL) was added diisopropylazodicarboxylate (0.79 mL, 3.9 mmol, 1.3 equiv.) dropwise during 5 minutes at –78 °C. After finishing the addition, the mixture was refluxed for three hours. Water (1 mL) was then added, volatiles were removed and 10 mL of ethyl ether/ethyl acetate mixture (4:1) was added, and stood at 0 °C overnight. Precipitates were collected to give 832 mg (61%) of pure **20**. Resulting residue was chromatographed on silica gel by 20% ethyl acetate in hexanes to give more products (230 mg, 17%): ^{1}H NMR (300 MHz, $CDCl_3$) δ 2.38 (2H, m, *J*=6.2Hz), 3.59 (2H, t, *J*=7.7Hz), 3.94 (6H, s), 4.14 (2H, t, *J*=5.9Hz), 7.79 (2H, d, *J*=1.4Hz), 7.88 (1H, d, *J*=7.8Hz), 8.0–8.05 (3H, m), 8.10 (2H, dd, *J*=6.4Hz, 9.3Hz), 8.17 (2H, d, *J*=7.7Hz), 8.30 (1H, s), 8.31 (1H, d, *J*=7.6Hz). ^{13}C NMR (75 MHz, $CDCl_3$) δ 29.651, 31.012, 52.403, 67.558, 119.878, 122.981, 123.189, 124.810, 124.876, 124.959, 124.984, 125.123, 125.861, 126.750, 127.377, 127.454, 128.768, 130.013, 130.888, 131.424, 131.777, 135.446, 159.111, 166.180. HRMS (FAB^+) [M = $C_{29}H_{24}O_5]^+$, calculated 452.1624 , found 452.1624.

Synthesis of **26**: To a suspension of $LiAlH_4$ (258 mg, 6.8 mmol, 4.0 equiv.) in anhydrous tetrahydrofuran, a solution of **20** (770 mg, 1.7 mmol, 1.0 equiv.) in anhydrous tetrahydrofuran was added dropwise. The mixture was then stirred for 5 hours until all the starting material was completely disappeared in TLC analysis. The

mixture was quenched by successive addition of 0.5 mL water, 1 mL of 15% NaOH, and 1.5 mL of water, and then filtered through celite pad. Volatiles were removed under reduced pressure, and dried under vacuum. The resulting residue was dissolved in 2:1 mixture of anhydrous tetrahydrofuran/dichloromethane (30 mL), and then 3.4 mL of 1.0 M phosphorous tribromide in dichloromethane (2.0 equiv.) was added under a nitrogen atmosphere, at 7 ^{o}C. The mixture was further stirred for 3 hours at room temperature, quenched with 1 mL of MeOH, diluted with 50 mL dichloromethane, added half-saturated sodium bicarbonate and extracted twice with 50 mL dichloromethane each. The combined organic layer was dried over magnesium sulfate, evaporated under reduced pressure. The resulting residue was filtered through small quantity of silica gel pad to give 710 mg of **26** (80%): ^{1}H NMR (300 MHz, $CDCl_3$) δ 2.35 (2H, m, *J*=7.0Hz), 3.56 (2H, t, *J*=7.7Hz), 4.05 (2H, t, *J*=6.0Hz), 4.43 (4H, s), 6.89 (2H, s), 7.02 (1H, s), 7.89 (1H, d, *J*=7.8Hz), 8.02–8.05 (3H, m), 8.08 (2H, dd, *J*= 6.1Hz, 9.0Hz), 8.18 (2H, d, *J*=7.6Hz), 8.30 (1H, d, *J*=9.3Hz). ^{13}C NMR (75 MHz, $CDCl_3$) δ 29.690, 31.064, 32.935, 67.160, 115.323, 121.837, 123.250, 124.832, 124.897, 124.974, 125.005, 125.134, 125.891, 126.765, 127.392, 127.467, 127.516, 127.784, 130.009, 130.917, 131.443, 135.599, 139.622, 159.444. HRMS (FAB^{+}) [M = $C_{27}H_{22}Br_2O]^{+}$, calculated 520.0037, found 520.0037.

Synthesis of **27**: **26** (350 mg, 0.67 mmol, 1.0 equiv.), di-(2-pyridylmethyl)amine (0.26 mL, 1.47 mmol, 2.2 equiv.), potassium iodide (244 mg, 1.47 mmol, 2.2 equiv.), and potassium carbonate (276 mg, 3.0 equiv.) were dissolved in acetonitrile (15 mL). The resulting mixture was stirred at slightly raised temperature for 16 hours. Volatiles were removed under reduced pressure, diluted with ethyl ether, half-saturated sodium bicarbonate solution, and extracted twice to 50 mL of ethyl ether each. Combined organic layer was dried over magnesium

sulfate, evaporated under reduced pressure, and then subjected to flash silica gel column chromatography. Gradient elution from chloroform to 10% methanol in chloroform gave 300 mg of **27** (43%): ^{1}H NMR (300 MHz, $CDCl_3$) δ 2.37 (2H, m, *J*=6.7Hz), 3.58 (2H, t, *J*=7.7Hz), 3.67 (4H, s), 3.83 (8H, s), 4.07 (2H, t, *J*=6.0Hz), 6.93(2H, s), 7.11(5H, m), 7.53(8H, m), 7.90(1H, d, *J*=7.8Hz), 7.96–8.18(7H, m), 8.33(1H, d, *J*=9.2Hz), 8.50(4H, d, *J*=4.7Hz).^{13}C NMR (75 MHz, $CDCl_3$) δ 29.718, 31.206, 58.607, 60.093, 66.834, 113.617, 121.517, 121.915, 122.696, 123.313, 124.771, 124.829, 124.918, 124.973, 125.101, 125.852, 126.711, 127.337, 127.415, 127.484, 127.792, 129.926, 130.867, 131.403, 135.814, 136.367, 140.667, 148.977, 159.214, 159.757. HRMS (FAB^+) [M+H = $C_{51}H_{47}N_6O]^+$, calculated 759.3811, found 759.3811.

Synthesis of **17**: To an aliquot of **27** (3.00 micromoles) in 0.2 mL of acetonitrile, zinc(II) nitrate hexahydrate (2.05 equiv., in 0.1 mL acetonitrile) was added slowly, stirred for 1 hour, and then solvent was removed under reduced pressure. The resulting residue was dried under vacuum and used without further purification. ^{1}H NMR (300 MHz, DMSO-d_6) δ 2.36(2H, br), 3.63(2H, d, *J*=7.4Hz), 3.73(4H, d, *J*=16Hz), 3.87(4H, s), 4.20(2H, t, *J*=7Hz), 4.34(4H, d, *J*=16Hz), 6.93(1H, s), 7.06(2H, s), 7.48(4H, d, *J*=7.8Hz), 7.65(4H, t, *J*=6.5Hz), 8.03–8.5(12H, m), 8.68(4H, d, *J*=4.7Hz). ^{13}C NMR (75 MHz, DMSO-d_6) δ 29.335, 31.162, 56.107, 57.411, 67.322, 118.190, 123.828, 123.892, 124.578, 124.720, 125.028, 125.331, 125.539, 126.695, 126.792, 127.116, 127.380, 127.769, 127.937, 128.110, 128.766, 129.903, 130.849, 131.359, 134.134, 136.472, 141.201, 148.374, 154.743, 159.334. HRMS (FAB^+) [M–NO_3 = $C_{51}H_{46}N_9O_{10}Zn_2]^+$, calculated 1072.1945, found 1072.1951.

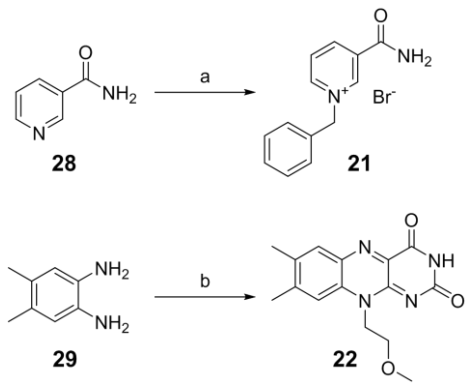

Scheme 1–18. Synthetic route to the model compounds for electrochemical studies, **21** and **22**. a) benzyl bromide, acetone; b) (i) $CH_3OCH_2CH_2Br$, DMF; (ii) alloxane monohydrate, boric acid, acetic acid.

Synthesis of **21**: To a stirred suspension of nicotinamide (**28**, 610 mg, 5 mmol, 1.0 equiv.) in acetone, benzyl bromide (0.77 mL, 6.5 mmol, 1.3 equiv.) were added, then gently heated for 2 days. The precipitate was collected by filtration to give pure benzylated nicotinamide, **21** (1.2 g, 82%). ^{1}H NMR (300 MHz, DMSO-d_6) δ 5.96 (2H, s) 7.43–7.46 (3H, m), 7.58–7.63 (2H, m), 8.19 (1H, br s), 8.27 (1H, dd, *J*=6.3Hz, 7.9Hz), 8.64 (1H, br s), 8.98 (1H, dd, *J*=1.0Hz, 8.0Hz), 9.35 (1H, d, *J*= 5.0Hz), 9.71 (1H, s). ^{13}C NMR (75 MHz, DMSO-d_6) 63.920, 128.747, 129.505, 129.678, 129.915, 134.441, 134.520, 144.310, 145.276, 146.837, 163.153. HRMS (FAB$^+$) [M–Br$^-$ = $C_{13}H_{13}N_2O]^+$, calculated 213.1022, found 213.1028.

Synthesis of **22**: To a stirred solution of 4,5-dimethylphenylene-1,2-diamine (**29**, 1.02 g, 7.5 mmol, 1.0 equiv.) and potassium carbonate (1.0 g, 7.5 mmol, 1.0 equiv.) in 20 mL DMF, 2-bromoethyl methyl ether (0.6 mL, 6.8 mmol, 0.9 equiv.) were added at 60 ^{o}C. The mixture was stirred for 6 hours, then the organic solvent was removed under vacuum. The resulting material was diluted with 150 mL of ethyl ether and washed with 3 portions of water. The ethereal layer was dried over

magnesium sulfate, and ether was removed under reduced pressure to give a dark brown liquid. The residue was re-dissolved in 30 mL of acetic acid then 3 g of boric acid (10% w/v to acetic acid) and 2.0 g of alloxan monohydrate (12.5 mmol, 1.67 equiv.) were added at room temperature. The resulting mixture was stirred overnight. Acetic acid was evaporated under vacuum, and resulting material was recrystallized from 25% MeOH in chloroform to give **22** (0.75 g, 33%). ^{1}H NMR (300 MHz, DMSO-d_6) δ 2.38(3H, s), 2.48(3H, s), 3.74(2H, t, *J*=5.7Hz), 4.77(2H, t, *J*=5.7Hz), 7.82(1H, s), 7.84(1H, s), 11.30(1H, br s). ^{13}C NMR (75 MHz, DMSO-d_6) 19.211, 21.117, 44.338, 58.906, 68.662, 117.125, 131.216, 131.808, 134.077, 136.207, 137.503, 146.722, 150.653, 155.968, 160.315. HRMS (FAB$^+$) [M+H = $C_{15}H_{17}N_4O_3$]$^+$, calculated 301.1301, found 301.1301.

4.3. Excited state population distribution of a mixture composed of two light-absorbing species

Let us consider a solution of A and B that they absorb an incident light independently. Then we can write an equation for the light absorption reaction of A and B as Eq. 1–1 and Eq. 1–2, respectively, whereas ε_A and ε_B are their corresponding absorptivity.

$$A + h\nu \xrightarrow{\varepsilon_A} A^* \qquad \text{(Eq. 1–1)}$$

$$B + h\nu \xrightarrow{\varepsilon_B} B^* \qquad \text{(Eq. 1–2)}$$

If we assume that the intensity of the light is weak enough, which is typical case for the photophysical experiments, the effective concentration of A and B at a

steady state are almost equal to the initial concentration of A and B, namely, A_0 and B_0, respectively (Eq. 1–3 and Eq. 1–4).

$$[\mathrm{A}] \approx \mathrm{A}_0 \qquad \text{(Eq. 1–3)}$$

$$[\mathrm{B}] \approx \mathrm{B}_0 \qquad \text{(Eq. 1–4)}$$

A light absorption reaction is an elementary reaction, thus the rate is proportional to both the concentration of substance and intensity of light. Therefore, if we consider a light intensity difference after passing through an infinitesimal distance (*dl*) of the solution is given by Eq. 1–5, which is a differential equation. A solution of the differential equation Eq. 1–5 is a very famous photophysical law, the Beer-Lambert law, which dictates that the overall absorbance is proportional to the product of the concentration of a light absorbing material and length of light path. (Eq. 1–6).

$$\frac{d\mathrm{I}}{dl} = -(\varepsilon_\mathrm{A}\mathrm{A}_0 + \varepsilon_\mathrm{B}\mathrm{B}_0) \cdot \mathrm{I}_l \qquad \text{(Eq. 1–5)}$$

$$\mathrm{I}_l = \mathrm{I}_0 \cdot e^{-(\varepsilon_\mathrm{A}\mathrm{A}_0+\varepsilon_\mathrm{B}\mathrm{B}_0)\cdot l} = \mathrm{I}_0 \cdot \mathrm{T}_l \qquad \text{(Eq. 1–6)}$$

Let us focus on the amount of light absorbed by each light absorbing materials. The light absorbed by A is the same as the amount of A* produced, which can be easily obtained by simple mathematical integration of Eq. 1–7.

$$\int_0^x \varepsilon_\mathrm{A}\mathrm{A}_0\, \mathrm{I}_l \mathrm{d}l = \varepsilon_\mathrm{A}\mathrm{A}_0\mathrm{I}_0 \int_0^\mathrm{x} e^{-(\varepsilon_\mathrm{A}\mathrm{A}_0+\varepsilon_\mathrm{B}\mathrm{B}_0)\cdot l}\mathrm{d}l \qquad \text{(Eq. 1–7)}$$

$$= \frac{\varepsilon_\mathrm{A}\mathrm{A}_0}{\varepsilon_\mathrm{A}\mathrm{A}_0 + \varepsilon_\mathrm{B}\mathrm{B}_0}\mathrm{I}_0\left(1 - e^{-(\varepsilon_A A_0+\varepsilon_B B_0)\cdot x}\right)$$

$$= \frac{\varepsilon_A A_0}{\varepsilon_A A_0 + \varepsilon_B B_0} I_0 (1 - T_x) \qquad \text{(Eq. 1–8)}$$

The fraction of light absorption by A (χ_A) is given by Eq. 1–9. Analogously, χ_B can be expressed as Eq. 1–10, meaning that the excited population is proportional to the fraction of the absorptivity.

$$\chi_A = \frac{A^*}{I_0 - I_l} = \frac{\varepsilon_A A_0}{\varepsilon_A A_0 + \varepsilon_B B_0} \qquad \text{(Eq. 1–9)}$$

$$\chi_B = \frac{B^*}{I_0 - I_l} = \frac{\varepsilon_B B_0}{\varepsilon_A A_0 + \varepsilon_B B_0} \qquad \text{(Eq. 1–10)}$$

Section 3. Molecular Recognition of cyclic-di-GMP

1. Introduction

Cyclic diguanosine monophosphate (c-di-GMP) is a cytoplasmic second messenger found in bacteria. It regulates a number of physiological processes that are critical to bacterial survival, such as biofilm formation, bacterial motility, and virulence gene expression.[68] Specifically, high level of c-di-GMP promotes biofilm formation and suppresses a bacterial motion and virulence. Also, an asymmetric distribution of c-di-GMP between mother and daughter bacteria during division process definitely signifies the regulatory effects of c-di-GMP (Figure 1–18).[69]

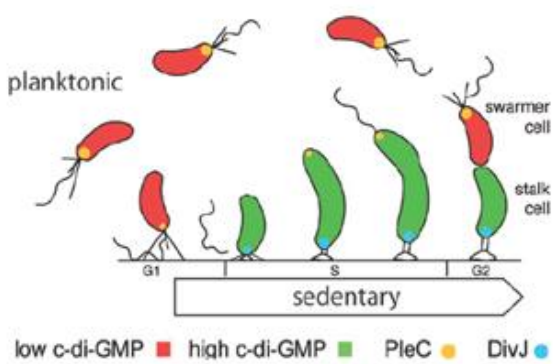

Figure 1–18. The cellular concentration of c-di-GMP in individual bacterium depending on its physical state. Copyright 2010 American Association for the Advancement of Science.

Figure 1–19 represents the chemical structure of c-di-GMP as well as its dimeric structure fitted in a binding site of a bacterial response regulator, PleD.[70,71] The dimeric structure of c-di-GMP is of particular interest because c-di-GMP spontaneously assembles into the dimeric structure which is often found as a building block in higher superstructures in the presence of monovalent cation.[72] For example, 10 μM of c-di-GMP and 40 μM of potassium formed G-quadruplex, whereas guanosine nucleotides did not form any stable G-quadruplex at the same condition, and the formation of G-quadruplex was successfully detected by the fluorescence enhancement of thiazolium orange (TO).

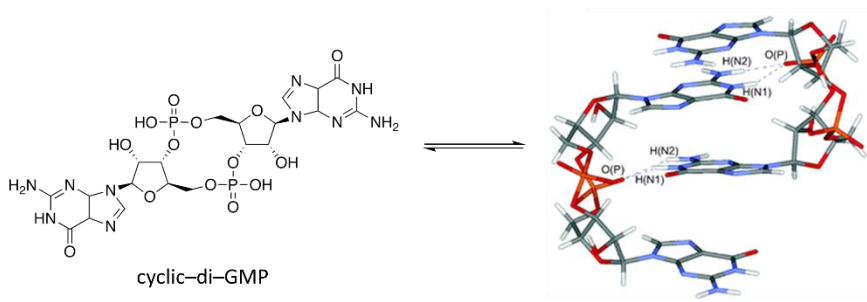

Figure 1–19. The chemical structure of c-di-GMP and its dimeric structure in a response regulator PleD complex. Reprinted by permission from reference 70. Copyright 2004 National Academy of Sciences.

Although there are several molecular and bimolecular probes that can detect c-di-GMP, a molecular probe that selectively detects c-di-GMP present in nanomolar concentration is still highly desirable for studying functions of c-di-GMP.

2. Result and discussion

2.1. Monomer–excimer strategy

The molecular structure of c-di-GMP is a macrocycle composed of two phosphates and two ribose. Therefore, the two phosphate groups are separated spatially so that they cannot come close enough to contact each other. This structural feature stimulated us to design a potential fluorescent probe by using monomer–excimer strategy. The designed molecular probe **30** and its expected binding mode to c-di-GMP is depicted in Scheme 1–19.

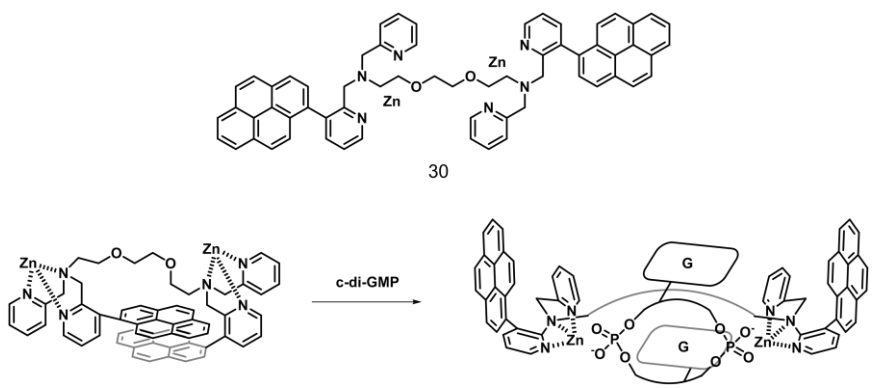

Scheme 1–19. The designed molecular structure of a potential c-di-GMP probe and its expected sensing mechanism.

The probe **30** was synthesized in a straightforward manner, following Scheme 1–20 (see Experimental section). Briefly, 2-(aminomethyl)-3-(pyrene-1-yl)pyridine was synthesized via Suzuki cross-coupling reaction followed by reduction with lithium aluminum hydride. The resulting amine was protected in the presence of Boc_2O, which was then N-alkylated with 2-(bromomethyl)pyridine in the presence of excess amount of sodium hydride. The Boc protective group was removed in

trifluoroacetic acid/dichloromethane mixture, and the resulting amine was N-alkylated with triethylene glycol bis(*p*-toluenesulfonate) and the zinc(II) chelation furnished the fluorescent probe **30**.

We evaluated the affinity of the probe **30** toward various phosphate-containing biomolecules including c-di-GMP by the fluorescence titration experiments. The fluorescence spectra are depicted in Figure 1–20 and the result was summarized in Table 1–1. Interestingly, only c-di-GMP showed monotonic decrease of the fluorescence of **30** while the addition of ATP, GTP and PPi increased the fluorescence of the probe **30** until 0.3 equivalents, and further addition of ATP, GTP, and PPi resulted in a decrement in the fluorescence intensity.

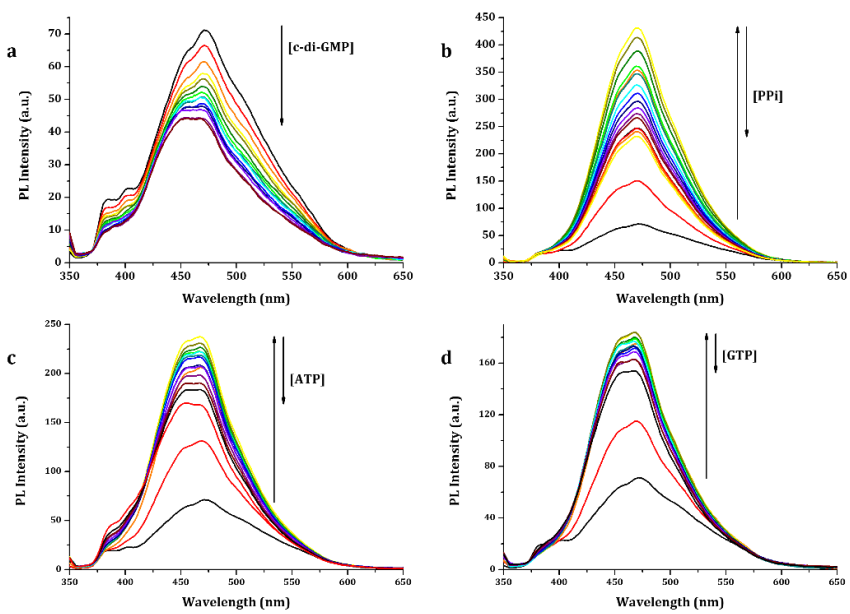

Figure 1–20. The fluorescence intensity change of 10 μM of **30** in 10 mM HEPES buffer (pH 7.42) in the increasing amount of guest molecules (0 ~ 50 μM), a, c-di-GMP; b, PPi; c, ATP; d, GTP.

Table 1–1. The fluorescence change pattern of **30** (10 μM) in the presence of various phosphate-containing biomolecules.[a]

	Signal change pattern	I_{max} / I_0	$I_{saturation} / I_0$
c-di-GMP	decrease	–	0.616
ATP	increase (~ 0.3 eq.) – decrease (0.3 eq. ~)	3.34	2.58
GTP	increase (~ 0.3 eq.) – decrease (0.3 eq. ~)	2.58	2.16
PPi	increase (~ 0.3 eq.) – decrease (0.3 eq. ~)	6.08	3.33

[a]10 mM HEPES (pH 7.42), λ_{ex} =344 nm, λ_{em} = 472 nm

The initial fluorescence spectra of the probe **30** undoubtedly involved excimer emission of pyrene, which is featureless and broad signal centered at 470 nm. In addition, there were two shoulder peaks at 380 nm and 400 nm, which is a typical monomeric emission pattern of pyrene. Therefore, our monomer–excimer strategy seemed to work. However, the fluorescence change upon addition of c-di-GMP did not coincide with our expectation. It showed only a small decrement in excimer emission without significant increment in monomer emission. The spectral change strongly implies that the binding event is not capable of inducing any conformational change of **30** from folded (excimer) into extended (monomer) form (*vide infra*).

In the formal section, we observed that a large amount of the $NADP^+$ did not reduce the excimer emission of **17**, which is presumably due to the weaker interaction between bis(Zn-DPA) and phosphate (see page 29~30). However, the phosphodiester group of c-di-GMP has smaller charge (–1) than phosphate (–2) at a physiological condition. Moreover, the probe **30** was designed to interact with phosphodiester groups with each of Zn-DPA complexes, which is smaller in charge

(+2) than bis(Zn-DPA) moiety (+4). Thus the interaction between Zn-DPA, and phosphodiester must be far weaker than that between bis(Zn-DPA) and phosphate. Therefore, the expected energy obtained by forming two ion pairs of Zn-DPA, and phosphodiester is insufficient to compensate the energy required to break the pyrene excimer into the monomer.

2.2. Biomimetic strategy

After getting a disappointing result with the monomer–excimer strategy, we designed another potential receptor for c-di-GMP with a biomimetic strategy. Figure 1–21 shows crystal structures of two independent c-di-GMP riboswitches (class I and class II) with bound c-di-GMP.[73] Although they are not homologs to each other, their molecular recognition pattern of c-di-GMP is almost identical. In detail, an adenine moiety (A47 and A70 for class I and class I riboswitches, respectively) intercalates between two guanine bases of c-di-GMP forming a sandwich structure that is enclosed by the rest of riboswitch through a complicated hydrogen bond network and a series of π stacking interactions. Especially, the hydrogen bonding interaction between N^6 of intercalating adenine with a phosphodiester of c-di-GMP in Hoogsteen face is noticeable. Also, we found that the ribose ring attached to that adenine moiety is located in close proximity to the other phosphodiester of c-di-GMP. Moreover, Strobel found that a point mutation at the intercalating adenine (A70) into guanine (G) or uracil (U) in class II c-di-GMP riboswitch virtually eliminated the affinity toward c-di-GMP.[74] This evolutionary convergent feature of riboswitches inspired us to design molecular receptors based on adenosine. Moreover, a recent study suggested the molecular structure of c-di-GMP in solution are not much different from that found in crystal structures (ΔG ~1.1 kcal mol^{-1}).[75]

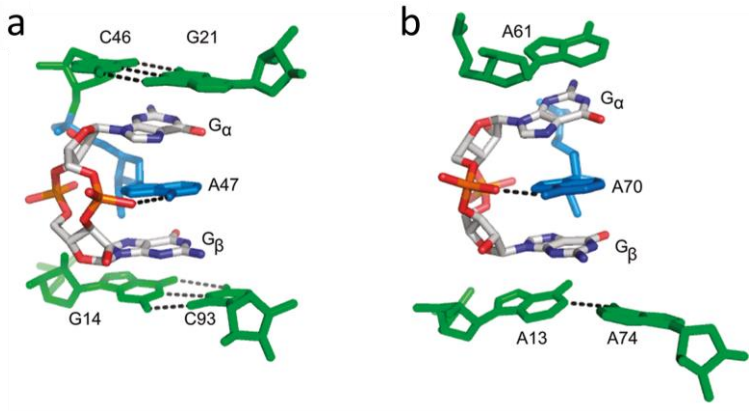

Figure 1–21. An analogous c-di-GMP molecular recognition pattern by (a) class I and (b) class II riboswitches. Reprinted by permission from reference 73. Copyright 2011 American Chemical Society.

Figure 1–22 represents the molecular structure of a receptor **31** designed for the recognition of c-di-GMP. We introduced phenylurea and Zn(II)-DPA moiety instead of amine (N^6) and 5'-hydroxyl group of 2'-deoxyadenosine in order to reinforce the intermolecular interactions, which would led favorable intercalation of adenine moiety into the cavity of c-di-GMP.

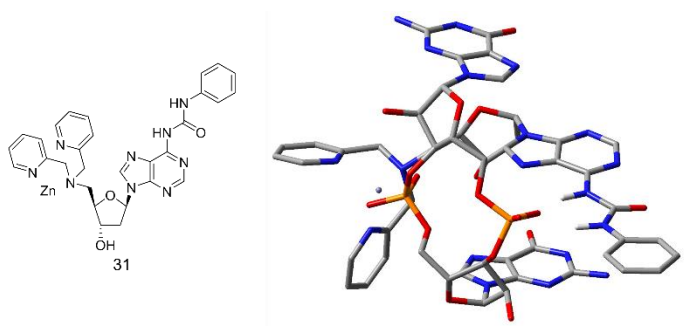

Figure 1–22. Molecular structure of **31** and the expected binding mode of **31** with c-di-GMP.

The molecular receptor **31** was efficiently synthesized from known nucleoside **32** by five synthetic steps. Briefly, the 5'-hydroxyl group was converted into 5'-amino group by successive treatment of methanesulfonyl chloride, sodium azide, and triphenylphosphine. Reductive alkylation at 5'-amino group in the presence of 2-pyridinecarboxaldehyde successfully constructed DPA moiety. The TBS protective group was removed by fluoride in THF, and chelation of zinc(II) ion in acetonitrile furnished the receptor **31**.

The isothermal titration calorimetry (ITC) experiment estimated the association constant of ~10^5 M^{-1} between receptor **31** and c-di-GMP. The affinity of **31** and c-di-GMP was remarkable in that the association constant exceeded to that between highly charged FMN (–2) and **17** (+4 cation). Moreover, **31** seemed to bind more strongly to c-di-GMP than PPi or GTP.

In order to obtain further insight in their binding behavior, we performed ^{1}H NMR titration experiments (Figure 1–23). Because D_2O/DMSO-d_6 solvent system completely diminished the resonances correspond to a urea protons, water containing D_2O (10%) and DMSO-d_6 (1-4%) was chosen as the solvent, and the water signal was suppressed by flipback-WATERGATE pulse sequence.[76,77] A set of resonances distinctive from that of **31** and c-di-GMP (e.g., resonances at 11.4, 8.3, 8.17, 8.16, 4.12, 3.17, 2.85, and 2.35 ppm) appeared transiently during titration, and c-di-GMP signals were greatly diminished when more than 2.0 equivalent of **31** was added, implying c-di-GMP was no more present in aqueous phase after titration. Indeed, white precipitates were formed gradually over the course of titration (Figure 1–24). Because **31** and c-di-GMP were clearly dissolved in the solvent system up to 6 and 10 mM, respectively, it is reasonable to assume that the precipitate would be **31**–c-di-GMP complex. These results suggested that **31** and c-di-GMP formed a stable and

hydrophobic complex with $K_a > 10^4$ M^{-1} that dissociated very slowly ($k_{off} > 2$ s^{-1}). However, the reason for slow exchange kinetics is of doubt.

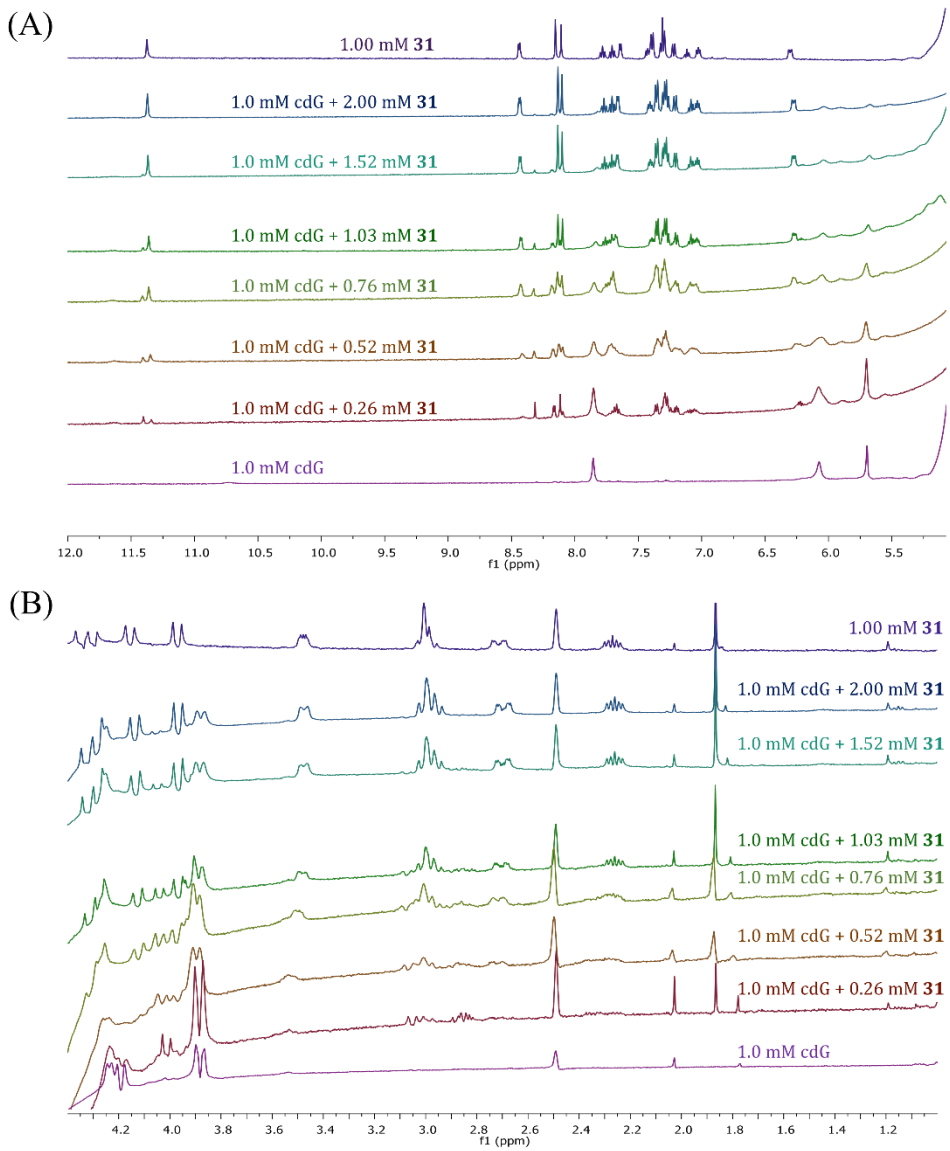

Figure 1–23. Partial ^{1}H NMR spectra of cyclic-di-GMP-**31** mixtures in (A) imidic/aromatic and (B) aliphatic region. The resonance at 2.5 ppm corresponds to the residual peak of DMSO-d_6.

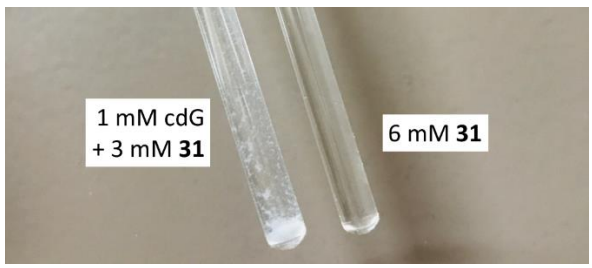

Figure 1–24. A picture of NMR tubes containing (left) 1 mM c-di-GMP and 3 mM **31** and (right) 6 mM **31**. Solvent = (left) 86.4% H_2O, 9.6% D_2O 4% DMSO-d_6, (right) 84.6% H_2O, 9.4% D_2O 6.5% DMSO-d_6

We then introduced a fluorophore into 3'-hydroxyl group for the fluorescent detection of c-di-GMP by the help of fluorescence quenching ability of guanine moiety (see Part III). A BODIPY-based Fluorophore was efficiently attached via carbamate forming reaction by hydroxyl quenching after Curtius rearrangement of carboxylic acid-terminated BODIPY. Final zinc(II) chelation in acetonitrile solution afforded **32**.

Probe **32** was titrated with c-di-GMP, GTP, and PPi using fluorescence. A fluorescence quenching was observed for all analytes, while weakest quenching was observed for c-di-GMP. The association constant between **32** and c-di-GMP was estimated to be 3.05×10^5 M^{-1} by fitting the fluorescence intensity at 549 nm with respect to analyte concentration, which is in accordance with the result of ITC experiment. On the other hand, we could not precisely determine the association constant of **32**-GTP and **32**-PPi complexes because they did not obey 1:1 binding isotherm. Nevertheless, the fluorescence of **32** similarly reached plateau after 5 equivalent of analytes were added, which implies that the association constants are similar to each other.

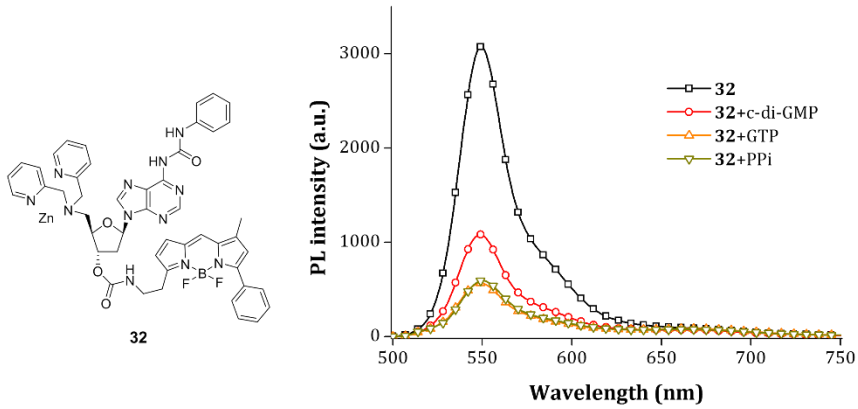

Figure 1–25. Molecular structure and fluorescence response of **32** (10 μM) to various anions (20 μM each) in 10 mM HEPES buffered solution (5% CH_3CN, 1% DMSO).

3. Conclusion

We rationally designed and synthesized molecular probes and receptors for c-di-GMP based on monomer–excimer and biomimetic strategies. We successfully demonstrated that the adenosine derivatives could be utilized as a fluorescent probe for c-di-GMP, as **32** exhibited a high association constant toward up to 3.05×10^5 M^{-1}, which is comparable to that between bis(Zn-DPA) and phosphate. However, probes **30** and **32** did not show any selectivity toward c-di-GMP against PPi or other nucleotides including GTP. We believe further optimization or screening is necessary to achieve selective detection. In another hand, a study on how **31** recognizes c-di-GMP using NMR spectroscopy is undergoing.

4. Experimental section

4.1. General information

All chemicals were purchased from either Sigma–Aldrich or Tokyo Chemical Industry (TCI) and were used as received except anhydrous solvents. Thin layer chromatography was performed over Merck silica gel 60 F254 on aluminum foil. Silicycle 60 was used for the stationary phase in chromatographic separation or silica pad filtration. Celite® 545 was used for celite filtration. All ^{1}H and ^{13}C NMR spectra were obtained from Bruker DRX-300 NMR spectrometer, Agilent 400MHz DD2MR400 spectrometer, or Varian 500 MHz NMR spectrometer. Fluorescence emission spectra were recorded on a JASCO FP-7300 spectrometer and the slit width was 3 or 5 nm for excitation and 5nm for emission. LRMS were taken by MALDI-TOF mass analyzer (Bruker instrument). HRMS were taken by Agilent 6890 Series, with FAB-positive mode.

4.2. Synthesis

Dichloromethane and tetrahydrofuran were distilled over calcium hydride and sodium/benzophenone ketyl, respectively. Other solvents were used without further purification. NMR samples were prepared by dissolving in DMSO-d_6, $CDCl_3$, acetone-d_6, or 10% D_2O in water. Multiplicities: s, singlet; d, doublet; t, triplet; m, multiplet; br, broad.

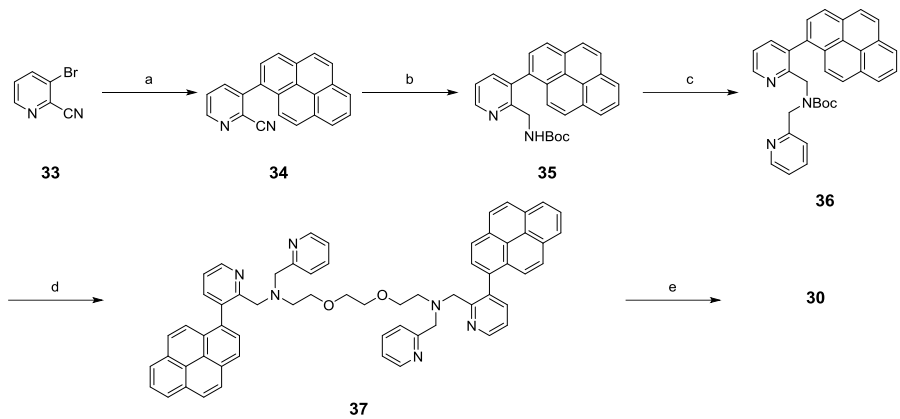

Scheme 1–20. Synthesis of probe 30. a, 3 mol–% tetrakis(triphenylphosphine)palladium(0), 1-pyreneboronic acid, THF/H_2O; b, $LiAlH_4$, THF, then Boc_2O; c, NaH, THF, then 2-bromomethylpyridine hydrobromide; d, 25% TFA in DCM; NaH, THF then triethylene glycol bis(*p*–toluenesulfonate); e, $Zn(ClO_4)_2 \cdot 6H_2O$, acetonitrile.

Synthesis of **34**: The solution of **33** (1.1 g, 6.0 mmol, 1.0 equiv.), 1-pyreneboronic acid (1.48 g, 6.0 mmol, 1.0 equiv.), tetrakis(triphenylphosphine) palladium(0) (208 mg, 0.18 mmol, 3 mol–%), and sodium bicarbonate (1.26 g, 15 mmol, 2.5 equiv.) in glyme-water mixture (4/1, 60 mL) was heated at 70 °C for 12 hours, during which time yellowish precipitates were formed. Volatiles were evaporated under reduced pressure, and the residue was diluted with water and dichloromethane (250 mL each). The organic phase was dried over anhydrous Na_2SO_4, filtered and evaporated to dryness. Ethyl ether (30 mL) was added and the suspension was sonicated for 3 hours. The precipitates were collected *via* filtration and washed with ethyl ether three times to give analytically pure product (1.52 g, 83 %). ^{1}H NMR (300 MHz, DMSO-d_6) δ 8.95 (d, J = 4.1 Hz, 1H), 8.52–8.21 (m, 7H), 8.16 (m, 2H), 7.98 (dd, J = 7.8, 4.8 Hz, 1H), 7.76 (d, J = 9.2 Hz, 1H). ^{13}C NMR (75 MHz, DMSO-d_6) δ 150.92, 141.33, 140.48, 133.58, 131.98, 131.27, 130.70, 130.55, 129.24, 128.92, 128.82, 128.32, 127.96, 127.75, 127.25, 126.55, 126.23,

125.31, 124.27, 124.14, 117.38. LRMS (MALDI-TOF) m/z: $[M+H]^+$ calcd for $C_{22}H_{13}N_2$ 305.1; found 305.2.

Synthesis of **35**: To a suspension of $LiAlH_4$ (486 mg, 12.8 mmol, 3.0 equiv.) and $AlCl_3$ (1.14 g, 8.54 mmol, 2.0 equiv.) in anhydrous tetrahydrofuran (100 mL) was added **33** (1.3 g, 4.27 mmol, 1.0 equiv.) in tetrahydrofuran (20 mL) at 0 °C. The mixture was gently refluxed for 12 hours. Excessive hydrides were destroyed by successive addition of water, 10% aqueous NaOH and water (1, 2, and 3 mL, respectively). The precipitates were removed by Celite® filtration and most of the volatiles were removed under reduced pressure. The residue was diluted by dichloromethane-water mixture before treated by di(tert-butyl) dicarbonate (1.4 g, 6.4 mmol, 1.5 equiv.). The biphasic mixture was stirred for 3 hours. The aqueous layer was extracted by dichloromethane twice, and the combined organic layer was dried over anhydrous Na_2SO_4, filtered and concentrated under reduced pressure. The crude product was purified by silica gel column chromatography by a gradient elution of ethyl acetate in hexanes (20 to 33 %) to give the analytically pure product (770 mg, 44 %). ^{1}H NMR (300 MHz, Acetone-d_6) δ 8.75 (dd, *J* = 4.8, 1.5 Hz, 1H), 8.39 (d, *J* = 7.8 Hz, 1H), 8.34 (d, *J* = 7.7 Hz, 1H), 8.29 (d, *J* = 7.5 Hz, 1H), 8.24 (s, 2H), 8.11 (dd, *J* = 16.3, 8.5 Hz, 2H), 7.99 (d, *J* = 7.8 Hz, 1H), 7.82 (dd, *J* = 7.6, 1.5 Hz, 1H), 7.65 (d, *J* = 9.2 Hz, 1H), 7.54 (dd, *J* = 7.5, 4.9 Hz, 1H), 6.27 (s, 1H), 4.18 (dd, *J* = 16.7, 4.9 Hz, 1H), 4.08 (dd, *J* = 16.7, 4.9 Hz, 1H), 1.30 (s, 9H). ^{13}C NMR (75 MHz, Acetone-d_6) δ 155.22, 154.91, 148.30, 138.56, 134.68, 133.07, 131.42, 131.31, 130.92, 128.82, 128.24, 127.84, 127.39, 127.29, 126.42, 125.63, 125.41, 124.91, 124.61, 124.50, 124.22, 122.12, 77.86, 43.72, 27.60. LRMS (MALDI-TOF) m/z: $[M+H]^+$ calcd for $C_{27}H_{25}N_2O_2$ 409.2; found 409.2.

Synthesis of **36**: To a suspension of NaH (60% in mineral oil, 120 mg, 3.0 mmol, 3.0 equiv.) in anhydrous THF (5 mL) was added **35** (408 mg, 1.0 mmol, 1.0 equiv.) at 0 °C and stirred for 30 minutes. The mixture was added 2-bromomethylpyridine hydrobromide (277 mg, 1.1 mmol, 1.1 equiv.) at 0 °C, and gently refluxed for 3 hours before being quenched by addition of 25 mL of water and 25 mL of water. The aqueous layer was extracted by dichloromethane three times. The combined organic layer was dried over anhydrous Na_2SO_4, filtered and evaporated under reduced pressure. The residue was chromatographed over silica gel by eluting ethyl acetate in hexanes (15 to 30 %) to give the analytically pure product (223 mg, 45 %). ^{1}H NMR (300 MHz, $CDCl_3$) δ 8.78 (d, *J* = 4.6 Hz, 1H), 8.39 (d, *J* = 4.4 Hz, 1H), 8.31–8.07 (m, 5H), 8.02 (dd, *J* = 16.5, 8.3 Hz, 2H), 7.84 (dd, *J* = 12.0, 7.8 Hz, 1H), 7.66 (t, *J* = 7.0 Hz, 2H), 7.53–7.31 (m, 2H), 7.23–6.90 (m, 2H), 4.83–4.23 (m, 4H), 1.22 (d, *J* = 35.5 Hz, 9H). ^{13}C NMR (75 MHz, $CDCl_3$) δ 158.70, 158.52, 155.53, 148.92, 148.67, 138.76, 138.41, 136.37, 136.29, 135.64, 134.87, 133.23, 131.32, 131.09, 130.84, 128.95, 128.85, 128.13, 127.81, 127.69, 127.33, 127.00, 126.22, 126.15, 125.53, 125.40, 125.27, 124.68, 124.41, 121.77, 121.60, 120.48, 79.66, 52.88, 52.65, 50.80, 28.17, 28.06. LRMS (MALDI-TOF) m/z: $[M+H]^+$ calcd for $C_{33}H_{30}N_3O_2$ 500.2; found 500.2.

Synthesis of **37**: A solution of **36** (220 mg, 0.44 mmol, 2.2 equiv.) in dichloromethane (5 mL) was treated by trifluoroacetic acid (1.25 mL). The mixture was stirred for 3 hours and quenched by adding 12 mL of saturated $NaHCO_3$ solution. The aqueous layer was extracted by dichloromethane three times. The combined organic layer was dried over anhydrous Na_2SO_4, filtered and concentrated under reduced pressure. The residue was redissolved in anhydrous acetonitrile (3 mL), and treated with triethyleneglycol bis(p-toluenesulfonate) (92 mg, 0.2 mmol, 1.0 equiv.)

and anhydrous K_2CO_3 (83 mg, 0.6 mmol, 3.0 equiv.) and the mixture was gently refluxed for 18 hours. Insoluble salts and volatiles were removed by Celite® filtration and rotary evaporator under reduced pressure. The residue was chromatographed over silica gel by a gradient elution of methanol in dichloromethane (0 to 15 %) to give the analytically pure product. (122 mg, 67 %). LRMS (MALDI-TOF) m/z: $[M+H]^+$ calcd for $C_{62}H_{53}N_6O_2$ 913.4; found 913.3.

Synthesis of **30**: 5 µmol of **36** in acetonitrile (0.1 mL) was treated with $Zn(ClO_4)_2 \cdot 6H_2O$ (3.82 mg, 10.25 µmol, 2.05 equiv.) in acetonitrile (0.1 mL). The mixture was shaken for 30 minutes, lyophilized, and used without further purification.

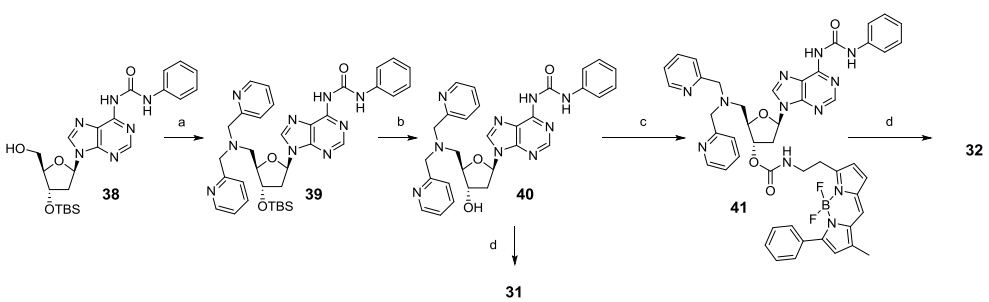

Scheme 1–21. Synthesis of receptor **31** and probe **32** for c-di-GMP. a, (i) methanesulfonyl chloride, triethylamine, DCM, (ii) NaN_3, DMF, reflux, (iii) PPh3, water, THF, (iv) 2-pyridinecarboxaldehyde, $NaBH(OAc)_3$, 1,2-dichloroethane; b, tetra-*n*-butylammonium fluoride, THF; c, **42**, pyridine, DCM; d, $Zn(ClO_4)_2 \cdot 6H_2O$, acetonitrile

Synthesis of **39**: To a suspension of **38** (484 mg, 1.0 mmol, 1.0 equiv.) in dichloromethane (7 mL) was successively added methanesulfonyl chloride (0.23 mL, 3.0 mmol, 3.0 equiv.) in dichloromethane (3 mL) and triethylamine (1.0 mL) at 0°C dropwisely. The mixture was stirred for additional 2 h after which the reaction

mixture became clear solution. The mixture was diluted with water (30 mL), extracted with dichloromethane three times. Combined organic layer was dried over anhydrous $MgSO_4$ and filtered. Volatiles were removed under reduced pressure. The residue was dissolved in DMF (5 mL) and added sodium azide (650 mg, 10 mmol, 10 equiv.) The mixture was gently refluxed for 16 h during which time TLC analysis indicated complete consumption of the starting materials. The mixture was concentrated in vacuo and the residue was diluted with ethyl acetate and water (30 mL each). Aqueous layer was extracted with ethyl acetate three times. Combined organic layer was dried over anhydrous $MgSO_4$ and filtered through a pad of silicate (1 cm). Volatiles were removed under reduced pressure. The residue was dissolved in wet THF (10 mL with 0.2 mL of water) and treated with PPh_3 (552 mg, 2 mmol, 2.0 equiv.). The mixture was heated at 50°C for 6 h and concentrated under reduced pressure. The residue was dissolved in 1,2-dichloromethane (12 mL), successively treated with 2-pyridinecarboxaldehyde (0.21 mL, 2.2 mmol, 2.2 equiv.) and $NaBH(OAc)_3$ (636 mg, 3 mmol, 3.0 equiv.), and stirred for 16 h. The mixture was concentrated under reduced pressure, diluted with water (20 mL), and extracted with dichloromethane three times. Combined organic layer was dried over anhydrous $MgSO_4$, filtered, and concentrated. The residue was chromatographed over silica gel by gradient elution of methanolic dichloromethane (0 to 5%) to give analytically pure product (217 mg, 33%). ^{1}H NMR (400 MHz, acetone-d_6) δ 12.05 (s, 1H), 8.95 (s, 1H), 8.62 (s, 1H), 8.54 (s, 1H), 8.47 (d, J = 4.3 Hz, 2H), 7.71 (d, J = 7.7 Hz, 2H), 7.65 (td, J = 7.6, 1.7 Hz, 2H), 7.54 (d, J = 7.8 Hz, 2H), 7.35 (t, J = 7.9 Hz, 2H), 7.26–7.11 (m, 2H), 7.08 (t, J = 7.4 Hz, 1H), 6.51 (t, J = 6.5 Hz, 1H), 4.60 (dt, J = 5.8, 4.1 Hz, 1H), 4.31–4.15 (m, 1H), 3.88 (dd, J = 42.9, 14.5 Hz, 4H), 3.01 (dd, J = 13.9, 4.7 Hz, 1H), 2.96–2.86 (m, 2H), 2.40 (ddd, J = 13.4, 6.6, 4.3 Hz, 1H), 0.88 (s, 9H), 0.09

(s, 3H), 0.06 (s, 3H). LRMS (MALDI-TOF) m/z: $[M+H]^+$ calcd for $C_{35}H_{44}N_9O_3Si$ 666.3; found 666.4.

Synthesis of **40**: **39** (200 mg, 0.3 mmol, 1.0 equiv.) in anhydrous THF (3 mL) was treated with tetra-*n*-butylammonium fluoride (0.9 mL, 1M in THF, 0.9 mmol, 3.0 equiv.) and stirred for 5 h. The mixture was concentrated under reduced pressure and the resulting residue was chromatographed over silica gel by gradient elution of methanolic dichloromethane (0 to 5%) to give analytically pure product (84 mg, 51%). ^{1}H NMR (400 MHz, acetone-d_6) δ 12.12 (s, 1H), 9.36 (s, 1H), 8.60 (s, 2H), 8.48 (d, J = 4.3 Hz, 2H), 7.75 (d, J = 7.8 Hz, 2H), 7.66 (td, J = 7.7, 1.5 Hz, 2H), 7.49 (d, J = 7.8 Hz, 2H), 7.36 (t, J = 7.8 Hz, 2H), 7.26–7.14 (m, 2H), 7.09 (t, J = 7.4 Hz, 1H), 6.51 (dd, J = 6.8, 5.3 Hz, 1H), 5.47 (s, 1H), 4.66 (dd, J = 11.5, 6.0 Hz, 1H), 4.24 (dd, J = 11.5, 6.3 Hz, 1H), 3.87 (d, J = 14.4 Hz, 4H), 3.12–2.78 (m, 4H), 2.54 (dt, J = 13.3, 6.6 Hz, 1H). LRMS (MALDI-TOF) m/z: $[M+H]^+$ calcd for $C_{29}H_{30}N_9O_3$ 552.2; found 552.3.

Synthesis of **41**: To a solution of 40 (20 mg, 0.036 mmol, 1.0 equiv.) in pyridine/dichloromethane mixture (0.3/1 mL) was treated with **42** (~0.1 mmol, 5 equiv.). The mixture was stirred for 16 h before being quenched by addition of ethanol. Volatiles were removed under reduced pressure and the residue was chromatographed over silica gel by gradient elution of ethyl acetate then methanolic dichloromethane (0 to 5%) to give analytically pure product. ^{1}H NMR (400 MHz, acetone-d_6) δ 12.02 (s, 1H), 8.82 (s, 1H), 8.48–8.42 (m, 2H), 7.95 (dd, J = 6.6, 2.8 Hz, 2H), 7.71 (d, J = 7.6 Hz, 3H), 7.62–7.57 (m, 2H), 7.54 (d, J = 7.8 Hz, 2H), 7.49–7.41 (m, 3H), 7.35 (t, J = 7.9 Hz, 3H), 7.23–7.15 (m, 2H), 7.16–7.11 (m, 2H), 7.08 (t, J = 7.4 Hz, 1H), 6.60–6.48 (m, 2H), 6.45–6.36 (m, 1H), 5.42–5.36 (m, 1H), 4.32 (s, 1H), 4.00–3.69 (m, 6H), 3.54 (dd, J = 13.2, 6.4 Hz, 2H), 3.16 (dd, J = 14.7, 10.2

Hz, 2H), 3.13–3.00 (m, 2H), 2.94 (ddt, J = 16.2, 13.9, 6.9 Hz, 2H), 2.52–2.44 (m, 1H), 2.35 (d, J = 11.1 Hz, 3H). LRMS (MALDI-TOF) m/z: $[M+H]^+$ calcd for $C_{48}H_{46}BF_2N_{12}O_4$ 903.4; found 903.5.

Synthesis of **31**: 8 μmol of **40** in acetonitrile (0.1 mL) was treated with $Zn(ClO_4)_2 \cdot 6H_2O$ (3.04 mg, 8.16 μmol, 1.02 equiv.) in acetonitrile (0.1 mL). The mixture was shaken for 30 minutes, lyophilized, and used without further purification.

Synthesis of **32**: 8 μmol of **41** in acetonitrile (0.1 mL) was treated with $Zn(ClO_4)_2 \cdot 6H_2O$ (3.04 mg, 8.16 μmol, 1.02 equiv.) in acetonitrile (0.1 mL). The mixture was shaken for 30 minutes, lyophilized, and used without further purification.

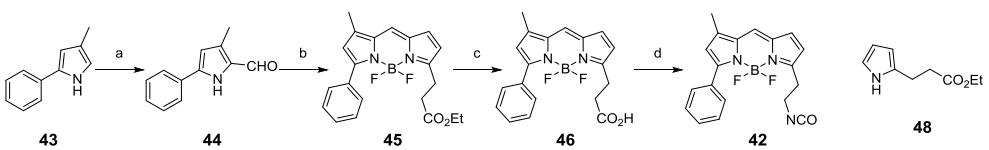

Scheme 1–22. Synthesis of BODIPY-NCO **47**. a, DMF, $POCl_3$, DCM; b, i. **48**, $POCl_3$, DCM; ii. $BF_3 \cdot OEt_2$, DIPEA, DCM; c, 6 M HCl, THF; d, i. ethyl chloroformate, N-methyl morpholine, THF; ii. NaN_3, THF, H_2O.

Synthesis of **44**: To a solution of N,N-dimethylformamide (0.38 mL, 5 mmol, 2.5 equiv.) in 5 mL of 1,2-dichloroethane was added phosphorous oxychloride (0.14 mL, 3 mmol, 1.5 equiv.) dropwisely at 0 °C to form Vilsmeier salt. To the solution of Vilsmeier salt was added **43**[78] (684 mg, 2 mmol, 1.0 equiv.) in dichloromethane (2 mL), and the mixture was stirred for an hour at ambient temperature. The mixture was treated with half-saturated sodium acetate solution (5 mL) and stirred for another

hour. The biphasic mixture was partitioned by ethyl acetate and water, and the organic layer was washed with water three times. The organic layer was dried over anhydrous $MgSO_4$, filtered, and concentrated under reduced pressure. The crude product was purified by silica gel column chromatography by a gradient elution of ethyl acetate in hexanes (10 to 20 %) to give the analytically pure product (330 mg, 89%). ^{1}H NMR (300 MHz, $CDCl_3$) δ 9.99 (br s, 1H), 9.66 (s, 1H), 7.73–7.59 (m, 2H), 7.44 (m, 2H), 7.35 (m, 1H), 6.46 (d, *J* = 2.5 Hz, 1H), 2.43 (s, 3H). ^{13}C NMR (75 MHz, $CDCl_3$) δ 177.04, 139.49, 134.32, 130.64, 130.16, 129.06, 128.52, 125.31, 110.51, 10.71. LRMS (MALDI-TOF) m/z: $[M+H]^+$ calcd for $C_{12}H_{12}NO$ 186.1; found 186.3.

Synthesis of **45**: To a solution of **44** (463 mg, 2.5 mmol, 1.0 equiv.) and **48**[79] (459 mg, 2.75 mmol, 1.1 equiv.) in 15 mL of dichloromethane was added phosphorous oxychloride (0.28 mL) dropwisely at –15 °C. The mixture was stirred for 4 hours at 0 °C and treated by N,N-diisopropylethylamine (3.0 mL, 17.5 mmol, 7.0 equiv.) and boron trifluoride etherate (0.62 mL, 5.0 mmol, 2.0 equiv.) successively. The reaction proceeded for 3 hours at room temperature. It was added 25 mL of water and the biphasic mixture was vigorously stirred for 2 hours to ensure complete quenching. The mixture was diluted with ethyl ether (30 mL) and water (30 mL), and the aqueous layer was extracted by ether twice. The combined organic layer was dried over anhydrous MgSO4, filtered, and concentrated under reduced pressure. The residue was chromatographed over silica gel by a gradient elution of ethyl acetate in hexanes (5 to 20 %) to obtain the analytically pure product (828 mg, 87 %). ^{1}H NMR (300 MHz, $CDCl_3$) δ 7.94 (m, 2H), 7.49 (m, 3H), 7.23 (s, 1H), 6.98 (d, *J* = 3.9 Hz, 1H), 6.47 (s, 1H), 6.35 (d, *J* = 4.0 Hz, 1H), 4.16 (q, *J* = 7.1 Hz, 2H), 3.32 (t, *J* = 7.5 Hz, 2H), 2.75 (t, *J* = 7.5 Hz, 2H), 2.33 (s, 3H), 1.26 (t, *J* = 7.1 Hz,

3H). ^{13}C NMR (75 MHz, $CDCl_3$) δ 172.45, 159.30, 159.12, 142.88, 142.74, 136.28, 133.86, 132.25, 129.83, 129.38, 129.33, 129.28, 129.15, 128.30, 124.76, 120.59, 118.05, 60.58, 33.32, 24.12, 14.22, 11.39. LRMS (MALDI-TOF) m/z: $[M+H]^+$ calcd for $C_{21}H_{22}BF_2N_2O_2$ 382.2; found 382.3.

Synthesis of **46**: To a solution of **45** (308 mg, 0.87 mmol) in 10 mL of tetrahydrofuran was treated with 10 mL of 6 M HCl solution. The mixture was stirred until TLC analysis indicates complete consumption of starting materials. Most of the tetrahydrofuran was evaporated under reduced pressure, and the aqueous layer was extracted by 2 % methanolic dichloromethane three times. The combined organic layer was dried over anhydrous Na_2SO_4, filtered, and evaporated. The residue was chromatographed over silica gel by a gradient elution of ethyl acetate in hexanes (70 to 100 %) to obtain the analytically pure product (195 mg, 62 %). ^{1}H NMR (300 MHz, Acetone-d_6) δ 10.80 (br, 1H), 8.0 (m, 2H), 7.69 (s, 1H), 7.48 (m, 3H), 7.18 (d, J = 3.9 Hz, 1H), 6.65 (s, 1H), 6.51 (d, J = 3.9 Hz, 1H), 3.27 (t, J = 7.7 Hz, 2H), 2.77 (t, J = 7.7 Hz, 2H), 2.39 (s, 3H). ^{13}C NMR (75 MHz, Acetone-d_6) δ 172.73, 159.59, 158.47, 143.45, 136.28, 134.10, 132.42, 129.75, 129.62, 129.38, 129.32, 129.27, 128.19, 125.86, 120.38, 118.03, 32.13, 23.93, 10.47. LRMS (MALDI-TOF) m/z: $[M+H]^+$ calcd for $C_{19}H_{18}BF_2N_2O_2$ 355.1; found 355.2.

Synthesis of **42**: A solution of **46** (125 mg, 0.35 mmol, 1.0 equiv.) in 4 mL of THF–DMF mixture (3:1) was successively treated with ethyl chloroformate (67μL, 0.71 mmol, 2.0 equiv.) and N-methylmorpholine (78μL, 0.71 mmol, 2.0 equiv.) and stirred for 30 minutes. The mixture was added an aqueous solution of NaN_3 (65 mg, 1 mmol, 3.0 equiv.) and was stirred for another 30 minutes. The mixture was diluted with dichloromethane and water (40 mL each), and the organic layer was washed with water three times. The organic layer was dried over anhydrous $MgSO_4$, filtered,

and evaporated under reduced pressure and below 30°C. The crude product was used in the next step without further purification.

Part II.

Molecular Receptors for Pyrophosphate

Section 1. Background

1. Binding event as a dynamic chemical equilibrium

A *dynamic chemical equilibrium* for a reversible reaction is a balanced state in which the rates of forward and reverse reaction are identical to each other so that the concentrations of reactants and products do not change with time. Two conditions to hold a dynamic chemical equilibrium are (1) the rates in both directions are the same; (2) the reactants and the products should be stable enough at a given temperature so that they do not undergo decomposition. In that regard, any simple binding event mediated by cumulative noncovalent interactions is a dynamic chemical equilibrium. Hence, a binding event can also be interpreted by means of thermodynamics and kinetics, analogously to any other chemical equilibrium or reaction.

1.1. Thermodynamics of a binding[80]

Gibbs free energy (G) is perhaps the most important parameter in thermodynamics. The negative value of Gibbs free energy represents a spontaneity for a given reaction manifesting the second law of thermodynamics. In addition, the Gibbs free energy change of given equilibrium gives another very special meaning other than indicating spontaneity of the reaction.

Eq. 2–1 represents Gibbs free energy change of a reversible reaction at arbitrary state, while ΔG^{o} denotes that at the standard state. When a reversible reaction reaches the equilibrium, no driving force for the reaction is present ($\Delta G_{rxn} = 0$), and Eq. 2–1 becomes Eq. 2–2, which equation is the most important consequence of the Gibbs free energy analysis as well as the special meaning mentioned above. It is very interesting that the concentration ratio of product to reactant directly connected to their intrinsic stability. This specific relation between energy difference of states and the populations occupying each state became Boltzmann-Gibbs distribution, one of the most famous distribution functions. If we consider a complexation reaction as of interest, we can deduce that the association constant reflects the overall free energy change of the complexation.

$$\Delta G_{\mathrm{rxn}} = \Delta G^{\mathrm{o}}_{\mathrm{rxn}} + \mathrm{RT}\ln Q \qquad \text{(Eq. 2–1)}$$

$$\Delta G^{\mathrm{o}}_{\mathrm{rxn}} = -\mathrm{RT}\ln K_{\mathrm{eq}} \qquad \text{(Eq. 2–2)}$$

Eq. 2–3, the definition of Gibbs free energy, reveals that Gibbs free energy is a state function. Therefore, a change of the Gibbs free energy for a complexation reaction at a constant temperature (ΔG) can be expressed as Eq. 2–4. The equation undoubtedly states that both the enthalpy and entropy of complexation affect the binding strength.

$$\mathrm{G} = \mathrm{H} - \mathrm{TS} \qquad \text{(Eq. 2–3)}$$

$$\Delta G = \Delta H_{\mathrm{comp}} - \mathrm{T}\Delta S_{\mathrm{comp}} \qquad \text{(Eq. 2–4)}$$

Hess's law is a powerful tool to analyze how the entropy and enthalpy affect the overall free energy change. Figure 2–1 shows a hypothetical route to form a host–guest complex according to Hess's law. The overall enthalpy change includes enthalpy changes during the solvation/desolvation process as well as that during the host-guest complex formation process. The same situation also applies to the entropy. Because the changes of enthalpy and entropy during solvation and desolvation does not necessarily cancel out each other, we can obtain an important consequence that the *nearby solvent molecules* must play significant roles in the complex forming reaction.

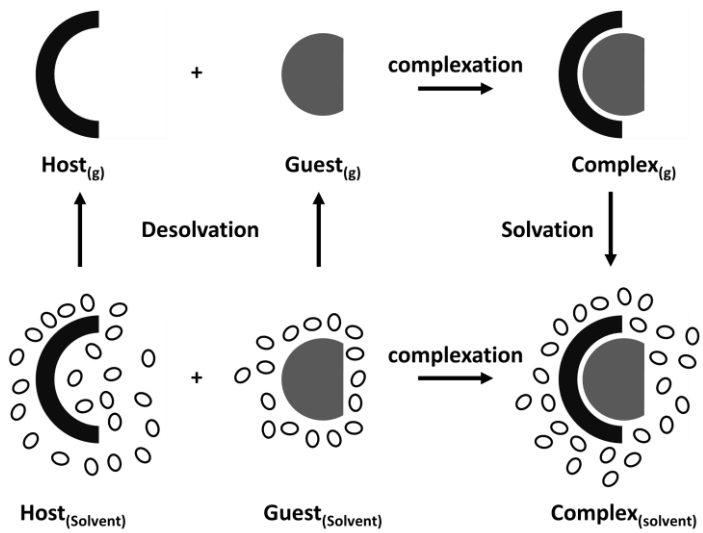

Figure 2–1. A hypothetical complexation according to Hess' law. Black arc, grey chord, and ellipsoids represent a host, guest and solvent molecules, respectively,

Let us consider a complexation behavior between a charged host and guest in an aqueous environment. If host and guest are weakly solvated, then the enthalpy change during complexation reaction predominantly comes from the charge-charge

interaction between the host and the guest, while solvation and desolvation enthalpy have marginal participation. In addition, water molecules are almost free at initial state, the conformational restriction of host and guest become the determinant factor of overall entropy change. On the other hand, when they are heavily solvated, the overall enthalpy change shifted positive, and release of solvent molecules result in the increase of entropy change. In this regard, we can reason a posteriori that a gain of enthalpy causes a loss of entropy, which situation termed by *enthalpy–entropy compensation*. Although there are many controversies[81-84] including whether the enthalpy–entropy compensation does actually exist, it has been extensively studied[85,86] not only in theory[87-91] but also in synthetic receptors[92-96] and many natural macromolecular receptors,[97-101]

1.2. Kinetics of a binding

For a binding between A and B satisfying Eq. 2–5, Eq. 2–6 holds under dynamic chemical equilibrium, which results in Eq. 2–7. Then, the relation between kinetics and thermodynamics of the binding becomes clear; increase in k_{on} and k_{off} results in the increment and decrement of K_a, respectively. Therefore, the molecular design could provide another powerful tool to manipulate an association constant since k_{on} and k_{off} largely depend on the molecular structure of a host.

$$\mathrm{A} + \mathrm{B} \underset{k_{\mathrm{off}}}{\overset{k_{\mathrm{on}}}{\rightleftarrows}} \mathrm{A} \cdot \mathrm{B} \qquad \text{(Eq. 2–5)}$$

$$k_{\mathrm{on}}[\mathrm{A}][\mathrm{B}] = k_{\mathrm{off}}[\mathrm{A} \cdot \mathrm{B}] \qquad \text{(Eq. 2–6)}$$

$$\frac{k_{\mathrm{on}}}{k_{\mathrm{off}}} = \frac{[\mathrm{A} \cdot \mathrm{B}]}{[\mathrm{A}][\mathrm{B}]} = K_{\mathrm{a}} \qquad \text{(Eq. 2–7)}$$

A combination of stopped-flow technique and Eq. 2–7 is particularly useful for studying detailed kinetic profiles of enzymes and biological receptors that obey Michaelis-Menten kinetics. If we assume $B_0 \gg A_0$, which is usual for enzymes, we obtain two mass balance equations Eq. 2–8 and 2–9, then we can obtain Eq. 2–10, a rate equation for Eq. 2–5. The solution of Eq. 2–10 is Eq. 2–11, which represents the change of concentration of A during the complexation reaction. Interestingly, the exponential factor is $-(k_{off}+k_{on}\,B_0)$. Therefore, we can obtain k_{on} and k_{off}, by plotting k_{obs} versus B_0.

$$A_0 = [A] + [A \cdot B] \qquad \text{(Eq. 2–8)}$$

$$B_0 = [B] + [A \cdot B] \approx B_0 \qquad \text{(Eq. 2–9)}$$

$$\frac{d[A]}{dt} = -k_{on}[A][B] + k_{off}[A \cdot B]$$

$$= k_{off}\,A_0 - (k_{on}B_0 + k_{off})[A] \qquad \text{(Eq. 2–10)}$$

$$[A] = \frac{k_{off}\,A_0}{k_{off} + k_{on}B_0} - \alpha \cdot e^{-(k_{on}B_0 + k_{off})t} \qquad \text{(Eq. 2–11)}$$

1.3. Relation between kinetics and thermodynamics of binding

Figure 2–2 represents a typical energy landscape for a spontaneous binding event between A and B. The activation energy of dissociation is obviously greater than overall free energy change of association. Therefore, an exceedingly strong binding increases the activation energy of dissociation. As a result, it necessarily retards the

rate of dissociation and as well as guest exchange reaction. Indeed, an association free energy of 11 kcal mol^{-1} (corresponds to $K_a \sim 10^8\ M^{-1}$) is significant compared to a typical activation energy of reaction, 20 kcal mol^{-1} ($t_{1/2} \sim 1$ min.).

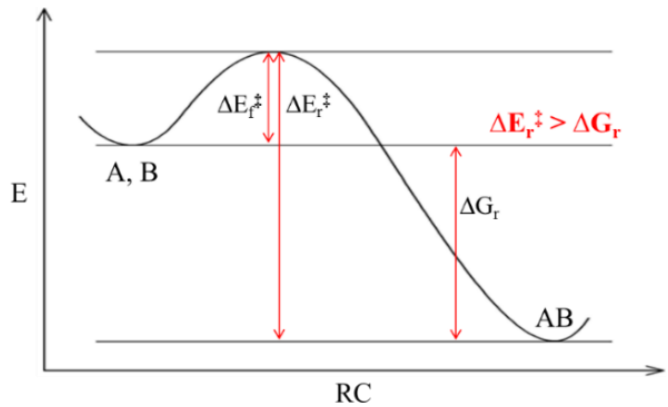

Figure 2–2. A typical energy diagram for a binding between A and B. RC = reaction coordinate, E = energy, G = Gibbs free energy, E = activation energy.

However, we must not ignore the very basic assumption that the association and dissociation reactions are elementary reactions. If they are not elementary reaction, the relation between kinetic and thermodynamic parameters changes dramatically. The representative is a molecular capsule **49** developed by Rebek and his colleagues.[102] They found that the guest exchange rate of inclusion complex in **49** dimer showed saturation kinetic behavior against the concentration of second guest molecule. Since we have seen that the exchange rate should be linear to the guest concentration (recall Eq. 2–11) when the association and dissociation reactions are elementary, the **49** dimer must follow another mechanism for guest exchange reaction. For the mechanism, they suggested that it proceeds through the formation

of solvent inclusion complex as an intermediate, which is the rate determining step (Figure 2–3).

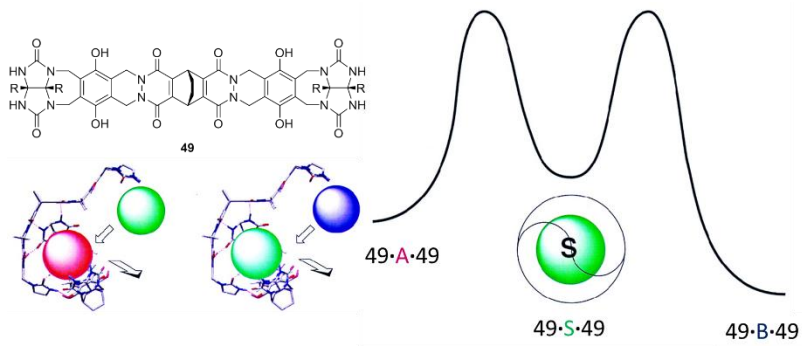

Figure 2–3. A proposed guest exchange mechanism of **49**·A·**49** to **49**·B·**49** through **49**·S·**49**. A, B, and S represents two possible guests and solvent molecules, respectively. Reprinted by permission from reference 102. Copyright 1999 National Academy of Sciences.

2. Estimation of an association constant

2.1. Isothermal titration calorimetry

ITC is the most important and widely used techniques because it can directly measure the enthalpy of association, including biological recognition process as well as molecular recognition in artificial systems.[103,104] The simultaneous determination of association constant and enthalpy of association gives detailed information about the association, such as Gibbs free energy, enthalpy, entropy, and heat capacity changes.

Figure 2–4 shows a typical instrumentation for isothermal titration calorimetry. Both cells of sample and reference are individually injected titrant sequentially

during which time a thermostat measures the heat flow for maintaining the internal temperature of both cells.

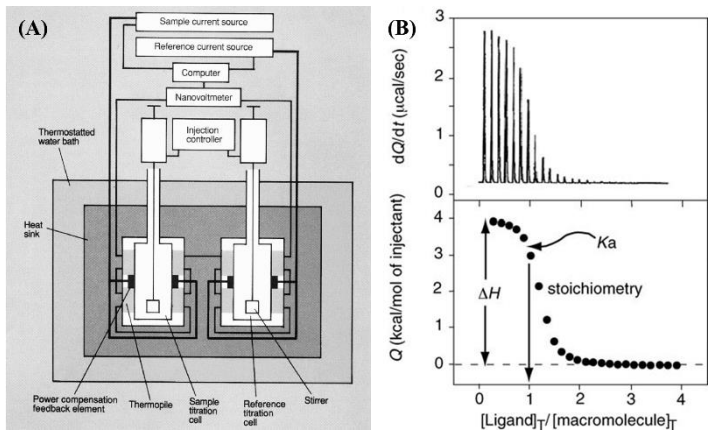

Figure 2–4. (A) Basic instrumental structure for ITC experiment. (B) A result of typical ITC experiment. Reprinted by permission from reference 103 and 104. Copyright 1990 American Chemical Society. Copyright 2001 John Wiley & Sons Inc.

2.2. Photophysical studies

Photophysical studies are of great interest because of its rapid response, high sensitivity and high accessibility. A visualization of the binding event is also highly desirable because it is the most intuitive mean of representation. The linearity between concentration and the photophysical activity (especially for absorbance) enables precise estimation of the concentration of chemical species. In addition, it is possible to monitor photophysical behaviors of various photophysically active chemical species simultaneously (recall Beer-Lambert law). However, observable molecules must be a photophysically active and embedding a suitable photophysical activity into a receptor is not always an easy task.

Photophysical studies are undoubtedly the most powerful tool for analyzing 1:1 binding event. Figure 2–5 shows a photophysical activity of a probe **50** in the presence of Zn(II) ion.[105] Probe **50** can accommodate single zinc ion in its binding site composed of DPA and salicylimine-type chelator and the presence of multiple isosbestic points strongly suggest 1:1 binding stoichiometry.

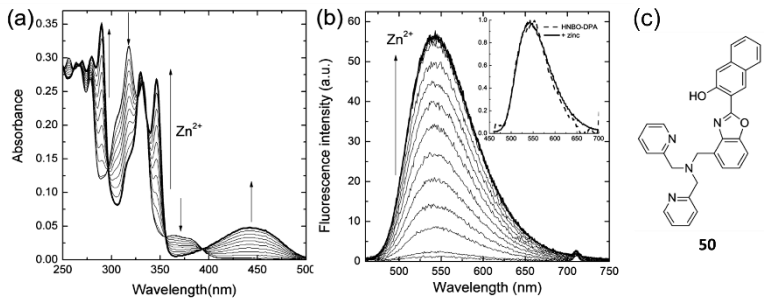

Figure 2–5. (a) UV–Vis and (b) photoluminescence spectra of **49** in the presence of increasing concentration of Zn(II) ion. (c) Chemical structure of **49**. Reprinted by permission from reference 105. Copyright 2012 American Chemical Society.

2.2.1. 1:1 binding

Let us consider a binding event between a host and a guest, namely H and G satisfying Eq. 2–12. Then, we can obtain two mass balance equations, Eq. 2–13 and Eq. 2–14.

$$\mathrm{H} + \mathrm{G} \overset{K_\mathrm{a}}{\rightleftarrows} \mathrm{HG} : K_\mathrm{a} = \frac{[\mathrm{HG}]}{[\mathrm{H}][\mathrm{G}]} \qquad \text{(Eq. 2–12)}$$

$$\mathrm{H}_0 = [\mathrm{H}] + [\mathrm{HG}] \qquad \text{(Eq. 2–13)}$$

$$\mathrm{G}_0 = [\mathrm{G}] + [\mathrm{HG}] \qquad \text{(Eq. 2–14)}$$

Multiplying of Eq. 2–13 and Eq. 2–14 then simplifying the equation about [HG] results in Eq. 2–15. Substitution of [H]+[G] and [H][G] using Eqs. From 2–12~14 results in Eq. 2–16, which is a quadratic function for [HG]. Choosing appropriate solution about [HG] gives Eq. 2–17, and accordingly are determined [H] and [G]. Eq. 2–17 helps us to predict the concentration of H, G, and HG by the total concentration of host and guest according to association constant. If HG and G absorb light, a solution of H and G follows Eq. 2–18 (Beer-Lambert Law). Therefore, we can determine the association constant from nonlinear fitting the titration experiment result by Eq. 2–19.

$$[\mathrm{HG}]^2 + ([\mathrm{H}] + [\mathrm{G}])[\mathrm{HG}] + [\mathrm{H}][\mathrm{G}] - \mathrm{H}_0\mathrm{G}_0 = 0 \qquad \text{(Eq. 2–15)}$$

$$[\mathrm{HG}]^2 - (\mathrm{H}_0 + \mathrm{G}_0 + K_\mathrm{a})[\mathrm{HG}] + \mathrm{H}_0\mathrm{G}_0 = 0 \qquad \text{(Eq. 2–16)}$$

$$[\mathrm{HG}] = \frac{\mathrm{H}_0 + \mathrm{G}_0 + K_\mathrm{a} - \sqrt{(\mathrm{H}_0 + \mathrm{G}_0 + K_\mathrm{a})^2 - 4\mathrm{H}_0\mathrm{G}_0}}{2} \qquad \text{(Eq. 2–17)}$$

$$\mathrm{A}_\mathrm{tot} = \varepsilon_\mathrm{HG}[\mathrm{HG}] + \varepsilon_\mathrm{G}[\mathrm{G}] \qquad \text{(Eq. 2–18)}$$

$$\mathrm{A} = \varepsilon_\mathrm{G}\mathrm{G}_0 + (\varepsilon_\mathrm{HG} - \varepsilon_\mathrm{G})[\mathrm{HG}] \qquad \text{(Eq. 2–19)}$$

There is another very famous equation for determining K_a value, which called Benesi-Hildebrand method. Eq. 2–20 shows the equation. However, we must keep in mind the assumption that a guest is present in large excess compared to host so that the change in concentration of a guest is negligible.

$$\frac{1}{\Delta\mathrm{A}} = \frac{\mathrm{c}}{K_\mathrm{a}}\mathrm{G}_0 + \mathrm{c} \qquad \text{(Eq. 2–20)}$$

2.2.2. 1:1:1 competition

Consider a competitive binding event among a host (H), a guest (G) and an indicator (I) that satisfies Eq. 2–21 and 2–22. Then, we obtain three mass balance equations, Eq. 2–23, 2–24 and 2–25, analogously to the previous.

$$\mathrm{H} + \mathrm{G} \overset{K_\mathrm{G}}{\rightleftarrows} \mathrm{HG} : K_\mathrm{G} = \frac{[\mathrm{HG}]}{[\mathrm{H}][\mathrm{G}]} \qquad \text{(Eq. 2–21)}$$

$$\mathrm{H} + \mathrm{I} \overset{K_\mathrm{I}}{\rightleftarrows} \mathrm{HI} : K_\mathrm{I} = \frac{[\mathrm{HI}]}{[\mathrm{H}][\mathrm{I}]} \qquad \text{(Eq. 2–22)}$$

$$\mathrm{H}_0 = [\mathrm{H}] + [\mathrm{HG}] + [\mathrm{HI}] \qquad \text{(Eq. 2–23)}$$

$$\mathrm{G}_0 = [\mathrm{G}] + [\mathrm{HG}] \qquad \text{(Eq. 2–24)}$$

$$\mathrm{I}_0 = [\mathrm{I}] + [\mathrm{HI}] \qquad \text{(Eq. 2–25)}$$

A new parameter K, the ratio of K_G over K_I, is defined by Eq. 2–26. If we assume that either guest or indicator is present in large enough amount so that [H] is close to zero, then we can replace of [G], [I] and [HI] in terms of [HG] resulting in Eq. 2–27. Choosing an appropriate solution for Eq. 2–27 gives a complicated equation, Eq. 2–28. Given the total concentration of host, guest, and indicator, we can calculate [HG] using Eq. 2–28, and [G], [I] and [HI] are determined accordingly. Therefore, we can determine K_G by fitting a titration result of an experiment that utilizes displacement of an indicator.

$$K = \frac{K_\mathrm{G}}{K_\mathrm{I}} = \frac{[\mathrm{HG}][\mathrm{I}]}{[\mathrm{G}][\mathrm{HI}]} \qquad \text{(Eq. 2–26)}$$

$$K = \frac{[\mathrm{HG}]\,(\mathrm{I}_0 - \mathrm{H}_0 + [\mathrm{HG}])}{(\mathrm{G}_0 - [\mathrm{HG}])\,(\mathrm{H}_0 - [\mathrm{HG}])} \qquad \text{(Eq. 2–27)}$$

$$[\mathrm{HG}] = \frac{\mathrm{b} - \sqrt{\mathrm{b}^2 - 4(K-1)\,K \cdot \mathrm{H}_0 \cdot \mathrm{G}_0}}{2(K-1)} \qquad \text{(Eq. 2–28)}$$

$$\text{where, } \mathrm{b} = (K-1) \cdot \mathrm{H}_0 + K \cdot \mathrm{G}_0 + \mathrm{I}_0$$

It is worth noting that a fitting should be performed *near the saturation point* because assumed is that the concentration of free host is close to zero.

2.3. Nuclear magnetic resonance

NMR is an unrivaled technique in providing structural information of a host–guest complex. For instance, it gives an evidence of which functional groups participate in the binding event, especially when the hydrogen bonding is the main driving force of complexation. Moreover, it can elucidate intermolecular contacts between a host and a guest by using special techniques called nuclear Overhouser effect spectroscopy (NOESY) or rotational frame nuclear Overhauser effect spectroscopy (ROESY).

Since the NMR signal appears at a weighted average of possible chemical species within NMR time scale (~ 1s), therefore we often can observe a gradual change of the NMR signal during titration experiments. Figure 2–6 shows a typical example of NMR signal change upon sequential addition of guest.[106] Fitting of a change in chemical shift (Δδ) by using Eq. 2–29 can determine binding affinity. However, a binding affinity greater than 10^6 M^{-1} could not be determined precisely, because it requires millimolar concentration for clear NMR spectra.

$$\Delta\delta = \frac{\Delta\delta_{\mathrm{tot}} K_{\mathrm{a}}[\mathrm{G}]}{1 + K_{\mathrm{a}}[\mathrm{G}]} \qquad \text{(Eq. 2–29)}$$

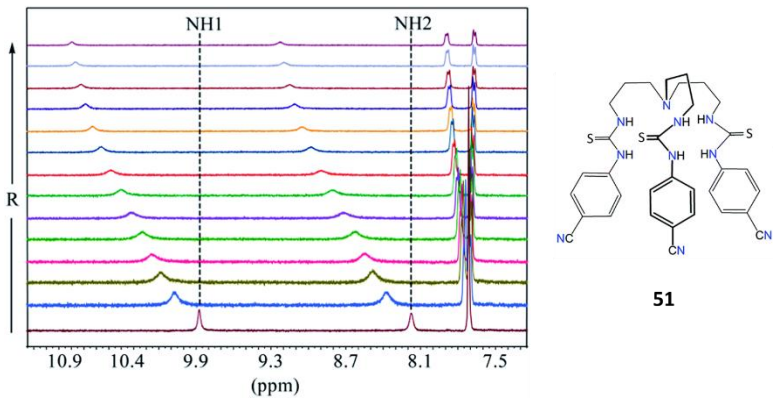

Figure 2–6. A partial ^{1}H NMR spectra of **51** in the presence of the increasing amount of sulfate (SO_4^{2-}) anion (from bottom to top, 0 equiv. to 10 equiv.). Reprinted by permission from reference 106. Copyright 2015 The Royal Society of Chemistry.

3. Selectivity issue for PPi against nucleotides

Monitoring an enzymatic reaction that produces PPi as a necessary byproduct often requires a high concentration of nucleotides (ATP for many cases) for ensuring maximum velocity. Therefore, a molecular probe that can specifically respond to a small amount of PPi is highly desirable but, to our best knowledge, such molecular receptor or probe has not yet been reported. Therefore, we established two conditions to be held by a suitable molecular probe for monitoring such enzymatic reactions in consideration of selectivity. The conditions of are: (1) it has a moderate association constant to ATP so that it mostly binds to ATP; (2) it has large enough association constant to PPi so that the addition of PPi quantitatively displaces ATP.

Table 2–1 predicts a complexation behavior at a given association constant and concentrations of PPi while other parameters are assumed to be: K_a(ATP) = 10^5 M^{-1}, [probe] = 5 μM and $[ATP]_{total}$ = 1 mM. A host having 4-order of magnitude

difference in association constant is capable of almost complete detection of added PPi (> 95%), while 3-order magnitude difference resulted in ~80% detection. Therefore, more than 3-order of magnitude difference in association constant is highly desirable.

Table 2–1. A theoretical mole fraction of probe–PPi complex ([probe–PPi]/$[PPi]_{total}$) according to various different $K_{a,PPi}$ and total PPi concentration. $K_{a,ATP} = 10^5\ M^{-1}$, [probe] = 5 μM, and $[ATP]_{total}$ = 1 mM are assumed.

	$K_{a,PPi}$ (M^{-1})		
$[PPi]_{total}$	10^7	10^8	10^9
1 μM	0.318	0.807	0.976
2 μM	0.304	0.775	0.970
3 μM	0.291	0.737	0.957

Section 2. Pyrophosphate Recognition of Extended bis(Zn-DPA) Derivatives

A part of this section was published in *Journal of Organic Chemistry*.[107]

1. Introduction

In 2007, Hong and colleagues developed the strongest artificial PPi receptor **52** having bis((6-acetamidopyridin-2-yl)methyl)amine (bapa) group instead of DPA.[108] It showed extremely high association constant toward PPi as high as 5.3×10^{10} M^{-1} by the combination of ion-ion interaction and hydrogen bonding (Figure 2–7). However, we recently observed that **52** exhibits very slow exchange kinetics, which is a critical problem for real-time monitoring. For instance, an exchange reaction from **52**-PV (pyrocatechol violet, $K_a \sim 6.0 \times 10^7$ M^{-1}) to **52**-PPi required more than 6 hours to completion, while probe **10** took only a few seconds to completion.

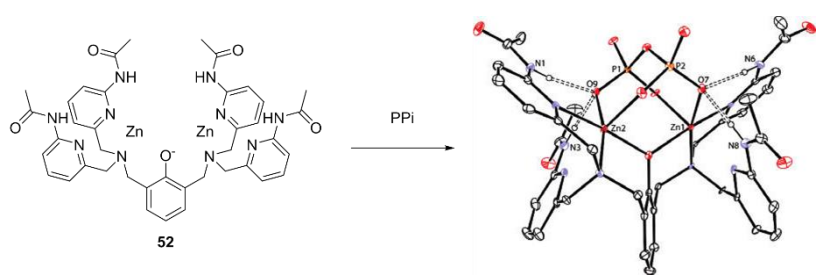

Figure 2–7. The molecular structure of **52** and its crystal structure with the presence of PPi ion.

Reprinted by permission from reference 108. Copyright 2007 American Chemical Society.

From the thermodynamic point of view, the difference in association free energy between **10**-PV (9.4 kcal mol^{-1}) and **52**-PV (10.6 kcal mol^{-1}) is only 1.2 kcal mol^{-1}, which is insufficient to reduce the rate of exchange more than 10-fold at an ambient temperature. Considering the molecular structure of **10** and **52**, there is no doubt that the presence of four acetamides retards guest exchange reactions. Figure 2–8 describes energy-minimized structures of the complexes of **52**, **53** and **54** with PPi. The space-filling models clearly show that the acetamide groups cover the captured pyrophosphate from the environment. Particularly, **52** forms almost complete inclusion complex, which structure prohibits the escape of PPi from the host molecule. In detail, the guest exchange reaction of **52** requires the simultaneous breakdown of at least two hydrogen bonds that are cooperatively involved with ion-ion interactions between Zn(II) ions and anionic oxygens of guests, creating extremely high energy of activation of the guest exchange. The situation encountered by **52** is very similar to aforementioned Rebek's molecular capsule **49**,[102] and we expected that reducing the number of hydrogen bond donor groups would enable rapid guest exchange reaction.

Appending a large substituent to a receptor is a well-known strategy to confer selectivity via steric interactions.[109] As shown in studies by Jolliffe[110] this strategy is perhaps best in discriminating PPi from the strongest competitors, nucleotide triphosphates (NTPs), because NTPs contain a large nucleotide monophosphate group. In that regard, we envisioned that the structure of hydrogen bond donor groups affect the PPi-binding strength and selectivity toward PPi against other competitors.

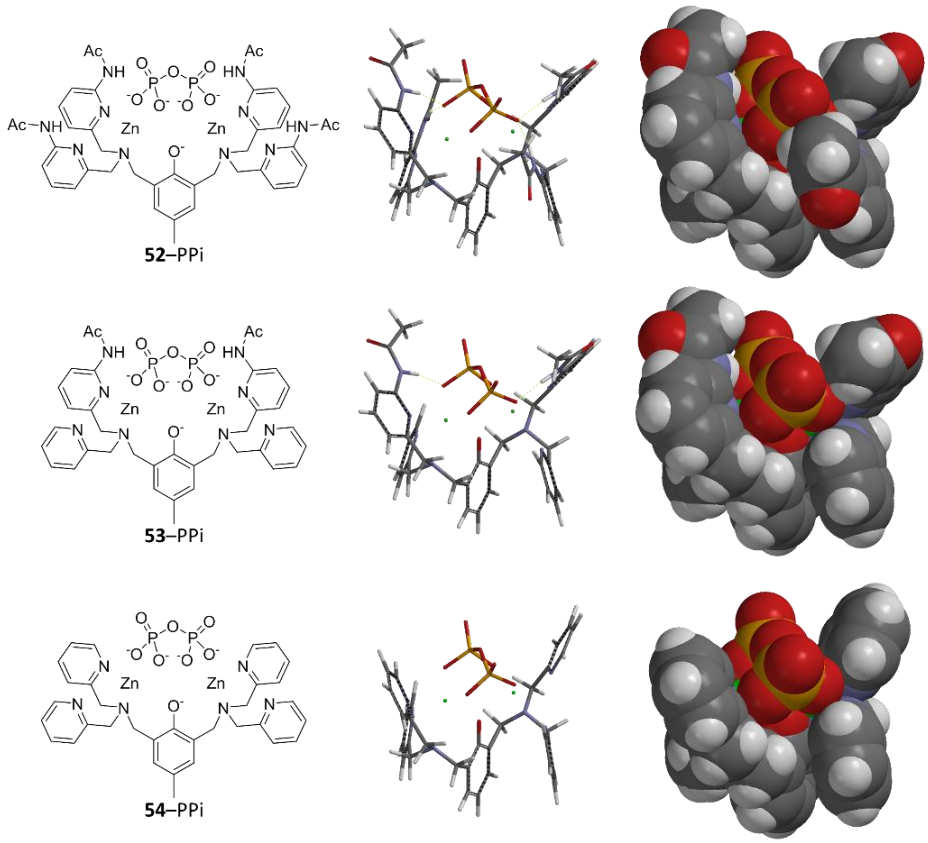

Figure 2–8. Energy-minimized structures of **52** (top), **53** (middle), and **54** (bottom) complexes with PPi. Left, molecular structure; middle, stick model; right, space-filling model. Methyl groups were omitted in molecular modeling.

2. Result and discussion

We first synthesized three molecular receptors **52**, **53**, and **54** by varying number of acetamides (Figure 2–8) and qualitatively examined the exchange kinetics of them. The color of PV was changed from yellow to blue instantaneously by the addition of

the receptors, which indicates the rates of associations are more or less the same. However, we observed a large difference in the successive addition of PPi. The color of PV was restored in a few seconds, 2 minutes, and more than 6 hours for **54**, **53**, and **52**, respectively. Therefore, there is not likely to be a linear relationship between the activation energy and the number of acetamide groups. Moreover, since the association reaction occurs very fast, the rate-determining step for guest exchange reaction is the dissociation of preexisting host–guest complex.

Since the presence of two acetamide groups did not significantly retard the rate of exchange, we decided to investigate how the structure of substituent affects the selectivity of PPi over ATP based on the structure of **53**. We prepared a series of receptors **55-59** (Scheme 2–1), which includes alkyl amides (**53** and **55**), aryl amides (**56** and **57**), and carbamates (**58** and **59**).

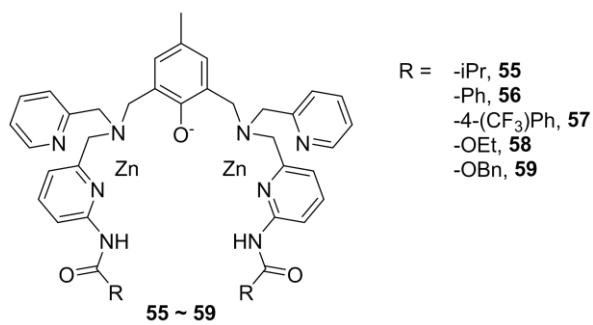

Scheme 2–1. The molecular structure of **55-59**.

We estimated affinity of the receptors toward PPi and ATP by means of the fluorescent competitive assay with **10** in a similar way of the previous report,[108] and Table 2–2 summarizes the result. In the fluorescence titration experiments, there are several noticeable observations. First, selectivities (K_a(PPi)/K_a(ATP)) of new receptors

were improved by a factor of 1.5 to 25 in comparison with **10**. Second, sterically demanding receptors (**55**, **56**, **57** and **59**) showed similar apparent association constants as that of **10**. In particular, the association constants of **53**-PPi and **58**-PPi were selectively improved, indicating that imposing steric hindrance into a receptor molecule controlled the selectivity toward PPi. Third, in case of **53**, **58**, and **59** having small substituents in close proximity to the binding pocket (carbonyl beta, hydrogen or one methylene), the fluorescence intensity changes were better fitted to the twofold concentration of the receptors, which may an involvement of different binding stoichiometry other than 1:1.

Table 2–2. Apparent association constants (log K_a, at 25°C) and their comparison (error ± 15%) according to fluorescence competition assay with **10**.

Host	PPi	ATP	$K_{a,PPi}/K_{a,ATP}$
10	8.46	7.23	17.1
52[108]	10.7	–	–
53	9.52 (8.69[a])	7.41	129 (19.1[a])
55	8.49	7.02	29.7
56	8.40	6.97	27.1
57	8.48	7.10	24.0
58	9.49 (8.78[a])	6.86	427 (83.2[a])
59	8.31 (7.78[a])	–	–

[a]Obtained by fitting the fluorescence intensity against twofold concentration of receptors.

An extraordinary selectivity of **58** led us to synthesize and evaluate additional receptors **60** and **61**, which had 2-methoyacetyl and (2-(2-(2-methoxy)-ethoxy)-

ethoxy)acetyl instead of an ethoxycarbonyl moiety, respectively (Scheme 2–2). Because it was recently suggested that photoexcited chemical species populated during photophysical experiments could provoke an overestimation of association constants, which was often pronounced in photoluminescence experiments,[111-113] we conducted UV-Vis competitive assays with PV for selected receptors (**10**, **52**, **53**, **55**, **58**, **60** and **61**) to determine association constants more precisely. As representatively depicted in Figure 2–9, we observed spectral changes during titration experiments that are suitable for determining association constants. Table 2–3 shows the affinities of the selected receptors toward PV, PPi, and ATP.

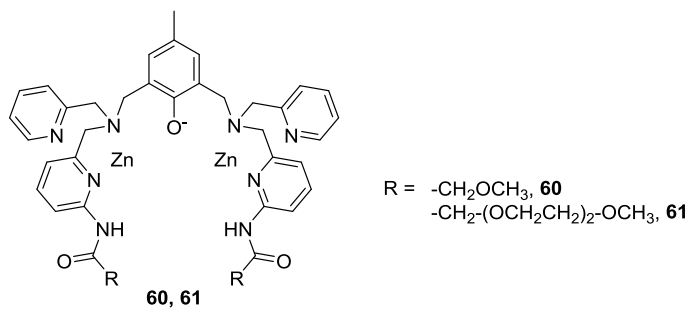

Scheme 2–2. Molecular structure of **60** and **61**.

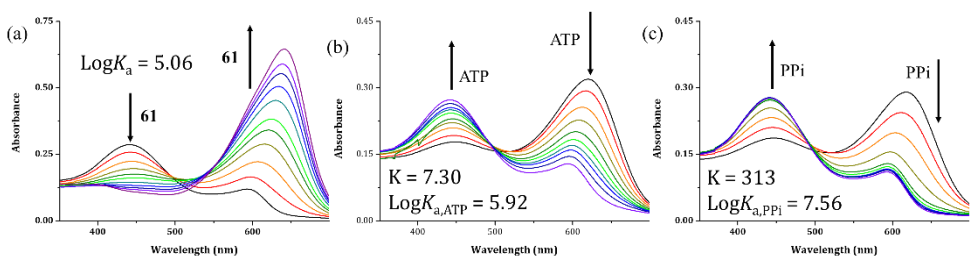

Figure 2–9. Spectral changes of (a) PV (20 μM) during titration with (a) **61** (0 ~ 180 μM), PV (20 μM) and **61**(30 μM) during titration with (b) ATP (0 ~ 80 μM) and (c) PPi (0 ~ 80 μM).

Table 2–3. Apparent association constants (LogK_a, column 2, 3, 4) and the selectivity factor (PPi/ATP, $K_{a,receptor–PPi}/K_{a,receptor–ATP}$) determined by UV-vis competitive assay.

Receptor	PV	PPi	ATP	PPi/ATP
10	6.90	8.47	7.44	10.7
52	7.78	8.76	7.83	8.46
53	5.23	7.17	5.85	20.9
55	5.30	7.17	6.26	8.12
58	5.38	7.18	6.05	13.7
60	5.53	8.04	6.47	37.1
61	5.06	7.56	5.92	42.8

Although the trend of association constant obtained by IDA experiments was not fully coincide with that obtained from fluorescence titration experiment, we could find several facts that are expected to help with designing a PPi-selective receptor. First, the receptors except **52** exhibited weaker binding to anions compared to **10**. Second, **60** showed the strongest binding to PPi, and **53** showed the weakest binding to ATP. Third, **60** and **61** having α-alkoxyacetyl substituents showed higher affinity toward PPi in comparison to other receptors. Fourth, **60** exhibited greater association constants compared to **58** regardless of the guest anion, and the PPi selectivity over ATP of **60** was approximately three times better than that of **58** with a similar structure. Because **58** and **60** were almost identical in terms of steric hindrance and hydrogen bond donating ability, stronger binding of **60** to anions could be rationalized by their preferential orientation of electron lone pairs on the sp^3-hybridized oxygen atoms, as in the selective molecular recognition of 8-

oxoguanosine by 8-oxoG-clamp,[13]. In detail, the oxygen lone electron pairs of **58** are inevitably directed toward the binding pocket, making the binding of anion less favorable, while those of **60** are preferentially oriented in the opposite direction without creating unfavorable interactions with guest anions (Figure 2–10). Finally, **61** showed the best selectivity toward PPi against ATP among the tested receptors (K = 42.8). These results suggest that steric effects is a primary factor in controlling the selectivity, and the acidity of hydrogen bond donors have only a minor effect.

Figure 2–10. Molecular modeling of a host having ethyl carbamate and 2-methoxyacetamide in each side with a bound PPi anion.

Because steric interactions play an important role in determining the selectivity, we wondered about the outcome if steric hindrance was maximized via macrocyclization. Therefore, **62**, a macrocyclic analogue of **61** was synthesized, and its association constants were evaluated by UV-vis competitive assay with PV. **62** showed the best selectivity toward PPi against ATP, by a factor of 130, which enabled us to detect 0.97 μM of PPi in the presence of 80 μM of ATP (Figure 2–11). However, the apparent association constants were disappointing (log $K_{a,PV}$ = 4.81, log $K_{a,PPi}$ = 5.98, and log $K_{a,ATP}$ = 3.86). In fact, inclusion of an anion within the

cavity of a crown ether-type receptor would be unfavorable due to the repulsive interactions between negative charges of a guest anion and ethereal oxygens of a receptor.[114] In that regard, the weakened binding strength is presumably attributed to the unavoidable repulsive interactions between the tetraethylene glycol ether tether and anionic guests forced by the macrocyclic structure, manifesting the principle of complementarity.[115]

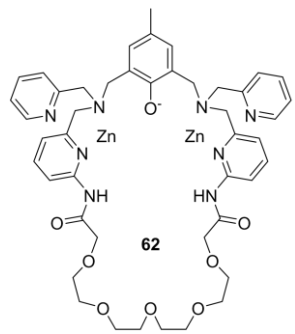

Scheme 2–3. The molecular structure of **62**.

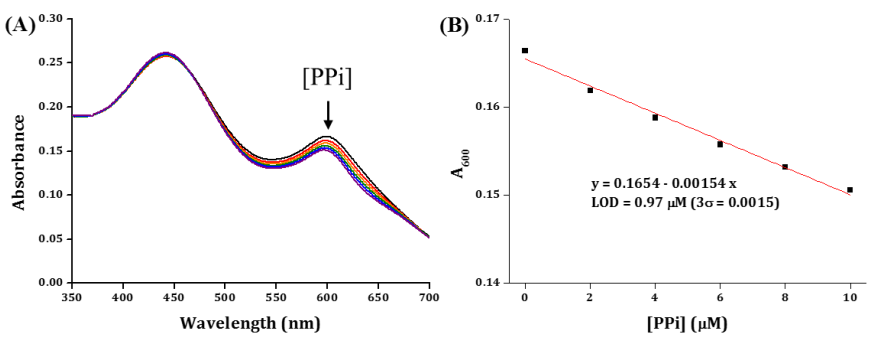

Figure 2–11. UV-Vis spectral changes of a mixture of PV (25 μM), **62** (15 μM), and ATP (80 μM) upon the addition of increasing concentrations of PPi and (B) linear relationship between absorbance at 600 nm and added PPi concentrations.

To gain deeper insight into the binding behavior of PPi receptors, we conducted isothermal titration calorimetry (ITC) experiments with **10**, **53**, **61**, and **62** and the results are summarized in Table 2–4. Considering that the additional hydrogen bond donor groups would significantly stabilize the anion-bound state, it seems reasonable to expect the larger heat released ($-\Delta H$) for the receptors with more hydrogen bond donors. However, receptors **53**, **61**, and **62** having two amide NHs released less heat compared to **10** having no amide NHs. For instance, the binding between **53** and ATP was almost an enthalpy-neutral process. We expected that the heat released ($-\Delta H$) during the binding process of the receptors having two amide groups would be in the order of **53** > **61** > **62** considering the repulsive interactions between the negative charges of guest anions and ethereal oxygens of receptors. Contrary to our expectations, however, we observed an opposite trend in the enthalpy change (ΔH) of binding, which was identical (**53** > **61** > **62** > **10**) regardless of the guest. These results strongly suggest a systematic difference in the initial state of the receptors (i.e. prior to the anion binding) according to their molecular structures. In that regard, it is well-documented that a hydrogen bond donor near a Zn(II)-aqua complex would facilitate deprotonation to afford a hydroxo-Zn(II) complex at physiological conditions,[116] and that crown ether-type macrocycles as well as their acyclic analogues would effectively lower the acidity of Zn(II)-bound water by stabilizing Zn(II)-coordinated acids (water) through hydrogen bond networks.[117-119] Therefore, it was expected that the water molecules bound to each receptor would be partially deprotonated, and the degree of deprotonation would be in the order of **53** > **61** > **62** (> **10**), which was the same trend as observed for the overall enthalpy changes. Since the dissociation of hydroxide from Zn(II) ion requires a greater enthalpy loss than that of neutral water, we believe that an identical trend is not a coincidence. Indeed, the same trend for the acidity (pK_a) of Zn(II)-bound water (**61**

(6.71) > **62** (6.84) > **10** (6.93)) by potentiometric titration experiments (except **53**, pK_a = 6.96) was observed. In addition, a larger enthalpy gain during the complexation between **61** and PPi in more acidic media (ΔH = –107 ± 1.2 kJ mol^{-1} at pH 6.0 MES buffer and –14.9 ± 1.6 kJ mol^{-1} at pH 8.9 CHES buffer) also supports our hypothesis of the partial deprotonation of Zn(II)-bound water molecules at the initial state.

Table 2–4. Thermodynamic parameters of the binding between anion guests and selected receptors according to isothermal titration calorimetry experiments

Guest	Receptor	LogK_a	ΔG(kJ/mol^{-1})	ΔH(kJ/mol^{-1})	ΔS(kJ/mol^{-1}K^{-1})
PPi	**10**	6.8 ± 0.1	–38 ± 1	–63 ± 3	–85 ± 8
	53	7.2 ± 0.1	–41 ± 0	–18 ± 1	78 ± 4
	61	7.0 ± 0.2	–39 ± 1	–28 ± 0	–35 ± 5
	62	4.9 ± 0.1	–28 ± 1	–56 ± 3	–92 ± 4
ATP	**10**	5.2 ± 0.2	–29 ± 1	–26 ± 1	10 ± 1
	53	5.8 ± 0.1[a]	–33 ± 1[a]	0 ± 0	112 ± 2
	61	5.5 ± 0.1	–31 ± 1	–10 ± 0	72 ± 4
	62	4.7 ± 0.1	–27 ± 1	–16 ± 1	38 ± 4

[a]from UV-vis competitive titration experiments

However, as the enthalpy changes cannot be explained by the pK_a shift alone (e.g. mismatch of **53** and large enthalpy difference compared to the pK_a difference), there is a strong indication that the additional roles of substituents (hydrogen bond acceptors and donors) as desolvating agents might be involved. As Lewis basic

oligoethylene glycol ether oxygens can replace solvating water molecules, it can be expected that **62** is hardly solvated while **53** encounters heavy solvation in aqueous media.[120] Then, the dramatic changes in thermodynamic parameters of **53** and **62** can be justified in part by well-known observations that binding between heavily solvated host and guest is often entropy-driven.[121]

3. Conclusion

The time required for the guest exchange reaction was shortened from more than 6 h to less than 15 min by controlling the number of hydrogen bond donor groups on the bis(Zn(II)-bapa) moiety of the receptors. In addition, a 12-fold increase in PPi selectivity was achieved by introducing a macrocyclic structure. This study revealed the effects of a hydrogen bond donating substituent at the 6-position of DPA on the guest selectivity (and sensitivity). The receptor composition, steric hindrance, and acidity in conjunction influence the thermodynamics and kinetics of the molecular recognition processes. The changes in thermodynamic parameters were rationalized in terms of the steric effect, hydrogen bond donating and accepting abilities, stereoelectronic effect, acidity of the zinc(II)-bound water molecules, and degree of desolvation according to the chemical nature of the receptors. It was also verified that imposing proper steric hindrance could be the most promising method for developing a highly selective receptor for PPi over NTPs.

4. Experimental section

4.1. General information

All chemicals were purchased from either Sigma-Aldrich or Tokyo Chemical Industry (TCI) and were used as received. Thin layer chromatography was performed over Merck silica gel 60 F254 on aluminum foil. Silicycle 60 was used for the stationary phase in chromatographic separation or silica pad filtration. Celite® 545 was used for celite filtration. All ^{1}H and ^{13}C NMR spectra were obtained from Bruker DRX 300 NMR spectrometer. Absorption and emission spectra were recorded on a V–730 spectrophotometer (JASCO) and FP-8300 spectrophotometer (JASCO), respectively. LRMS were taken by MALDI-TOF mass analyzer (Bruker instrument). Gas chromatography-high resolution tandem mass spectrometry data were taken by 6890 Series (Agilent, USA, GC) and JMS-700 (JEOL, Japan, double-focusing mass analyzer, FAB-positive mode). Molecular geometry optimizations were carried out using Spartan 08 software (Wavefunction Inc.) at AM1 semi-empirical level. The initial geometries were deduced from the previously reported crystal structures. Raw data were graphed and fitted with Origin 8 program (OriginLab Corp.).

4.2. Synthesis of the receptors

Dichloromethane and tetrahydrofuran were distilled over calcium hydride and sodium/benzophenone ketyl, respectively. NMR samples were prepared by dissolving in DMSO-d_6, $CDCl_3$ or acetone-d_6. Multiplicities: s, singlet; d, doublet; t, triplet; m, multiplet; br, broad. It should be noted that some chemical compounds showed complicated NMR spectra due to restricted rotations.

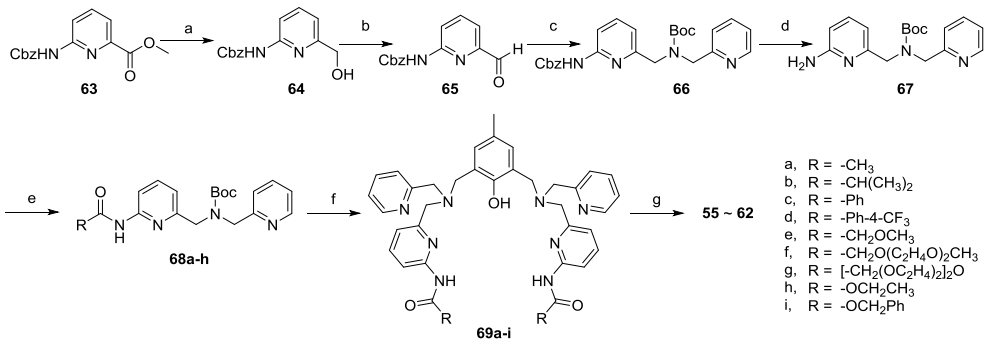

Scheme 2–4. Synthesis of the receptors. a, $NaBH_4$, EtOH; b, DMSO, $(COCl)_2$, DCM, then Et_3N; c, 2-picolyl amine, $NaBH(OAc)_3$, DCE, then Boc_2O; d, cat. $Pd(OAc)_2$, cat. Et_3N, Et_3SiH, DCM, then $NaHCO_{3\,(aq)}$; e, acyl chlorides or chloroformates, Et_3N, DCM; f, TFA, DCM, then 2-hydroxy-5-methylisophthaladehyde, $NaBH(OAc)_3$, DCE; g, $Zn(ClO_4)_2 \cdot 6H_2O$, acetonitrile.

Synthesis of **64**: **63**[122] (11.6 g, 40.5 mmol) in 125 mL of absolute ethanol was added sodium borohydride (2.3g, 60.8 mmol, 1.5 equiv.) at 0 °C. The reaction mixture was stirred for 4 hours during which time the suspension became a clear solution. Most of the ethanol was removed under reduced pressure, and the residue was diluted with water. The aqueous layer was extracted by ethyl ether three times, and the combined ethereal layer was dried over anhydrous $MgSO_4$ and filtered through a 3-cm pad of silicate. Volatiles were removed under reduced pressure to give analytically pure **64** (9.15 g, 87% yield). ^{1}H NMR (300 MHz, $CDCl_3$) δ 8.67 (s, 1H), 7.84 (d, *J* = 8.3 Hz, 1H), 7.55 (t, *J* = 7.9 Hz, 1H), 7.32 (s, 5H), 6.92 (d, *J* = 7.4 Hz, 1H), 5.16 (s, 2H), 4.58 (s, 3H). ^{13}C NMR (75 MHz, $CDCl_3$) δ 158.4, 153.2, 151.1, 139.1, 135.8, 128.6, 128.3, 128.2, 115.7, 111.0, 67.1, 64.2. HRMS (FAB) m/z: $[M+H]^+$ Calcd for $C_{14}H_{15}N_2O_3$ 259.1077; Found 259.1086.

Synthesis of **65**: To a solution of dimethyl sulfoxide (3.79 mL, 53.1 mmol, 1.5 equiv.) in anhydrous dichloromethane (80 mL) was added oxalyl chloride (3.64 mL, 42.5 mmol, 1.2 equiv.) dropwisely at –78 °C and the mixture was stirred for 10

minutes. To the solution was transferred **64** (9.13g, 35.4 mmol, 1.0 equiv.) dissolved in a minimal amount of THF and stirred for 30 minutes, during which time white precipitates were formed. Triethylamine (12.3 mL, 88.5 mmol, 2.5 equiv.) was added and further stirred for 1h. The reaction was quenched by adding 250 mL of water and diluted with 200 mL of ethyl ether. The organic layer was washed with water three times, dried over anhydrous $MgSO_4$, filtered, and concentrated under reduced pressure. The residue was chromatographed over silica gel by a gradient elution of ethyl ether in hexanes (40 to 60%) to give analytically pure **65** (5.5g, 61%). ^{1}H NMR (300 MHz, $CDCl_3$) δ 9.91 (s, 1H), 8.27 (d, *J* = 8.3 Hz, 1H), 8.04 (s, 1H), 7.88 (t, *J* = 7.9 Hz, 1H), 7.65 (d, *J* = 7.4 Hz, 1H), 7.39 (s, 5H), 5.24 (s, 2H). ^{13}C NMR (75 MHz, $CDCl_3$) δ 192.4, 153.0, 152.0, 150.9, 139.4, 135.5, 128.7, 128.6, 128.3, 117.5, 117.0, 67.5. HRMS (FAB) m/z: $[M+H]^+$ Calcd for $C_{14}H_{13}N_2O_3$ 257.0921; Found 257.0924.

Synthesis of **66**: To a solution of **65** (5.6 g, 21.9 mmol, 1.0 equiv.) and 2-(aminomethyl)pyridine (2.37 mL, 23 mmol, 1.05 equiv.) in 120 mL of anhydrous 1,2-dichloroethane was added sodium triacetoxyborohydride (6.0 g, 28.5 mmol, 1.3 equiv.) portionwisely. The suspension was stirred overnight before most of the solvent was vaporized under reduced pressure. Excessive hydrides are destroyed by addition of 10 mL of 1 M HCl solution. The solution was neutralized by addition of saturated $NaHCO_3$ solution and extracted by dichloromethane three times. Combined organic layers were dried over anhydrous Na_2SO_4, filtered and concentrated under reduced pressure. The residue was re-dissolved in 80 mL of acetonitrile and treated by di-tert-butyl dicarbonate (5.3 g, 24.3 mmol, 1.11 equiv.) in 10 mL of acetonitrile. The reaction mixture was stirred for 2 hours before being concentrated under reduced pressure, and resulting residue was dissolved in diethyl ether. The ethereal layer was washed with water three times, dried over anhydrous

MgSO4, filtered and evaporated. The crude product was purified by silica gel column chromatography with elution of ethyl acetate in dichloromethane (35 %) to obtain analytically pure **66** (8.51 g, 87 %). ^{1}H NMR (300 MHz, $CDCl_3$) δ 8.45 (d, *J* = 4.4 Hz, 1H), 8.31 (d, *J* = 29.0 Hz, 1H), 7.79 (d, *J* = 8.3 Hz, 1H), 7.54 (t, *J* = 7.8 Hz, 2H), 7.24 (d, *J* = 16.4 Hz, 5H), 7.14–7.00 (m, 1H), 6.85 (dd, *J* = 32.1, 7.3 Hz, 1H), 5.12 (s, 2H), 4.52 (t, *J* = 36.8 Hz, 4H), 1.36 (s, 9H). ^{13}C NMR (75 MHz, $CDCl_3$) δ 158.4, 158.1, 156.8, 156.4, 155.8, 153.1, 151.2, 149.2, 146.7, 138.8, 138.7, 136.6, 136.4, 136.0, 128.5, 128.2, 128.0, 122.1, 121.9, 121.7, 120.7, 116.5, 115.7, 110.7, 110.5, 85.0, 80.1, 66.8, 65.8, 60.3, 52.8, 52.5, 52.2, 51.9, 28.3, 27.3, 15.3. HRMS (FAB) m/z: $[M+H]^+$ Calcd for $C_{25}H_{29}N_4O_4$ 449.2183; Found 449.2186.

Synthesis of **67**: To a solution of **66** (8.5 g, 19.0 mmol, 1.0 equiv.), palladium(II) acetate (233 mg, 0.95 mmol, 5 mol-%), and triethylamine (0.40 mL, 15 mol-%) in dichloromethane (125 mL) was added triethylsilane (4.3 mL, 26.5 mmol, 1.4 equiv.) dropwisely. The mixture was heated to reflux for 16 hours before being quenched by adding 50 mL of saturated $NaHCO_3$ solution. The biphasic mixture was vigorously stirred for additional 4 hours. The aqueous layer was extracted by ethyl ether three times. The combined organic layer was dried over anhydrous Na_2SO_4, filtered through a 4-cm pad of Celite® and concentrated under reduced pressure. The crude product was purified by silica gel column chromatography with gradient elution of methanol in ethyl acetate (0 to 3 %) to obtain analytically pure **67** (3.8 g, 64 %). ^{1}H NMR (300 MHz, $CDCl_3$) δ 8.53 (d, *J* = 3.8 Hz, 1H), 7.65 (t, *J* = 7.6 Hz, 1H), 7.39 (t, *J* = 7.7 Hz, 1H), 7.32–7.10 (m, 2H), 6.59 (dd, *J* = 26.5, 6.6 Hz, 1H), 6.36 (d, *J* = 8.0 Hz, 1H), 4.55 (m, 6H), 1.43 (d, *J* = 8.1 Hz, 9H). ^{13}C NMR (75 MHz, $CDCl_3$) δ 158.7, 158.2, 158.1, 156.7, 156.3, 156.1, 156.0, 149.2, 138.3, 138.2, 136.6, 136.5, 122.0, 121.8, 121.5, 120.5, 111.4, 110.5,

107.0, 106.7, 80.1, 52.7, 52.4, 52.2, 28.3. HRMS (FAB) m/z: $[M+H]^+$ Calcd for $C_{17}H_{23}N_4O_2$ 315.1816; Found 315.1815.

General procedure for the syntheses of **68a-h**: To a stirred solution of **67** (314 mg, 1.0 mmol, 1.0 equiv.) in 8 mL of dichloromethane was treated by acyl halides (commercial or synthesized by carboxylic acid and oxalyl chloride, 1.2 mmol in 1 mL of dichloromethane, 1.2 equiv.) and triethylamine (0.28 mL, 2.0 mmol, 2.0 equiv.) successively. The mixture was stirred for 4 hours before being quenched by addition of water (10 mL). The aqueous layer was extracted by dichloromethane three times. The combined organic layer was dried over anhydrous Na_2SO_4, filtered, and concentrated under reduced pressure. The crude product was chromatographed over silica gel by eluting ethyl acetate to give analytically pure products.

68a: 312 mg (87 % yield). ^{1}H NMR (300 MHz, $CDCl_3$) δ 8.65 (d, *J* = 8.0 Hz, 1H), 8.42 (d, *J* = 4.0 Hz, 1H), 7.95 (d, *J* = 7.4 Hz, 1H), 7.54 (m, 6.8 Hz, 2H), 7.17 (dd, *J* = 30.2, 7.2 Hz, 1H), 7.09–7.00 (m, 1H), 6.87 (dd, *J* = 30.2, 7.2 Hz, 1H), 4.48 (t, *J* = 41.5 Hz, 4H), 2.08 (s, 3H), 1.32 (s, 9H). ^{13}C NMR (75 MHz, $CDCl_3$) δ 169.1, 158.3, 158.0, 156.5, 156.1, 155.8, 151.0, 149.1, 138.8, 138.7, 136.7, 136.5, 122.1, 122.0, 121.8, 120.8, 117.3, 116.5, 112.2, 112.0, 80.3, 52.6, 52.4, 52.1, 51.9, 28.2, 24.5. HRMS (FAB) m/z: $[M+H]^+$ Calcd for $C_{19}H_{25}N_4O_3$ 357.1921; Found 357.1928.

68b: 307 mg (80 % yield). ^{1}H NMR (300 MHz, $CDCl_3$) δ 8.42 (d, *J* = 4.1 Hz, 1H), 8.17 (d, *J* = 9.6 Hz, 1H), 8.00 (d, *J* = 8.2 Hz, 1H), 7.54 (m, 2H), 7.18 (dd, *J* = 33.6, 7.5 Hz, 1H), 7.06 (dd, *J* = 6.9, 5.5 Hz, 1H), 6.87 (dd, *J* = 32.7, 7.3 Hz, 1H), 4.42 (dd, *J* =41.7, 38.5 Hz, 4H), 2.48 (quint, *J* = 6.8 Hz, 1H), 1.33 (s, 9H), 1.13 (d, *J* = 6.9 Hz, 6H). ^{13}C NMR (75 MHz, $CDCl_3$) δ 175.7, 158.3, 158.0, 156.5, 156.2, 155.9, 155.8, 151.0, 149.1, 138.8, 138.7, 136.6, 136.5, 122.1, 121.9, 121.7, 120.7, 117.3,

116.4, 112.2, 111.9, 80.2, 52.7, 52.5, 52.1, 52.0, 36.4, 28.2, 19.4. HRMS m/z: (FAB) $[M+H]^+$ Calcd for $C_{21}H_{29}N_4O_3$ 385.2234; Found 385.2240.

68c: 303 mg (72 % yield). ^{1}H NMR (300 MHz, $CDCl_3$) δ 8.82 (d, *J* = 7.2 Hz, 1H), 8.45 (d, *J* = 4.3 Hz, 1H), 8.20 (d, *J* = 8.2 Hz, 1H), 7.87 (d, *J* = 7.4 Hz, 2H), 7.64 (t, *J* = 8.0 Hz, 1H), 7.58 (t, *J* = 7.8 Hz, 1H), 7.43 (dt, *J* = 23.5, 7.0 Hz, 3H), 7.21 (dd, *J* = 36.9, 7.5 Hz, 1H), 7.11–7.05 (m, 1H), 6.96 (dd, *J* = 33.8, 7.2 Hz, 1H), 4.53 (dd, *J* = 40.7, 34.5 Hz, 4H), 1.37 (s, 9H). ^{13}C NMR (75 MHz, $CDCl_3$) δ 165.7, 158.3, 158.0, 156.7, 156.4, 155.8, 151.1, 149.1, 139.0, 138.9, 136.7, 136.5, 134.2, 132.1, 128.7, 127.3, 122.2, 122.0, 121.9, 120.8, 117.9, 116.9, 112.5, 112.3, 80.3, 52.8, 52.6, 52.2, 52.0, 28.3. HRMS (FAB) m/z: $[M+H]^+$ Calcd for $C_{24}H_{27}N_4O_3$ 419.2078; Found 419.2083.

68d: 368 mg (76 % yield). ^{1}H NMR (300 MHz, $CDCl_3$) δ 9.06 (s, 1H), 8.48 (s, 1H), 8.18 (d, *J* = 8.1 Hz, 1H), 8.02 (d, *J* = 8.0 Hz, 2H), 7.68 (d, *J* = 7.1 Hz, 2H), 7.66–7.56 (m, 2H), 7.23 (dd, *J* = 35.7, 7.1 Hz, 1H), 7.16–7.09 (m, 1H), 7.01 (dd, *J* = 30.1, 7.1 Hz, 1H), 4.56 (dd, *J* = 42.8, 33.4 Hz, 4H), 1.39 (s, 9H). ^{13}C NMR (75 MHz, $CDCl_3$) δ 168.6, 164.5, 158.2, 158.0, 156.8, 156.5, 155.8, 150.8, 149.0, 139.2, 139.0, 137.5, 136.9, 136.7, 133.8, 133.4, 130.1, 127.9, 125.7, 125.6, 125.4, 122.3, 122.1, 122.0, 121.8, 120.9, 118.3, 117.4, 112.8, 112.5, 80.4, 52.7, 52.4, 52.0, 51.9, 28.3. LRMS (MALDI-TOF) m/z: $[M+H]^+$ Calcd for $C_{25}H_{26}F_3N_4O_3$ 487.2; Found 487.1.

68e: 292 mg (76 % yield). ^{1}H NMR (300 MHz, $CDCl_3$) δ 8.70 (s, 1H), 8.46 (d, *J* = 4.4 Hz, 1H), 8.04 (d, *J* = 8.2 Hz, 1H), 7.6 (m, 2H), 7.22 (dd, *J* = 32.9, 7.6 Hz, 1H), 7.10 (dd, *J* = 6.9, 5.3 Hz, 1H), 6.95 (dd, *J* = 35.4, 7.3 Hz, 1H), 4.54 (t, *J* = 34.6 Hz, 4H), 3.96 (s, 2H), 3.43 (s, 3H), 1.37 (s, 9H). ^{13}C NMR (75 MHz, $CDCl_3$) δ 168.1, 158.4, 158.0, 156.9, 156.5, 155.9, 150.0, 149.2, 138.9, 138.7, 136.6, 136.5, 122.1, 121.9, 121.8, 120.7, 117.9, 117.0, 112.2, 112.0, 80.3, 71.9, 59.2, 52.9, 52.7, 52.2,

52.1, 28.3. HRMS (FAB) m/z: $[M+H]^+$ Calcd for $C_{20}H_{27}N_4O_3$ 387.2027; Found 387.2028.

68f: 339 mg (71% yield). ^{1}H NMR (300 MHz, $CDCl_3$) δ 8.97 (s, 1H), 8.48 (d, *J* = 4.2 Hz, 1H), 8.07 (d, *J* = 8.2 Hz, 1H), 7.62 (m, 2H), 7.24 (m, 1H), 7.13 (m, 1H), 6.97 (dd, *J* = 34.9, 7.2 Hz, 1H), 4.56 (dd, *J* = 33.0, 26.6 Hz, 4H), 4.11 (s, 2H), 3.69 (m, 6H), 3.53 (m, 2H), 3.30 (s, 3H), 1.39 (s, 9H). ^{13}C NMR (75 MHz, $CDCl_3$) δ 168.6, 158.0, 156.9, 155.9, 150.2, 149.2, 138.7, 136.6, 122.1, 121.8, 120.7, 117.7, 116.8, 112.3, 112.1, 80.3, 71.9, 71.3, 70.8, 70.6, 70.3, 59.0, 52.8, 52.6, 52.3, 28.3. HRMS (FAB) m/z: $[M+H]^+$ Calcd for $C_{24}H_{35}N_4O_6$ 475.2551; Found 475.2558.

68g: 231 mg (51% yield). ^{1}H NMR (300 MHz, $CDCl_3$) δ 8.93 (d, *J* = 8.8 Hz, 2H), 8.42 (d, *J* = 4.1 Hz, 2H), 8.01 (d, *J* = 8.2 Hz, 2H), 7.57 (m, 4H), 7.18 (dd, *J* = 33.6, 7.8 Hz, 2H), 7.10–7.02 (m, 2H), 6.92 (dd, *J* = 34.1, 7.2 Hz, 2H), 4.50 (dd, *J* = 33.6, 26.9 Hz, 8H), 4.05 (s, 4H), 3.74–3.49 (m, 16H), 1.34 (s, 18H). ^{13}C NMR (75 MHz, $CDCl_3$) δ 168.6, 158.3, 157.9, 156.9, 156.5, 155.8, 150.2, 149.1, 138.9, 138.7, 136.6, 136.5, 122.1, 122.0, 121.7, 120.7, 117.6, 116.8, 112.3, 112.0, 80.2, 71.2, 70.7, 70.6, 70.3, 52.8, 52.6, 52.3, 52.2, 28.3. HRMS (FAB) m/z: $[M+H]^+$ Calcd for $C_{46}H_{63}N_8O_{11}$ 903.4611; Found 903.4617.

68h: 280 mg (72 % yield). ^{1}H NMR (300 MHz, $CDCl_3$) δ 8.46 (d, *J* = 4.3 Hz, 1H), 7.87 (d, *J* = 26.2 Hz, 1H), 7.77 (d, *J* = 8.3 Hz, 1H), 7.57 (m, 2H), 7.23 (dd, *J* = 24.8, 7.5 Hz, 1H), 7.09 (m, 1H), 6.87 (dd, *J* = 33.2, 7.1 Hz, 1H), 4.53 (t, *J* = 36.8 Hz 4H), 4.15 (q, *J* = 6.9 Hz, 2H), 1.36 (s, 9H), 1.22 (t, *J* = 7.0 Hz, 3H). ^{13}C NMR (75 MHz, $CDCl_3$) δ 158.4, 158.1, 156.7, 156.3, 155.9, 153.3, 151.2, 149.2, 138.8, 138.7, 136.6, 136.4, 122.1, 121.9, 121.7, 120.6, 116.4, 115.6, 110.6, 110.4, 80.2, 61.2, 52.8, 52.6, 52.1, 51.9, 28.3, 14.4. HRMS (FAB) m/z: $[M+H]^+$ Calcd for $C_{20}H_{27}N_4O_3$ 387.2027; Found 387.2029.

General procedure for the syntheses of **69a-i**: To a solution of Boc-protected DPA derivatives (0.5 mmol, 2.27 equiv.) in anhydrous dichloromethane (4 mL) was treated by 1 mL of trifluoroacetic acid. The solution was stirred for 3 hours. The mixture was added 6 mL of saturated $NaHCO_3$ solution and the aqueous layer was extracted by dichloromethane three times. The combined organic layer was dried over anhydrous Na_2SO_4, filtered and evaporated under reduced pressure. The residue was re-dissolved in 4 mL of 1,2-dichloroethane with 2-hydroxy-5-methylisophthalaldehyde[123] (36 mg, 0.22 mmol, 1.0 equiv.). The homogeneous solution was treated by $NaBH(OAc)_3$ (139 mg, 0.66 mmol, 3.0 equiv.) and stirred overnight. Volatiles were removed under reduced pressure and the residue was diluted by water and dichloromethane. Aqueous layer was extracted by dichloromethane three times. The combined organic layer was dried over anhydrous Na_2SO_4, filtered, and concentrated. The residue was chromatographed over silica gel by gradient elution of methanol in dichloromethane (0 to 7 %) to give analytically pure free ligands.

69a: 172 mg (53% yield). ^{1}H NMR (300 MHz, acetone-d_6) δ 10.76 (br, 1H), 9.39 (s, 2H), 8.53 (d, J = 4.2 Hz, 2H), 8.05 (d, J = 8.2 Hz, 2H), 7.70 (m, 4H), 7.53 (d, J = 7.8 Hz, 2H), 7.26 (d, J = 7.6 Hz, 2H), 7.22 (m, 2H), 7.00 (s, 2H), 3.85 (s, 4H), 3.75 (s, 4H), 3.73 (s, 4H), 2.20 (s, 3H), 2.18 (s, 6H). ^{13}C NMR (75 MHz, acetone-d_6) δ 168.7, 159.2, 157.8, 153.8, 151.6, 148.8, 138.4, 136.4, 129.8, 126.9, 123.7, 122.8, 122.0, 118.0, 111.4, 59.3, 59.1, 54.5, 23.5, 19.8. HRMS (FAB) m/z: $[M+H]^+$ Calcd for $C_{37}H_{41}N_8O_3$ 645.3296; Found 645.3297.

69b: 211 mg (60% yield). ^{1}H NMR (300 MHz, acetone-d_6) δ 10.86 (br, 1H), 9.29 (s, 2H), 8.53 (d, J = 4.2 Hz, 2H), 8.12 (d, J = 8.2 Hz, 2H), 7.67 (dd, J = 10.6, 5.2 Hz, 4H), 7.52 (d, J = 7.8 Hz, 2H), 7.26 (d, J = 7.5 Hz, 2H), 7.20 (dd, J = 6.6, 5.2

Hz, 2H), 7.02 (s, 2H), 3.85 (s, 4H), 3.75 (d, *J* = 3.7 Hz, 8H), 2.82 (quint, *J* = 6.8 Hz, 2H), 2.21 (s, 3H), 1.20 (d, *J* = 6.8 Hz, 12H). ^{13}C NMR (75 MHz, acetone-d_6) δ 175.7, 159.2, 157.8, 153.8, 151.8, 148.9, 138.5, 136.5, 129.9, 127.0, 123.8, 122.8, 122.0, 117.9, 111.6, 59.4, 59.1, 54.6, 35.6, 19.9, 19.0. HRMS (FAB) m/z: $[M+H]^+$ Calcd for $C_{41}H_{49}N_8O_3$ 701.3922; Found 701.3930.

69c: 305 mg (79% yield). ^{1}H NMR (300 MHz, acetone-d_6) δ 11.06 (br, 1H), 9.51 (s, 2H), 8.49 (d, *J* = 4.3 Hz, 2H), 8.21 (d, *J* = 8.2 Hz, 2H), 8.04 (d, *J* = 7.3 Hz, 4H), 7.75 (t, *J* = 7.9 Hz, 2H), 7.67 (m, 2H), 7.59 (dd, *J* = 7.3, 3.3 Hz, 4H), 7.52 (t, *J* = 7.4 Hz, 4H), 7.31 (d, *J* = 7.5 Hz, 2H), 7.25–7.13 (m, 2H), 7.10 (s, 2H), 3.87 (s, 4H), 3.83 (s, 8H), 2.24 (s, 3H). ^{13}C NMR (75 MHz, acetone-d_6) δ 165.3, 159.5, 158.0, 153.6, 151.5, 148.8, 138.7, 136.4, 134.4, 132.0, 130.0, 128.6, 127.5, 127.2, 124.0, 122.7, 122.0, 118.2, 111.9, 59.5, 58.8, 54.4, 19.8. HRMS (FAB) m/z: $[M+H]^+$ Calcd for $C_{47}H_{45}N_8O_3$ 769.3609; Found 769.3612.

69d: 302 mg (67% yield) ^{1}H NMR (300 MHz, Acetone-d_6) δ 10.96 (s, 1H), 9.72 (s, 2H), 8.50 (d, *J* = 4.2 Hz, 2H), 8.23 (d, *J* = 8.1 Hz, 4H), 8.18 (d, *J* = 8.3 Hz, 2H), 7.89 (d, *J* = 8.2 Hz, 4H), 7.76 (t, *J* = 7.9 Hz, 2H), 7.69 (td, *J* = 7.7, 1.6 Hz, 2H), 7.57 (d, *J* = 7.8 Hz, 2H), 7.35 (d, *J* = 7.5 Hz, 2H), 7.18 (m, 2H), 7.06 (s, 2H), 3.87 (s, 4H), 3.82 (s, 4H), 3.81 (s, 4H), 2.23 (s, 3H). ^{13}C NMR (75 MHz, Acetone-d_6) δ 164.3, 159.3, 158.2, 153.7, 151.2, 148.8, 138.7, 138.3, 136.4, 132.9, 132.5, 130.1, 128.4, 127.1, 125.5, 125.5, 123.9, 122.8, 122.0, 118.7, 112.1, 59.4, 58.8, 54.4, 19.8. LRMS (MALDI-TOF) m/z: $[M+H]^+$ Calcd for $C_{49}H_{42}F_6N_8O_3$ 904.3; Found 904.4.

69e: 263 mg (74% yield). ^{1}H NMR (300 MHz, acetone-d_6) δ 10.84 (br, 1H), 8.96 (s, 2H), 8.51 (d, *J* = 4.4 Hz, 2H), 8.07 (d, *J* = 8.2 Hz, 2H), 7.76–7.65 (m, 4H), 7.56 (d, *J* = 7.8 Hz, 2H), 7.31 (d, *J* = 7.5 Hz, 2H), 7.20 (dd, *J* = 6.4, 5.3 Hz, 2H), 7.07 (s, 2H), 4.03 (s, 4H), 3.86 (s, 4H), 3.80 (s, 8H), 3.50 (s, 6H), 2.23 (s, 3H). ^{13}C NMR

(75 MHz, acetone-d_6) δ 167.9, 159.4, 158.2, 153.8, 150.4, 148.8, 138.8, 136.4, 129.9, 126.9, 123.8, 122.7, 122.0, 118.5, 111.3, 71.7, 59.4, 58.8, 58.6, 54.3, 19.8. HRMS (FAB) m/z: $[M+H]^+$ Calcd for $C_{39}H_{45}N_8O_5$ 705.3507; Found 705.3522.

69f: 162 mg (37% yield). ^{1}H NMR (300 MHz, acetone-d_6) δ 9.25 (s, 2H), 8.53 (d, *J* = 4.5 Hz, 2H), 8.09 (d, *J* = 8.1 Hz, 2H), 7.73 (m, 4H), 7.55 (d, *J* = 7.8 Hz, 2H), 7.35 (d, *J* = 7.5 Hz, 2H), 7.22 (dd, *J* = 6.7, 5.4 Hz, 2H), 7.05 (s, 2H), 4.15 (s, 4H), 3.87 (s, 4H), 3.78 (d, *J* = 9.7 Hz, 12H), 3.70 (m, 4H), 3.64 (m, 4H), 3.51 (m, 4H), 3.26 (s, 6H), 2.23 (s, 3H). ^{13}C NMR (75 MHz, acetone-d_6) δ 168.6, 159.2, 158.3, 153.8, 150.6, 148.9, 138.7, 136.5, 129.9, 127.0, 123.8, 122.8, 122.1, 118.5, 111.4, 71.8, 71.2, 70.4, 70.2, 70.1, 59.4, 59.1, 58.0, 54.4, 19.9. HRMS (FAB) m/z: $[M+H]^+$ Calcd for $C_{47}H_{61}N_8O_9$ 881.4556; Found 881.4560.

69g: 54 mg (13% yield). ^{1}H NMR (300 MHz, acetone-d_6) δ 10.67 (br, 1H), 9.33 (s, 2H), 8.48 (d, *J* = 4.2 Hz, 2H), 8.11 (d, *J* = 8.2 Hz, 2H), 7.80–7.71 (m, 2H), 7.68 (dd, *J* = 7.6, 1.6 Hz, 2H), 7.53 (d, *J* = 7.8 Hz, 2H), 7.33 (d, *J* = 7.5 Hz, 2H), 7.19 (dd, *J* = 6.6, 5.3 Hz, 2H), 7.08 (s, 2H), 4.15 (s, 4H), 3.93–3.67 (m, 28H), 2.24 (s, 3H). ^{13}C NMR (75 MHz, Acetone-d_6) δ 168.8, 159.3, 158.1, 153.7, 150.8, 148.9, 138.8, 136.4, 129.6, 127.2, 123.9, 122.7, 122.0, 118.4, 111.5, 100.0, 71.4, 70.5, 70.4, 70.4, 69.9, 59.4, 59.0, 54.1, 19.9. HRMS (FAB) m/z: $[M+H]^+$ Calcd for $C_{45}H_{55}N_8O_8$ 835.4137; Found 835.4150.

69h: 232 mg (66% yield). ^{1}H NMR (300 MHz, acetone-d_6) δ 10.79 (br, 1H), 8.76 (s, 2H), 8.52 (d, *J* = 4.2 Hz, 2H), 7.83 (d, *J* = 8.2 Hz, 2H), 7.77–7.63 (m, 4H), 7.57 (d, *J* = 7.8 Hz, 2H), 7.22 (dd, *J* = 10.5, 7.3 Hz, 4H), 7.01 (s, 2H), 4.17 (q, *J* = 7.1 Hz, 4H), 3.87 (s, 4H), 3.76 (d, *J* = 3.4 Hz, 8H), 2.20 (s, 3H) 1.25 (t, *J* = 7.1 Hz, 6H). ^{13}C NMR (75 MHz, acetone-d_6) δ 159.3, 158.0, 153.8, 153.3, 151.7, 148.8, 138.5, 136.4, 129.8, 126.9, 123.8, 122.8, 122.0, 117.4, 110.0, 60.7, 59.4, 58.9, 54.5,

19.8, 13.9. HRMS (FAB) m/z: $[M+H]^+$ Calcd for $C_{39}H_{45}N_8O_5$ 705.3507; Found 705.3521.

69i: 284 mg (68% yield). ^{1}H NMR (300 MHz, acetone-d_6) δ 10.73 (br, 1H), 9.04 (s, 2H), 8.51 (d, *J* = 4.4 Hz, 2H), 7.85 (d, *J* = 8.2 Hz, 2H), 7.71–7.62 (m, 4H), 7.54 (d, *J* = 7.8 Hz, 2H), 7.40 (t, *J* = 6.6 Hz, 6H), 7.33 (dd, *J* = 9.2, 7.3 Hz, 4H), 7.21 (m, 4H), 6.99 (s, 2H), 5.20 (s, 4H), 3.85 (s, 4H), 3.74 (d, *J* = 4.3 Hz, 8H), 2.18 (s, 3H). ^{13}C NMR (75 MHz, acetone-d_6) δ 159.3, 158.0, 153.8, 153.3, 153.2, 151.6, 148.8, 138.6, 136.7, 136.4, 129.8, 128.4, 128.0, 127.9, 126.9, 123.7, 122.8, 122.0, 117.5, 110.1, 66.2, 59.4, 58.9, 54.5, 19.8. HRMS (FAB) m/z: $[M+H]^+$, Calcd for $C_{49}H_{49}N_8O_5$ 829.3820; Found 829.3816.

General procedure for the syntheses of **53-62**: 5 μmol of free ligand in acetonitrile (0.1 mL) was treated with $Zn(ClO_4)_2 \cdot 6H_2O$ (3.82 mg, 10.25 μmol, 2.05 equiv.) in acetonitrile (0.1 mL). The mixture was shaken for 30 minutes and lyophilized, and used without further purification.

4.3. Isothermal titration calorimetry.

Isothermal titration calorimetry was conducted using an Affinity ITC (TA Instruments). The experimental procedures for each titration are detailed in the Supporting Information. The thermodynamic parameters, K_a, ΔG, ΔH, and ΔS, were obtained by non-linear regression analysis on the software supplied by TA Instruments. Otherwise noted, the average values and standard deviations are obtained from two separate experiments for each titration.

4.4. Potentiometric titration.

Potentiometric titration experiments were conducted with FiveEasy Plus pH Meter (Mettler Toledo). The receptor solutions (0.91 mM in deionized water, containing 0.10 M NaCl and 9.09% DMSO for **10**, **61** and **62**, or 0.83 mM in deionized water, containing 0.10 M NaCl and 8.26% DMSO for **53**) were titrated with portions of 0.198 M $NaOH_{(aq)}$ at 27°C. All pH values were reproduced in 0.03 pH units. $[OH^-]_{total}$/[receptor] values were calibrated by the first inflection point (equivalent point to $HClO_4$), which was within a 3% margin of error.

Section 3. Pyrophosphate Recognition of Chiral bis(Zn-DPA) Derivatives

1. Introduction

Nature usually utilizes single enantiomer (or diastereomer) such as amino acids. For the use of single enantiomer, enzymes have evolved to reach an exceptional specificity to the corresponding substrates. Recent study suggested that ATP could induce chirality of a supramolecular assembly composed of **70** (Figure 2–12) by the intrinsic chirality of ATP.[124] Since Zn-DPA units are located at the edge of **70**, the chiral information of ATP must be efficiently transferred into the center of the supramolecular structure through binding event. Therefore, in a course of the development of a highly selective PPi receptor using bis(Zn-DPA) complexes, we envisioned that a suitably designed chiral bis(Zn-DPA) complex can selectively recognize PPi against ATP as nature does.

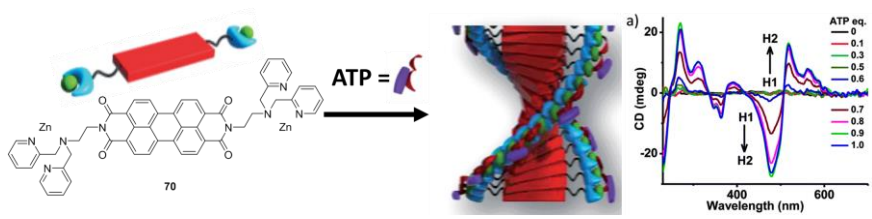

Figure 2–12. An atp-induced helical supramolecular structure composed of **86**. Reproduced by permission from reference 124. Copyright 2014 Royal Society of Chemistry

We realized that even though the receptors based on phenoxy-bridged bis(Zn-DPA) such as **9** and **52** have no stereocenter, their complexes with PPi have two-fold symmetry, which is an axial chirality. As evident in Figure 2–7, two benzylic carbons of the free ligand are the essential prochiral centers. Therefore, we assumed that the axial chirality of the complex would be determined according to the absolute stereochemistry of the benzylic carbon (Scheme 2–5). Then, we might observe diastereoselective molecular recognition between axially chiral host and intrinsically chiral guest ATP. On the other hand, an achiral guest PPi would bind to two enantiomeric hosts with the same affinity.

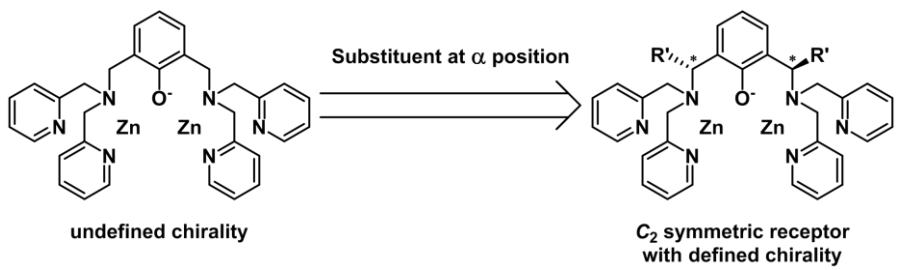

Scheme 2–5. A molecular design strategy for controlling an axial chirality of a bis(Zn-DPA) receptor.

2. Result and discussion

We have seen that phenoxy-bridged bis(Zn-DPA) derivatives take unique geometry that resembles an adamantane structure, we designed a series of chiral receptor molecules (Scheme 2–6). The steric hindrance of the receptors were controlled by the size of silyl protective groups (**71-73**). **74** lacking the central hydroxyl group was also prepared. The receptor molecules were synthesized in very straightforward manner. The synthetic strategy includes a modified Sharpless' asymmetric

aminohydroxylation,[125] Sharpless' asymmetric epoxidation,[126] stereospecific S_N2 reactions, deprotective cyclization, and reductive alkylation of amines. During the syntheses, we installed chiral centers with almost complete stereoselectivity (>98% ee), which was verified by chiral HPLC analysis.

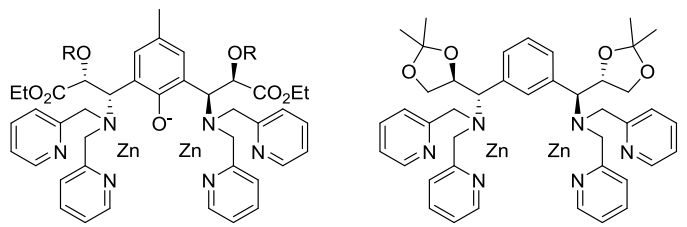

Scheme 2–6. The molecular structure of chiral PPi receptors, **71**-**74**.

We calculated the association constants of the receptors by means of IDA technique using PV as an indicator. As summarized in Table 2–8, the association constants of receptors with PPi ranged from 5.8×10^4 M^{-1} to 1.7×10^8 M^{-1}, and that between receptors and ATP ranged from 1.6×10^4 M^{-1} to 2.1×10^7 M^{-1}. In addition, we observed that the receptors in (*R,R*)-form commonly exhibit better selectivity factor ($K = K_{a,PPi}/K_{a,ATP}$) than that in (*S,S*)-form, which clearly shows that there is a diastereoselectivity in molecular recognition of ATP.

To investigate the diastereoselectivity of the receptors in detail, we defined K_R/K_S as a new parameter *Q*. We observed a negative and linear correlation between $\log(K_a)$ and *Q*-values that is a clear indication of the trade-off between the binding strength and diastereoselectivity (Figure 2–13), and we termed this phenomenon as *diastereoselectivity–sensitivity compensation*. Although we successfully embedded

diastereoselectivity into the bis(Zn-DPA) scaffold, the lower selectivity factors of receptors than **54** (K = 10.7) without a chiral component claims the ineffectiveness of the new chiral receptors in selectively detecting pyrophosphate against ATP. Indeed, larger slope for PPi than ATP in LogK_a-Q graph (Figure 2–13) suggests that the selectivity would be maximized when no diastereoselectivity was present (Q = 1.0). However, interesting was that the receptors formed a good linearity regardless of whether the central hydroxyl group is present or not. This result suggests that the presence of the central hydroxyl group is, perhaps, not essential for achieving exceptional selectivity.

Table 2–5. Apparent association constants (Log$K_{a,receptor–guest}$, column 2, 3, and 4), the selectivity factor (PPi/ATP, $K_{a,receptor–PPi}/K_{a,receptor–ATP}$), and Q-value K_R/K_S.

Receptor	**PV**	**PPi**	**ATP**	**PPi/ATP**	***Q***
(*S*,*S*)-**71**	5.17	6.44	5.87	3.8	1.73
(*R*,*R*)-**71**	5.51	6.90	6.09	6.6	
(*S*,*S*)-**72**	4.74	5.22	4.74	3.1	2.08
(*R*,*R*)-**72**	4.92	5.66	4.85	6.4	
(*S*,*S*)-**73**	4.66	4.76	4.22	3.5	2.22
(*R*,*R*)-**73**	4.74	5.37	4.48	7.8	
(*S*,*S*)-**74**	6.81	8.28	7.33	8.9	1.17
(*R*,*R*)-**74**	6.72	8.28	7.25	10.4	

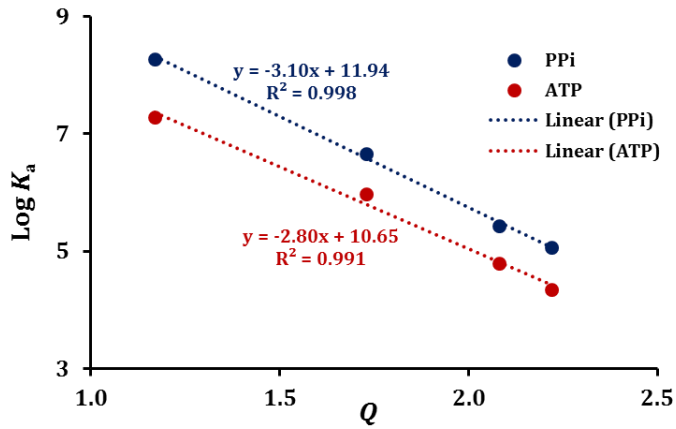

Figure 2–13. A linear relationship between association constant (LogK_a) and Q-value.

Then, why do we observe a reduction in the affinity? We have seen that the four pyridines of bis(Zn-DPA) moiety are so closely packed that a slight extension of bis(Zn-DPA) completely blocks even a water molecule that approaches from the equatorial side. We also found that the receptor having bigger substituent tends to show higher Q-value. Therefore, the reason for the reduction of presumably originates from the steric effect of the substituent. Figure 2–14 shows the computer-generated molecular structure of PPi complexes with selected receptors, **52**, **71** and **73**. It clearly reveals a geometrical distortion of PPi-bound bis(Zn-DPA) structures in the presence of side chain. We also found that the unique adamantane-like structure composed of a PPi ion, two Zn ions, and an oxygen atom lost its C_2-symmetry, and became more skewed with a bigger side chain. This computational result strongly suggests that the binding of PPi to bis(Zn-DPA) becomes less favorable with the greater steric interaction.

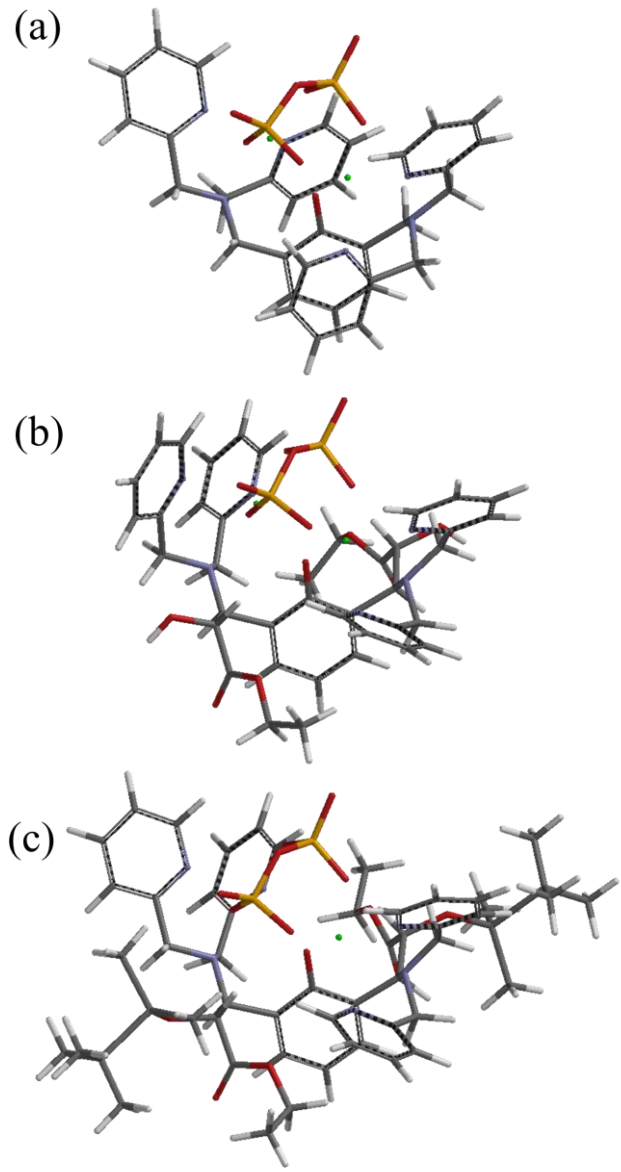

Figure 2–14. Computer-aided molecular models of (a) **54**-PPi, (b) (*S*,*S*)-**71**-PPi, and (c) (*S*,*S*)-**73**-PPi.

3. Conclusion

We have synthesized and analyzed a series of chiral receptors and their affinity to ATP by means of IDA technique. We figured out that ATP favors the binding to a receptor of (*S*,*S*)-form than that of (*R*,*R*)-form, which presumably originates from the diastereoselectivitiy in molecular recognition. However, the overall selectivity was decreased. Moreover, the installation of a chirality at the benzylic position reduced the degree of preorganization of bis(Zn-DPA) moiety, which results in the negative effect in the affinity and selectivity. In consideration with that the structural changes in binding site is more or less the same for the binding of PPi and ATP, we think that there would be an attractive interaction, such as van der Waals, between the AMP moiety and the added group for installing the chiral centers.[127] Therefore, controlling the axial chirality by introducing chiral center at the benzylic position is of minute merit for enhancing selectivity toward PPi against ATP.

4. Experimental section

4.1. General information

All chemicals were purchased from either Sigma-Aldrich or Tokyo Chemical Industry (TCI) and were used as received except anhydrous solvents. Thin layer chromatography was performed over Merck silica gel 60 F254 on aluminum foil. Silicycle 60 was used for the stationary phase in chromatographic separation or silica pad filtration. Celite® 545 was used for celite filtration. All ^{1}H and ^{13}C NMR spectra were obtained from Bruker DRX 300 NMR spectrometer. Absorption spectra were

recorded on a JASCO V–730 spectrometer. LRMS were taken by MALDI-TOF mass analyzer (Bruker instrument).

4.2. Synthesis of the receptors

Dichloromethane and tetrahydrofuran were distilled over calcium hydride and sodium/benzophenone ketyl, respectively. NMR multiplicities: s, singlet; d, doublet; t, triplet; m, multiplet; br, broad. Enantiomeric excesses (ee) were determined by chiral HOLC analysis over CHIRALPAK-IA with elution of IPA/hexane (5%, 1mL min^{-1}) detecting at 220 nm.

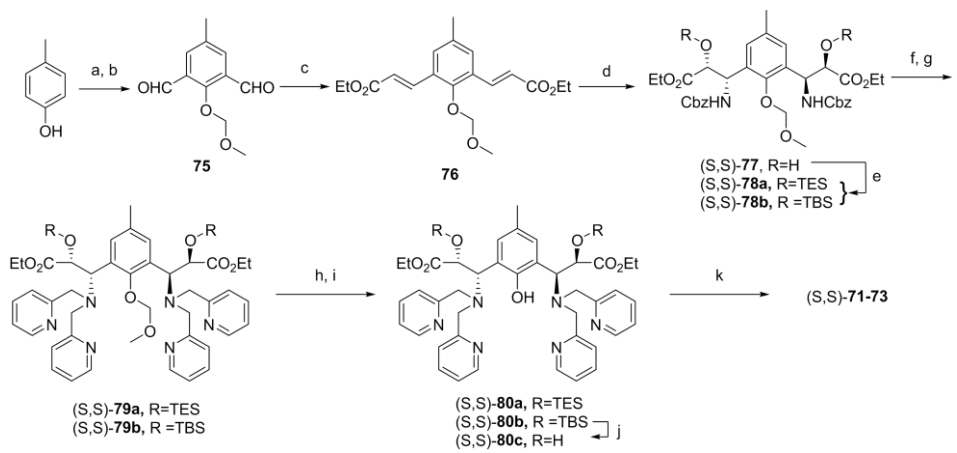

Scheme 2–7. Synthetic procedure for the receptors **71-73**. a, hexamethylenetetramine, TFA, 2 d; b, chloromethyl methyl ether, N,N-diisopropyl ethylamine, DCM; c, triethyl phosphonoacetate, NaH, THF; d, OsO_4 (3.0 mol-%), $(DHQ)_2PHAL$ (3.6 mol-%), benzyl N-(4-chlorobenzoyloxy)carbamate, acetonitrile/water (6:1); e, R_3SiCl, imidazole, DMF; f, Pd/C, H_2, ethyl acetate; g, 2-pyridinecarboxaldehyde, $NaBH(OAc)_3$, DCE; h, 20% TFA/DCM; i, 1.0 M HCl in EtOH; j, TBAF, THF; k, $Zn(ClO_4)_2 \cdot 6H_2O$, acetonitrile.

Synthesis of **75**: To a solution of hexamethylenetetramine (84g, 0.6 mol, 4.0 equiv.) in TFA (450 mL) was added 16.2 g of *p*-cresol (0.15 mol, 1.0 equiv.). The mixture was stirred for 2 days at 80°C and concentrated under reduced pressure. The residue was diluted by 4 M aqueous HCl (3 L) and stirred for 6 hours, during which time yellow precipitates were formed. The solid was collected via filtration using sintered glass funnel and washed with water (2 L × 3). The solid was re-dissolved in dichloromethane (1 L) and washed with water twice. The organic layer was dried over anhydrous Na_2SO_4, filtered, and concentrated under reduced pressure. The residue (~ 21 g, ~ 0.12 mol) was dissolved in anhydrous dichloromethane (250 mL). The solution was successively treated with N,N-diisopropyl ethylamine (25 mL, 0.14 mol) and chloromethyl methyl ether (10.0 mL, 0.13 mol), and stirred for 3 hours. The solution was quenched by adding 200 mL of water, and the organic layer was successively washed with water, half-saturated $NaHCO_3$, and brine. The organic layer was dried over anhydrous $MgSO_4$ and filtered through a pad of silica gel (5 cm). The filtrate was concentrated under reduced pressure to give 22.4 g of analytically pure **75** (72% in two steps). ^{1}H (300 MHz, $CDCl_3$) δ 10.35 (s, 2H), 7.92 (s, 2H), 5.20 (s, 2H), 3.61 (s, 3H), 2.44 (s, 3H). ^{13}C (75 MHz, $CDCl_3$) δ 189.2, 160.3, 135.5, 135.3, 130.1, 102.9, 58.3, 20.6. LRMS (MALDI-TOF) m/z: $[M+H]^+$ Calcd for $C_{11}H_{13}O_4$ 209.1; Found 209.2.

Synthesis of **76**: To a suspension of NaH (2.2 g, 55 mmol, 2.2 equiv.) in anhydrous THF (250 mL) was slowly added triethyl phosphonoacetate (10.9 mL, 55 mmol, 2.2 equiv.) at 0°C. The mixture was stirred at the same temperature until the solution becomes clear and no more gas evolution was observed. To the solution was added a solution of **75** (5.21 g, 25 mmol, 1.0 equiv.) in THF (50 mL) via cannula. The homogeneous solution was stirred for 6 hours after which time most of THF was

evaporated. The residue was diluted with water (300 mL), which was then extracted with ethyl ether (2 × 200 mL). The combined ethereal layer was dried over anhydrous MgSO4, filtered, and evaporated. The residue was subjected for flash column chromatography with a gradient elution of ethyl ether in hexanes (30 to 50%) to give analytically pure **76** (7.6 g, 87%). ^{1}H (300 MHz, $CDCl_3$) δ 8.01 (d, *J*=16.2Hz, 2H), 7.44 (s, 2H), 6.4 (d, *J*=16.2Hz, 2H), 5.00 (s, 2H), 4.28 (q, *J*=7.1Hz, 4H), 3.67 (s, 3H), 2.37 (s, 3H), 1.35 (t, *J*=7.1Hz, 6H). ^{13}C (75 MHz, $CDCl_3$) δ 166.8, 153.6, 139.4, 134.4, 129.7, 129.0, 119.7, 101.4, 60.5, 58.2, 20.9, 14.3. LRMS (MALDI-TOF) m/z: $[M+H]^+$ Calcd for $C_{19}H_{25}O_6$ 349.2; Found 349.3.

Synthesis of (*S*,*S*)-**77**: To a suspension of $(DHQ)_2PHAL$ (141 mg, 0.18 mmol, 3.6 mol–%) and benzyl N-(4-Chlorobenzoyloxy)carbamate (4.6 g, 15.3 mmol, 3.0 equiv.) in 120 mL of acetonitrile was added 0.96 mL of OsO_4 in water (4 wt%, 38.5 mg, 0.15 mmol, 3.0 mol–%) at an ambient temperature. The mixture was stirred for 10 minutes and cooled to –15 °C. To the solution was successively added **76** (1.8 g, 5.1 mmol, 1.0 equiv.), and water (19 mL). The mixture was stirred at the same temperature for 16 hours at which time a TLC analysis indicates the complete consumption of **76**. After removing acetonitrile, the residue was diluted with saturated $Na_2S_2O_3$ and ethyl acetate (150 mL each). The biphasic mixture was vigorously stirred for additional 30 minutes. The organic layer was washed with saturated $NaHCO_3$ solution three times, dried over anhydrous Na_2SO_4, filtered, and concentrated. The residue was subjected to flash chromatography (50% EA in Hex) for the removal of catalyst to afford analytically pure (*S*,*S*)-**77** (2.2g, 63%, 98% ee) (*R*,*R*)-form was synthesized analogously using $(DHQD)_2PHAL$ instead of $(DHQ)_2PHAL$.

(*S*,*S*)-**77**: ^{1}H (300 MHz, Acetone-d_6) δ 7.35 (br, 12H), 6.76 (d, *J*=9.6 Hz, 2H), 5.68 (dd, *J*=9.5, 1.8 Hz, 2H), 5.41 (dd, *J*=27, 3.0 Hz, 2H), 5.00 (q, *J*=12 Hz, 4H), 4.48 (s, 2H), 4.37 (d, *J*=5.4Hz, 2H), 4.20 (m, 4H), 3.76 (br, 3H), 2.28 (s, 3H), 1.98 (s, 2H), 1.21 (m, 6H). LRMS (MALDI-TOF) m/z: $[M+H]^+$ Calcd for $C_{35}H_{43}N_2O_{12}$ 683.3; Found 683.3. retention time: 12.2 min.

(*R*,*R*)-**77**: (2.0g, 57%, 99% ee) ^{1}H (300 MHz, Acetone-d_6) δ 7.35 (br, 12H), 6.76 (d, *J*=9.6 Hz, 2H), 5.70 (dd, *J*=9.0, 1.9 Hz, 2H), 5.41 (dd, *J*=27, 3.1 Hz, 2H), 5.04 (q, *J*=12 Hz, 4H), 4.48 (s, 2H), 4.32 (d, *J*=5.4Hz, 2H), 4.23 (m, 4H), 3.72 (br, 3H), 2.28 (s, 3H), 1.78 (s, 2H), 1.21 (m, 6H). LRMS (MALDI-TOF) m/z: $[M+H]^+$ Calcd for $C_{35}H_{43}N_2O_{12}$ 683.3; Found 683.3. retention time: 13.2 min.

Synthesis of **78**: A solution of **77** (680 mg, 1.0 mmol, 1.0 equiv.) in DMF (8 mL) was successively treated with imidazole (224 mg, 3.3 mmol, 3.3 equiv.) and silyl chlorides (3.0 mmol, 3.0 equiv.). The mixture was stirred for 3 hours before being quenched by addition of water (50 mL). The aqueous layer was extracted with ethyl ether (2 × 50 mL), and the combined ethereal layer was dried over anhydrous $MgSO_4$, filtered, and concentrated under reduced pressure. The residue was chromatographed over silica gel by a gradient elution of ethyl acetate in hexanes (0 to 25 %) to give analytically pure **78**.

(*S*,*S*)-**78a**: ^{1}H (300 MHz, $CDCl_3$) δ 7.34 (br, 10H), 7.1–7.0 (m, 2H), 5.78 (d, *J*=9.1 Hz, 2H), 5.58 (d, *J*=8.1Hz, 2H), 5.4–4.9 (m, 6H), 4.7–4.3 (m, 2H), 4.28–4.16 (m, 4H), 3.71 (d, *J*=22 Hz, 3H), 2.26 (d, *J*=6.2Hz, 1H), 1.30 (t, *J*=7.0Hz, 6H), 0.94–0.74 (m, 18H), 0.36 (m, 12H). LRMS (MALDI-TOF) m/z: $[M+H]^+$ Calcd for $C_{47}H_{71}N_2O_{12}Si_2$ 911.4; Found 911.6.

(*R*,*R*)-**78a**: ^{1}H (300 MHz, $CDCl_3$) δ 7.34 (br, 10H), 7.1–7.0 (m, 2H), 5.78 (d, *J*=9.1 Hz, 2H), 5.58 (d, *J*=8.1Hz, 2H), 5.4–4.9 (m, 6H), 4.7–4.3 (m, 2H), 4.28–4.16

(m, 4H), 3.71 (d, *J*=22 Hz, 3H), 2.26 (d, *J*=6.2Hz, 1H), 1.30 (t, *J*=7.0Hz, 6H), 0.94–0.74 (m, 18H), 0.35 (m, 12H). LRMS (MALDI-TOF) m/z: $[M+H]^+$ Calcd for $C_{47}H_{71}N_2O_{12}Si_2$ 911.4; Found 911.6.

(*S*,*S*)-**78b**: ^{1}H (300 MHz, $CDCl_3$) δ 7.34 (br, 10H), 7.1–7.0 (m, 2H), 5.78 (d, *J*=9.1 Hz, 2H), 5.58 (d, *J*=8.1Hz, 2H), 5.4–4.9 (m, 6H), 4.7–4.3 (m, 2H), 4.28–4.16 (m, 4H), 3.71 (d, *J*=22 Hz, 3H), 2.26 (d, *J*=6.2Hz, 1H), 1.30 (t, *J*=7.0Hz, 6H), 0.94–0.73 (m, 18H), -0.1–-0.48 (m, 12H). LRMS (MALDI-TOF) m/z: $[M+H]^+$ Calcd for $C_{47}H_{71}N_2O_{12}Si_2$ 911.4; Found 911.5.

(*R*,*R*)-**78b**: ^{1}H (300 MHz, $CDCl_3$) δ 7.34 (br, 10H), 7.1–7.0 (m, 2H), 5.78 (d, *J*=9.1 Hz, 2H), 5.58 (d, *J*=8.1Hz, 2H), 5.4–4.9 (m, 6H), 4.7–4.3 (m, 2H), 4.28–4.16 (m, 4H), 3.71 (d, *J*=22 Hz, 3H), 2.26 (d, *J*=6.2Hz, 1H), 1.30 (t, *J*=7.0Hz, 6H), 0.94–0.73 (m, 18H), -0.1–-0.48 (m, 12H). LRMS (MALDI-TOF) m/z: $[M+H]^+$ Calcd for $C_{47}H_{71}N_2O_{12}Si_2$ 911.4; Found 911.5.

Synthesis of **79**: To a solution of **78** in ethyl acetate (10 mL/mmol) was hydrogenated in the presence of Pd/C (10 wt%) for 6 hours. The reaction was monitored by the disappearance of benzylic proton of protection. The insoluble catalyst was removed by celite filtration (~5 cm) and the remaining solvent was removed under reduced pressure. The residue was redissolved in 1,2-dichloroethane (5 mL/mmol), and successively treated with 2-pyridinecarboxaldehyde (6.0 equiv.) and $NaBH(OAc)_3$ (8.0 equiv.), which was then stirred overnight. After the removal of solvent, the residue was diluted with water and extracted with dichloromethane. The combined organic layer was dried over anhydrous Na_2SO_4, filtered, and concentrated. The residue was chromatographed over silica gel by eluting ethyl acetate to give analytically pure **79**.

(*S*,*S*)-**79a**: ^{1}H (300 MHz, $CDCl_3$) δ 8.42 (d, *J*=4.5Hz, 2H), 7.64–7.56 (m, 10H), 7.06 (t, *J*=5.1 Hz, 4H), 4.81 (d, *J*=4.0 Hz, 2H), 4.66 (d, *J*=4.0 Hz, 2H), 4.49 (d, *J*=15.3 Hz, 4H), 4.14 (m, 4H), 3.97 (d, *J*=15.3 Hz, 4H), 2.98 (s, 3H), 2.40 (s, 3H), 1.16 (t, *J*=7.2 Hz, 6H), 0.84 (m, 18H), 0.39 (m, 6H). LRMS (MALDI-TOF) m/z: $[M+H]^+$ Calcd for $C_{55}H_{79}N_6O_8Si_2$ 1007.5; Found 1007.8.

(*R*,*R*)-**79a**: ^{1}H (300 MHz, $CDCl_3$) δ 8.42 (d, *J*=4.5Hz, 2H), 7.64–7.56 (m, 10H), 7.06 (t, *J*=5.1 Hz, 4H), 4.81 (d, *J*=4.0 Hz, 2H), 4.66 (d, *J*=4.0 Hz, 2H), 4.49 (d, *J*=15.3 Hz, 4H), 4.14 (m, 4H), 3.97 (d, *J*=15.3 Hz, 4H), 2.98 (s, 3H), 2.40 (s, 3H), 1.16 (t, *J*=7.2 Hz, 6H), 0.84 (m, 18H), 0.39 (m, 6H). LRMS (MALDI-TOF) m/z: $[M+H]^+$ Calcd for $C_{55}H_{79}N_6O_8Si_2$ 1007.5; Found 1007.8.

(*S*,*S*)-**79b**: ^{1}H (300 MHz, $CDCl_3$) δ 8.42 (d, *J*=4.5Hz, 2H), 7.64–7.56 (m, 10H), 7.06 (t, *J*=5.1 Hz, 4H), 4.81 (d, *J*=4.0 Hz, 2H), 4.66 (d, *J*=4.0 Hz, 2H), 4.49 (d, *J*=15.3 Hz, 4H), 4.14 (m, 4H), 3.97 (d, *J*=15.3 Hz, 4H), 2.98 (s, 3H), 2.40 (s, 3H), 1.16 (t, *J*=7.2 Hz, 6H), 0.89 (s, 18H), -0.05 (s, 6H), -0.23 (s, 6H). LRMS (MALDI-TOF) m/z: $[M+H]^+$ Calcd for $C_{55}H_{79}N_6O_8Si_2$ 1007.5; Found 1007.8.

(*R*,*R*)-**79b**: ^{1}H (300 MHz, $CDCl_3$) δ 8.42 (d, *J*=4.5Hz, 2H), 7.64–7.56 (m, 10H), 7.06 (t, *J*=5.1 Hz, 4H), 4.81 (d, *J*=4.0 Hz, 2H), 4.66 (d, *J*=4.0 Hz, 2H), 4.49 (d, *J*=15.3 Hz, 4H), 4.14 (m, 4H), 3.97 (d, *J*=15.3 Hz, 4H), 2.98 (s, 3H), 2.40 (s, 3H), 1.16 (t, *J*=7.2 Hz, 6H), 0.89 (s, 18H), -0.05 (s, 6H), -0.23 (s, 6H). LRMS (MALDI-TOF) m/z: $[M+H]^+$ Calcd for $C_{55}H_{79}N_6O_8Si_2$ 1007.5; Found 1007.8.

Synthesis of **80b-c**: A solution of **79** was dissolved in anhydrous DCM (2 mL/mmol) was treated by TFA–DCM (4 mL/mmol, 1:1) at 0 °C and stirred for 2.5 hours at the same temperature. The mixture was poured into 20 mL of half-saturated $NaHCO_3$ solution, and the aqueous layer was extracted with dichloromethane (40 mL × 3). The combined organic layer was dried over anhydrous $MgSO_4$, filtered,

and concentrated under reduced pressure. The residue was re-dissolved by 1M HCl in EtOH (4 mL/mmol) and stirred for 6 hours. The solution was neutralized by adding solid $NaHCO_3$. Volatiles were removed in vacuo, and the residue was diluted with water. The aqueous layer was extracted with dichloromethane, and the combined organic layer was dried over anhydrous Na_2SO_4, filtered, and evaporated under reduced pressure. The residue was chromatographed over silica gel by a gradient elution of methanol in ethyl acetate (0 to 5 %) to give analytically pure **81** (1.47g, 42 %). **82** was analogously synthesized using **80** instead of **79**.

(*S*,*S*)-**80a**: ^{1}H (300 MHz, $CDCl_3$) δ 8.42 (d, *J*=4.2 Hz, 4H), 7.59 (t, *J*=7.4 Hz, 4H), 7.45 (d, *J*=7.7 Hz, 4H), 7.32 (s, 2H), 7.08 (t, *J*=5.9 Hz, 4H), 5.07 (d, *J*=4.8 Hz, 2H), 4.79 (d, *J*=4.8 Hz, 2H), 4.36 (d, *J*=15 Hz, 4H), 3.95 (d, *J*=15 Hz, 4H), 4.12–3.91 (m, 4H), 2.26 (s, 3H), 1.02 (t, *J*=7.2 Hz, 6H), 0.82 (m, 18H), 0.42 (m, 12H). LRMS (MALDI-TOF) m/z: $[M+H]^+$ Calcd for $C_{53}H_{75}N_6O_7Si_2$ 963.5; Found 963.6.

(*R*,*R*)-**80a**: ^{1}H (300 MHz, $CDCl_3$) δ 8.42 (d, *J*=4.2 Hz, 4H), 7.59 (t, *J*=7.4 Hz, 4H), 7.45 (d, *J*=7.7 Hz, 4H), 7.32 (s, 2H), 7.08 (t, *J*=5.9 Hz, 4H), 5.07 (d, *J*=4.8 Hz, 2H), 4.79 (d, *J*=4.8 Hz, 2H), 4.36 (d, *J*=15 Hz, 4H), 3.95 (d, *J*=15 Hz, 4H), 4.12–3.91 (m, 4H), 2.26 (s, 3H), 1.02 (t, *J*=7.2 Hz, 6H), 0.82 (m, 18H), 0.42 (m, 12H). LRMS (MALDI-TOF) m/z: $[M+H]^+$ Calcd for $C_{53}H_{75}N_6O_7Si_2$ 963.5; Found 963.6.

(*S*,*S*)-**80b**: ^{1}H (300 MHz, $CDCl_3$) δ 8.42 (d, *J*=4.2 Hz, 4H), 7.59 (t, *J*=7.4 Hz, 4H), 7.45 (d, *J*=7.7 Hz, 4H), 7.32 (s, 2H), 7.08 (t, *J*=5.9 Hz, 4H), 5.07 (d, *J*=4.8 Hz, 2H), 4.79 (d, *J*=4.8 Hz, 2H), 4.36 (d, *J*=15 Hz, 4H), 3.95 (d, *J*=15 Hz, 4H), 4.12–3.91 (m, 4H), 2.26 (s, 3H), 1.02 (t, *J*=7.2 Hz, 6H), 0.93 (s, 18H), 0.02 (s, 6H), -0.06 (s, 6H). LRMS (MALDI-TOF) m/z: $[M+H]^+$ Calcd for $C_{53}H_{75}N_6O_7Si_2$ 963.5; Found 963.6.

(*R*,*R*)-**80b**: ^{1}H (300 MHz, $CDCl_3$) δ 8.42 (d, *J*=4.2 Hz, 4H), 7.59 (t, *J*=7.4 Hz, 4H), 7.45 (d, *J*=7.7 Hz, 4H), 7.32 (s, 2H), 7.08 (t, *J*=5.9 Hz, 4H), 5.07 (d, *J*=4.8 Hz, 2H), 4.79 (d, *J*=4.8 Hz, 2H), 4.36 (d, *J*=15 Hz, 4H), 3.95 (d, *J*=15 Hz, 4H), 4.12–3.91 (m, 4H), 2.26 (s, 3H), 1.02 (t, *J*=7.2 Hz, 6H), 0.93 (s, 18H), 0.02 (s, 6H), -0.06 (s, 6H). LRMS (MALDI-TOF) m/z: $[M+H]^+$ Calcd for $C_{53}H_{75}N_6O_7Si_2$ 963.5; Found 963.6.

Synthesis of **80c**: To an aliquot of **80b** (10 μM) in anhydrous THF (1 mL) was treated with 0.1 mL of tetrabutylammonium fluoride (1M THF) and the mixture was shaken for 30 minutes. Most of the solvent was removed under reduced pressure and used for next complexation without purification.

Synthesis of **71-73**: 5 μmol of free ligand in acetonitrile (0.1 mL) was treated with $Zn(ClO_4)_2{\cdot}6H_2O$ (3.82 mg, 10.25 μmol, 2.05 equiv.) in acetonitrile (0.1 mL). The mixture was shaken for 30 minutes and lyophilized and used without further purification.

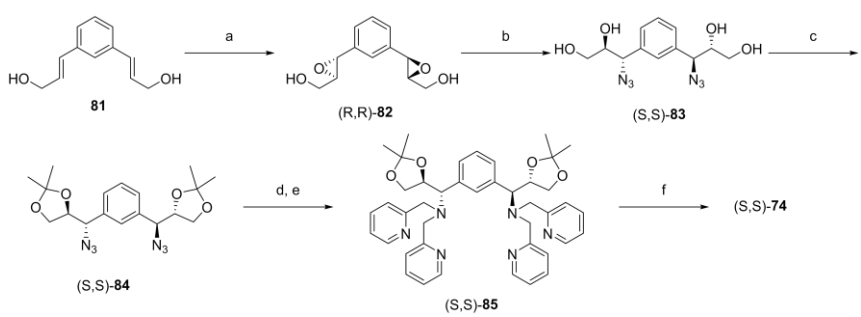

Scheme 2–8. Synthetic procedure for the receptors **74**. a. (D)-(–)-diisopropyl tartrate (10 mol–%), $Ti(OiPr)_4$ (10 mol–%), cumene hydroperoxide; b, NH_4Cl, NaN_3, THF/water (1:1); c, 2,2-dimethoxypropane, pyridinium *p*-toluenesulfonate, DCM; d, PPh_3, THF/water (8:1); e, 2-pyridinecarboxaldehyde, $NaBH(OAc)_3$, DCE; f, $Zn(ClO_4)_2{\cdot}6H_2O$, acetonitrile.

Synthesis of **82**: To a two-necked round-bottomed flask charged with (D)-(–)-diisopropyl tartrate (for (*R*,*R*)-form, 84 μL, 0.4 mmol, 0.1 equiv.), flame-dried 4Å MS (1.5 g), and a Teflon-coated magnetic stirring bar was added titanium(IV) isopropoxide (0.11 mL, 0.4 mmol, 0.1 equiv.) in DCM (20 mL) at –15 °C. The mixture was stirred for 30 minutes, added cumene hydroperoxide (80%, 3.0 mL, 16 mmol, 4.0 equiv.), and stirred for additional 30 minutes, during which time the colorless solution became yellow. To the yellow solution was added a solution of **81**[128] (760 mg, 4.0 mmol, 1.0 equiv.) in THF (10 mL), and stood in a refrigerator for 2 days. The insoluble was removed by Celite filtration (~5 cm) and the solvent was removed under reduced pressure. The residue was directly chromatographed over silica gel by a gradient elution of ethyl acetate in hexane (0 to 80%) to give analytically pure product.

(*R*,*R*)-**82**: 554 mg, 62% yield, 99% ee. ^{1}H (300 MHz, DMSO-d_3) δ 7.35 (t, *J*=7.9 Hz, 1H), 7.25–7.18 (m, 3H), 4.98 (t, *J*=5.82 Hz, 2H), 3.85 (s, 2H), 3.68 (m, 2H), 3.55 (m, 2H), 3.14 (br, 2H). ^{13}C (75 MHz, $CDCl_3$) δ 108.2, 103.1. LRMS (MALDI-TOF) m/z: $[M+H]^+$ Calcd for $C_{12}H_{15}O_4$ 223.1; Found 223.1.

(*S*,*S*)-**82**: 540 mg, 61%, 99% ee. ^{1}H (300 MHz, DMSO-d_3) δ 7.35 (t, *J*=7.9 Hz, 1H), 7.25–7.18 (m, 3H), 4.98 (t, *J*=5.82 Hz, 2H), 3.85 (s, 2H), 3.68 (m, 2H), 3.55 (m, 2H), 3.14 (br, 2H). ^{13}C (75 MHz, $CDCl_3$) δ 108.2, 103.1. LRMS (MALDI-TOF) m/z: $[M+H]^+$ Calcd for $C_{12}H_{15}O_4$ 223.1; Found 223.1.

Synthesis of **83**: To a solution of **82** (444 mg, 2.0 mmol, 1.0 equiv.) in THF (6 mL) was added aqueous solution (3 mL) of NH_4Cl (64 mg, 1.2 mmol, 0.6 equiv.) and NaN_3 (455 mg, 7 mmol, 3.5 equiv.). The mixture was stirred for 16 hours, and diluted with water and ethyl acetate. The organic layer was washed with water, dried over Na_2SO_4, filtered, and concentrated under reduced pressure. The residue was

used in the next step without further purification. LRMS (MALDI-TOF) m/z: [M+H]+ Calcd for $C_{12}H_{17}N_6O_4$ 308.1; Found 308.1

Synthesis of **84**: To a solution of **83** (1.0 equiv.), 2,2-dimethoxypropane (4.0 equiv.) in dichloromethane (5 mL/mmol **83**) was added pyridinium *p*-toluenesulfonate (10 mol–%). The mixture was stirred for 4 hours before being quenched by addition of half-saturated $NaHCO_3$ solution. The aqueous layer was extracted with DCM, and the combined organic layer was dried over anhydrous $MgSO_4$, filtered, and concentrated. The residue was chromatographed over silica gel by eluting ethyl acetate in hexane (33%) to give analytically pure products.

Synthesis of **85**: To a solution of **84** (1.0 equiv.) in THF-water (8:1, 9 mL/mmol) was added triphenylphosphine (PPh_3, 3.0 equiv.). The mixture was gently heated at 70 °C for 3 hours, during which time a complete consumption of **102** was observed. The mixture was diluted with water and extracted with ethyl acetate three times. The combined organic layer was dried over anhydrous Na_2SO_4, filtered, and concentrated. The residue was redissolved in 1,2-dichloroethane, and treated with 2-pyridinecarboxaldehyde (6.0 equiv.) and $NaBH(OAc)_3$ (8.0 equiv.). The mixture was stirred overnight and concentrated under reduced pressure. The residue was diluted with water and extracted with dichloromethane three times. The combined organic layer was dried over anhydrous Na_2SO_4, filtered, and concentrated. The crude product was chromatographed over silica gel by a gradient elution of methanol in DCM (0 to 10 %) to give analytically pure product.

(*S*,*S*)-**85**: 540 mg, 61%. ^{1}H (300 MHz, Acetone-d_6) δ 8.53 (d, *J*=4.2 Hz, 4H), 7.79 (m, 5H), 7.61 (d, *J*=7.8 Hz, 4H), 7.53 (m, 3H), 7.24 (q, *J*=4.0 Hz, 4H), 5.05 (m, 2H), 4.33 (t, *J*=7.1 Hz, 2H), 4.05 (d, *J*=14 Hz, 4H), 3.81 (t, *J*=8.0 Hz, 4H) 3.55 (d,

J=14 Hz, 4H), 1.22 (s, 6H), 1.09 (s, 6H). LRMS (MALDI-TOF) m/z: $[M+H]^+$ Calcd for $C_{42}H_{49}N_6O_4$ 701.4; Found 701.3.

(*R*,*R*)-**85**: 540 mg, 61%. ^{1}H (300 MHz, Acetone-d_6) δ 8.53 (d, *J*=4.2 Hz, 4H), 7.79 (m, 5H), 7.61 (d, *J*=7.8 Hz, 4H), 7.53 (m, 3H), 7.24 (q, *J*=4.0 Hz, 4H), 5.05 (m, 2H), 4.33 (t, *J*=7.1 Hz, 2H), 4.05 (d, *J*=14 Hz, 4H), 3.81 (t, *J*=8.0 Hz, 4H) 3.55 (d, *J*=14 Hz, 4H), 1.22 (s, 6H), 1.09 (s, 6H). LRMS (MALDI-TOF) m/z: $[M+H]^+$ Calcd for $C_{42}H_{49}N_6O_4$ 701.4; Found 701.3.

Syntheses of **74**: 5 μmol of free ligand in acetonitrile (0.1 mL) was treated with $Zn(ClO_4)_2 \cdot 6H_2O$ (3.82 mg, 10.25 μmol, 2.05 equiv.) in acetonitrile (0.1 mL). The mixture was shaken for 30 minutes and lyophilized and used without further purification.

Section 4. Pyrophosphate Recognition of Homo- and Hetero-bimetallic Complexes

1. Introduction

In a previous section, we verified that the appended acetamides of **52** retard the guest exchange reaction by effectively blocking the access of molecular entities to the host–guest complex. As a result, we demonstrated that controlling the number of substituents is an effective strategy for accelerating the exchange reaction.

We then wondered what would happen if zinc(II) ion is replaced by other metal ions. In order to facilitate exchange reaction without significant distortion in molecular geometry, the replacement metal ion should satisfy following conditions. First, the ion should be bigger than zinc(II) ion so that the complex is sufficiently solvated. Second, the ion should make a complex with DPA derivatives. Finally, the charge of the ion is preferably greater than 2+ to compensate the weaken interaction due to a longer distance between ion and PPi.

Indium, in that regard, is the most promising candidate. In(III) is the only stable oxidation state of indium ion, with an ionic radius of 94 pm, which is about 7% bigger than Zn(II) ion (88 pm).[129] Also, it forms stable complexes with various amine chelators.[130,131] Therefore, we chose In(III) as a replacement for Zn(II) ion.

2. Result and discussion

In order to investigate the effect of indium substitution, we synthesized four new dinuclear complexes **86** to **89** (Scheme 2–9). **86** and **88** are heterobimetallic (Zn, In) complexes, while **87**, **89** are diindium(III) complexes. Since the chelation of DPA to zinc(II) ion is stronger than that to indium(III) ion, we successively chelated indium(III) ion and zinc(II) ion. With the MALDI-TOF mass analysis we confirmed that the heterodinuclear complex was synthesized as the major species (m/*e* = 708.1 and 936.2 for **86** and **88**, respectively). Although we prepared their naphthyl derivatives based on the free ligand of **10**, the probes containing at least one indium ion did not exhibit any fluorescence. We, therefore, had no choice but the IDA for analyzing their association behaviors.

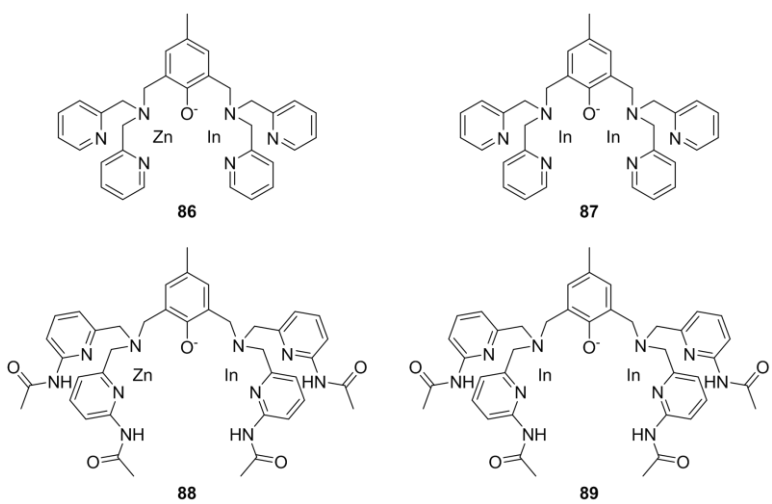

Scheme 2–9. Molecular structures of **86**-**89**.

We conducted titration experiments with PV. As depicted in Figure 2–15, all receptors induced spectral changes of PV. The addition of the **86** and **87** failed to show an isosbestic point during the titration experiments, which proves that the binding stoichiometry is not one-to-one. This might be because the enlarged cavity size by the substitution of Zn(II) for In(III) is capable of accommodating more than one PV molecule. The maximum absorbance reached to 609 nm when excessive amount of **86** and **87** was added, which also indicates the multiple binding of PV. Interestingly, the absorption spectra of PV was changed more drastically when added was **87** than **86**. Considering that charge of the blue-colored PV species is –2, the overall charge of **86**-PV and **87**-PV are likely to be +2 and +3, respectively. In that sense **87**-PV is far better receptor for PV than **86**-PV. Furthermore, hard character of indium(III) ion is advantageous to zinc(II) ion in binding to a oxyanionic catecholate moiety.

Meanwhile, **88** and **89** exhibited clear isosbestic points at 375 nm and 501 nm, which is strong indication of 1:1 binding stoichiometry. Also the absorption maxima reaching to 641nm at a plateau is a typical absorption maximum when PV binds to bis(Zn-DPA) receptor. Since the only difference of **88** and **89** from **86** and **87** is the presence of the four acetamide moieties, there is without a doubt that the amides suppresses the second binding of PV to **88** and **89**, possibly by its cavity size-confining effect. Because the 1:1 binding stoichiometry is more beneficial for analysis, further experiments were mainly conducted using **88** and **89**. Moreover, we observed almost identical binding behavior of PV to **88** and **89**.

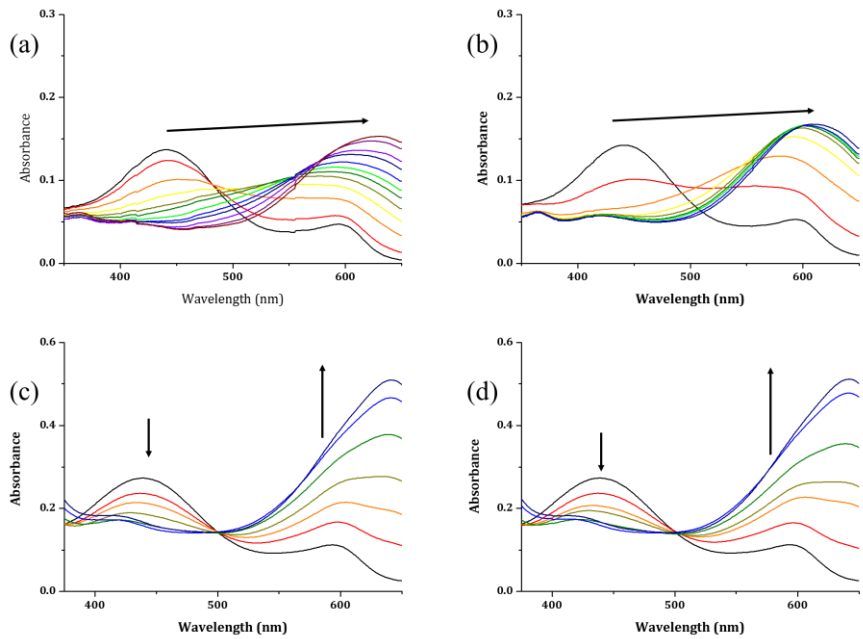

Figure 2–15. UV–Vis spectral change of PV (10 μM for a, and b, 20 μM for c, and d) upon gradual addition of (a) **86**, (b) **87**, (c) **88**, and (d) **89**.

Then we quantitatively analyzed the exchange kinetics. We prepared two vials containing a receptor solution those were successively added PPi and PV, or in a reversed order. After that, we measured the time elapsed for reaching the same color. Figure 2–16 shows a picture of **88** and **89** after 5 minutes of addition of anionic guests. Specifically, **89** reached the same color within 6 minutes, while **88** took about 3 hours. Considering that **52** requires more than 6 hours for the completion, there is certainly a cation size effect on the rate of exchange. As expected, we observed the faster exchange for the more In(III) substituted receptor.

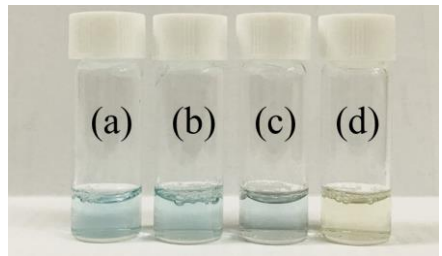

Figure 2–16. A picture of vials 5 minutes after mixing. Mixing order: (a) **89**, PV, then PPi, (b) **89**, PPi, then PV, (c) **88**, PV, then PPi, (d) **88**, PPi, then PV.

Since we identified a potential of **89** as a PPi receptor for real-time monitoring, we conducted an IDA experiment with PPi and ATP. Figure 2–17 shows the UV–Vis spectral changes of **89**-PV(30 μM and 20 μM, respectively) ensemble solution. We observed a clear absorbance change for PPi, while ATP induced barely visible changes. However, we could not reach a plateau until the addition of 80 μM PPi, which implies the binding between **89** and PPi is very weak. Indeed, we failed to calculate relative association constant of PPi against PV.

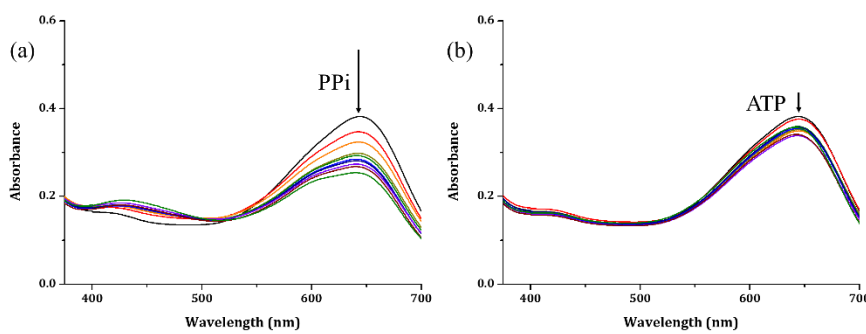

Figure 2–17. UV–Vis spectral changes of **89**–PV ensemble (30 μM and 20 μM, respectively) by gradual addition of (a) PPi or (b) ATP (0 ~ 80 μM).

3. Conclusion

We synthesized a series of bimetallic complexes by substituting Zn(II) ion by In(III) ion. The substitution enlarged the cavity size, which turned the one-to-one binding stoichiometry of **52** into a sophisticated binding behavior of **86** and **87**. Meanwhile, the presence of four amide groups forced to maintain the binding stoichiometry as one-to-one. Moreover, In(III) ion remarkably accelerated the rate of exchange. However, the **89**-PV ensemble system seemed not suitable for detecting PPi due to exceptional stability of **89**-PV complex.

4. Experimental section

4.1. General information

All chemicals were purchased from either Sigma–Aldrich or Tokyo Chemical Industry (TCI) and were used as received except anhydrous solvents. Thin layer chromatography was performed over Merck silica gel 60 F254 on aluminum foil. Silicycle 60 was used for the stationary phase in chromatographic separation or silica pad filtration. Celite® 545 was used for celite filtration. All ^{1}H and ^{13}C NMR spectra were obtained from Bruker DRX 300 NMR spectrometer. Absorption spectra were recorded on a JASCO V-730 spectrometer. LRMS were taken by MALDI-TOF mass analyzer (Bruker instrument).

4.2. Synthesis of the receptors

Synthesis of **86** and **88**: To an aliquot of free ligand (5 μM) in acetonitrile (0.1 mL) was treated by 51 μL of 0.1 M $InCl_3 \cdot 3H_2O$ in water, which was shaken for 10 minutes. The mixture was then treated with 51 μL of 0.1 M $Zn(ClO_4)_2 \cdot 6H_2O$ in acetonitrile and further shaken for 30 minutes. The mixture was lyophilized and used for spectroscopic experiments without further purification.

86: LRMS(MALDI-TOF) m/e: $[M]^+$ calcd for 708.1; found and 708.1.

88: LRMS(MALDI-TOF) m/e: $[M]^+$ calcd for 936.2; found and 936.0.

Synthesis of **87** and **89**: To an aliquot of free ligand (5 μM) in acetonitrile (0.1 mL) was treated by 102 μL of 0.1 M $InCl_3 \cdot 3H_2O$ in water, which was shaken for 30 minutes. The mixture was lyophilized and used for spectroscopic experiments without further purification.

86: LRMS(MALDI-TOF) m/e: $[M]^+$ calcd for 759.1; found and 759.1.

88: LRMS(MALDI-TOF) m/e: $[M]^+$ calcd for 987.2; found and 987.1.

Part III.

Molecular Probes for Pyrophosphate

Section 1. Background

1. Requirements of a highly selective molecular probe for pyrophosphate against ATP

PPi probes are highly beneficial in monitoring some enzymatic reactions that consume ATP and produces PPi. In many cases, a high concentration of ATP (> 1 mM) is required to ensure the maximum turnover rate of the enzymes, which is large excess compared to the amount of PPi produced during the analysis of the reaction.[132,133] Therefore, a probe that emits bright fluorescence only when it is bound to PPi is highly desirable for that purpose. However, ATP contains the entire structure of PPi, and the charge of ATP is identical to that of PPi at a physiological condition. These facts make it extremely difficult to achieve high selectivity toward PPi over ATP, as evident by the limited number of such probes.

The most straightforward approach for achieving high selectivity toward PPi over ATP is to make the probe to bind only to PPi. We developed a receptor that has an association constant as low as M^{-1} to ATP. However, even that receptor is almost fully saturated with 1 mM level of ATP. Incidentally, I have an opinion that the binding of ATP is inevitable unless we find another prominent structure than bis(Zn-DPA), or utilize another kind of intermolecular forces than charge-charge interaction. Therefore, we need to compromise on affinity issue.

Then, it is clearly the next step to make our probes to exhibit different signals when it forms a complex with PPi or ATP. Indeed, some of the probes developed so far satisfy the condition.[36] However, many of them have drawbacks, such as turn-off, and a small difference in emission intensity. Because it is without a doubt that a turn-on system is the most desirable for analyzing the (enzymatic) reactions, it is still urgent to develop a highly sensitive probe that shows turn-on and turn-off responses to PPi and ATP, respectively.

2. Energy levels of fluorophores and nucleobases

From the late-1990s, several research articles reported that nucleobases are capable of quenching the fluorescence of several famous fluorophores, including coumarin, fluorescein, BODIPY, and rhodamine by a PeT mechanism (Figure 3–1).[134-136] Guanine is the strongest quencher among nucleobase thanks to the lowest oxidation potential of 1.47 V (vs NHE). Adenine is in the second place with the oxidation potential at 1.9 V (vs NHE), which still have the ability to quench a number of fluorophores. The energy levels of the nucleobases seem so low that it is capable of quenching only a few fluorophores, Siedel pointed out that the electron transfer from nucleobase to excited fluorophores gains additional water-specific free energy that possibly comes from coupled proton transfer and a hydrophobic effect. Although the main quenching mechanism is PeT, nucleobases cannot compete with conventional quenchers based on FRET mechanism. However, these studies so far are meaningful in that they provide an opportunity to develop a quencher-free sensing system.

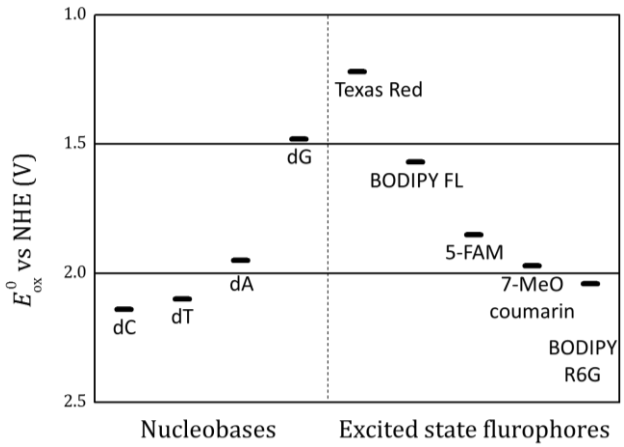

Figure 3–1. Oxidation potentials of nucleobases and excited state fluorophores. Recreated by permission from reference 134 and 135. Copyright 1996 American Chemical Society, 2001 The Japan Society for Analytical Chemistry.

Interestingly, our biological system manifests the opportunity of the quencher-free system. Flavin species are very famous biomolecules that emit fluorescence. Especially, riboflavin, also known as vitamin B_2, emits bright fluorescence with a fluorescence quantum yield (Φ_F) up to 26%. However, the intrinsic fluorescence of FAD is completely quenched (Φ_F = 0.03),[137] which is attributed by the close proximity of bases (isoalloxazine and adenine) as well as extremely fast electron transfer rate (adenine to excited isoalloxazine) mediated by strong electronic coupling.[138] Therefore, we expected that a properly designed molecular probe that contains a fluorophore such as isoalloxazine, fluorescein, or some of BODIPY family exhibit turn-off response specifically to ATP with help of a PeT mechanism.

Section 2. Molecular Probes with FRET–PeT Strategy

1. Introduction

The binding of anions to a metal complex restores the inherent property of the free ligand. It consequently forces the signal of a metal complex to change in a similar direction regardless of which anion is binding.[25] For instance, Probe **10** shows fluorescence turn-on responses to both PPi and ATP,[40] whereas some other ones exhibit turn-off responses.[139,140] Therefore, we envisioned that the combination of the turn-on response of **10** and fluorescence quenching ability of ATP might enable the complete spectroscopic differentiation of PPi from ATP.

Hong and colleagues recently reported an ensemble system that employs **10** and a boronic acid-based FRET quencher (**BA**).[141] At the initial state, **10** and BA form a complex to emit marginal fluorescence. Since boronic acids can bind to diol of nucleotides, the subsequent binding of nucleotide brings a quencher (**BA**) to a close proximity to the fluorophore, which results in the fluorescence quenching. Meanwhile, **10**–PPi complex, which lacks diol functional group, cannot form a covalent bond with BA, hence is fluorescent. It demonstrates a selective quenching of the fluorescence by using a unique property of nucleotide, but none of PPi.

2. Result and discussion

Since the quenching ability of nucleotides arises from the nucleobases, we envisioned that we could selectively quench the fluorescence of the probes by using it. The new strategy only requires single molecular sensor but a quencher, it would be more desirable than the previous ensemble system. Scheme 3–1 outlines our strategy to distinguish PPi and ATP, which utilizes two electronically separated fluorophores, one is the fluorescent core of **10** (**HPN**), and the other one is what we defined as a *mediator fluorophore*. A mediator fluorophore ought to reflect the fluorescence response of **10**, as well as the presence of adenine base through a quenching mechanism. Therefore, it should be quenched by adenine base and it is a potential energy transfer pair (Förster or Dexter) to **HPN** simultaneously. We selected isoalloxazine and 2',7'-dichlorofluorescein as mediator fluorophores because they have sufficiently low HOMO energy level to undergo a-PeT mechanism from adenine as well as absorption spectra that overlap with the emission spectrum of **10**-PPi complex.

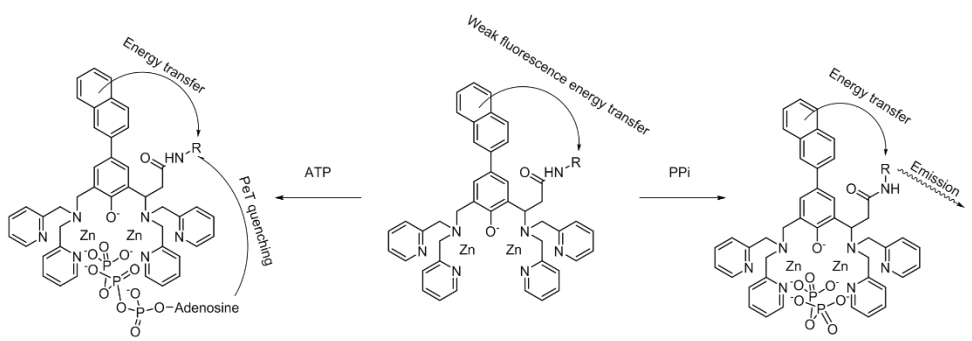

Scheme 3–1. A spectroscopic discrimination between PPi and ATP. R = mediator fluorophore

An efficient PeT quenching requires close proximity between two participants. In this case, the fluorophore needs to be near the adenine moiety or the binding site. Therefore, we decided to incorporate mediator fluorophores at the equatorial position to the bis(Zn-DPA) structure by means of the method developed in a previous section. We designed and synthesized probes **90** and **91** (Scheme 3–2) by a number of steps including Suzuki cross-coupling, asymmetric aminohydroxylation, deprotective cyclization, acyl transfer reaction, and amide coupling (See experimental section).

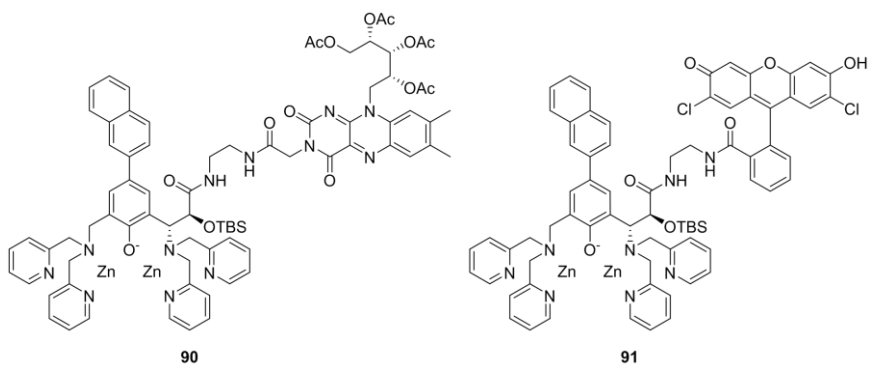

Scheme 3–2. The molecular structure of probes **90** and **91**.

To our regret, **90** and **91** did not show any change in fluorescence intensity during titration experiments with PPi and ATP. Moreover, they are essentially nonfluorescent even when no anionic guests are present, which implies the presence of additional intramolecular quenching mechanisms that have not been intended. The absence of the fluorescence of isoalloxazine fluorophore of **90** under selective excitation condition (λ_{ex} = 452 nm) also supports this hypothesis. In order to figure out the reason why they are nonfluorescent, we synthesized additional probes **92**, **93** and **94** that possesses different functional groups (Scheme 3–3).

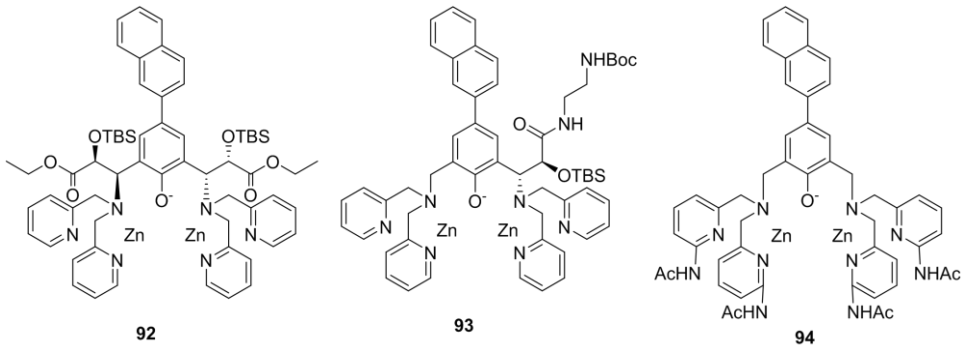

Scheme 3–3. The molecular structure of probes **92**-**94**.

The probe **92** was the only probe that responded to the addition of PPi and ATP. Because the binding of PPi (or ATP) to bis(Zn-DPA) moiety is tolerant toward every functional group that constitutes probes **90**-**94**, as evident by numerous probes reported, this result highlights that amide, carbamate and aminopyridine derivatives are potential quenchers to the fluorescence of the **HPN** core. In addition, the incapability of these functional groups to absorb visible light and the structural similarity of the probes strongly suggest that neither energy transfer (FRET or Dexter) nor a chelation (i. e., CHEF) is the mechanism of quenching. However, it should not be ignored that there is still a strong possibility of FRET between **HPN** core and attached fluorophores (isoalloxazine or fluorescein), which results in the complete quenching of **HPN** fluorescence.

Therefore, we suspected PeT as the responsible quenching mechanism. Figure 3–2 summarizes the typical energy levels of relevant functional groups and fluorophores involved in.[142-144] HOMO energy level of **HPN** is located at 0.95 V (vs NHE) which is high enough to quench most fluorophores that have sufficiently low HOMO energy level to be quenched by adenine. In other words, **HPN** is a powerful

quencher to any fluorophore that could be quenched by adenine. Then, the situation seems analogous to the fluorescent sensing of FMN by **17** (see Part I, Section 2), in which two fluorophores involved in the sensing system (pyrene/isoalloxazine and **HPN**/isoalloxazine derivatives, respectively) are a pair of not only FRET but also PeT. Therefore, it is very likely that **HPN** and flavin are in a mutually quenching relationship with extremely high quenching efficiency, while **17** did not fully quench the fluorescence of isoalloxazine moiety. We believe that the difference in quenching efficiency largely is attributed to whether the mechanism occurs in intermolecular or intramolecular scale. Moreover, 2-aminopyridine occupies similar HOMO energy level to that of **HPN,** 2-aminopyridine is also a potential quencher of the fluorophores.

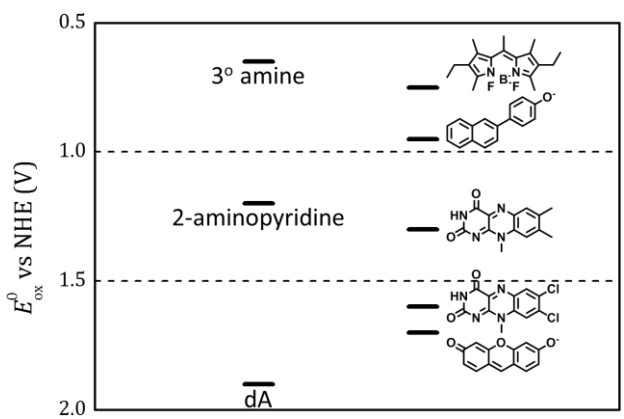

Figure 3–2. Energy diagram for selected functional groups and fluorophores.

3. Conclusion

The FRET–PeT strategy encounters an unavoidable problem that arises from the intrinsic energy level of the functional groups involved in the sensing system. Moreover, the large dependency of HOMO energy level of **HPN** to the corresponding phenol moiety strongly suggests that a molecular probe that shows selective turn-on response to PPi using PeT mechanism requires the absence of **HPN** core structure, at least phenol moiety.[145]

4. Experimental section

4.1. General information

All chemicals were purchased from Sigma-Aldrich or Tokyo Chemical Industry (TCI) and used as received. Thin layer chromatography was performed over Merck silica gel 60 F254 on aluminum foil. Silicycle 60 was used for the stationary phase in chromatographic separation. Celite® 545 was used for celite filtration. ^{1}H and ^{13}C NMR spectra were obtained from Bruker DRX 300 NMR spectrometer. Fluorescence spectra were recorded on a FP–8300 spectrophotometer (JASCO). LRMS were taken by MALDI-TOF mass analyzer (Bruker instrument).

4.2. Synthesis of the probes

Dichloromethane and tetrahydrofuran were distilled over calcium hydride and sodium/benzophenone ketyl, respectively. NMR samples were prepared by

dissolving in $CDCl_3$ or acetone-d_6. Multiplicities: s, singlet; d, doublet; t, triplet; m, multiplet; br, broad. Enantiomeric excesses (ee) were determined by chiral HOLC analysis over CHIRALPAK-IA with elution of IPA/hexane (5%, 1mL min^{-1}) detecting at 220 nm.

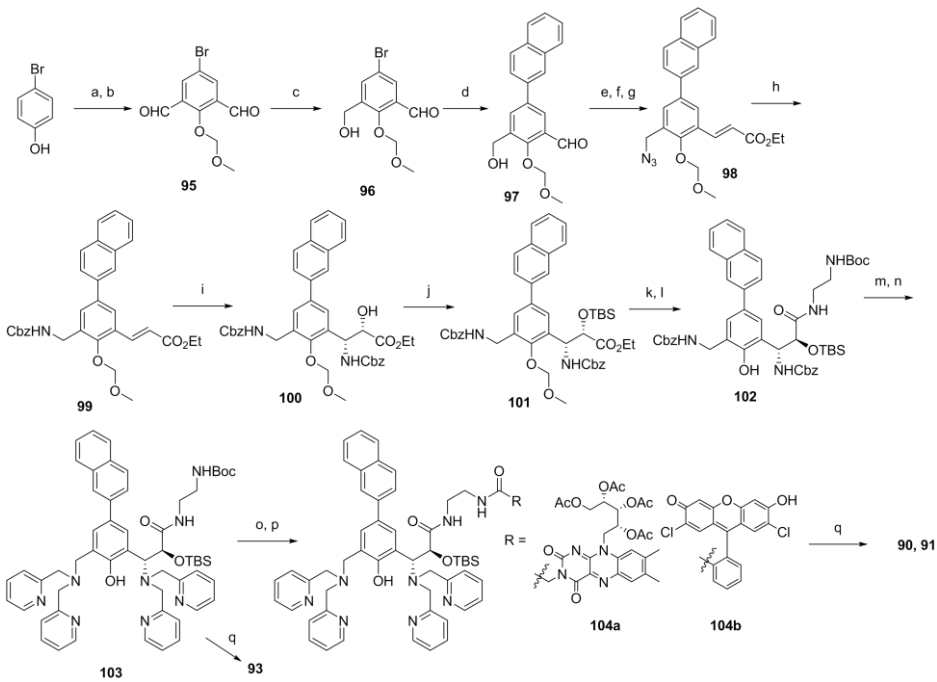

Scheme 3–4. Synthetic procedure for the probes **90**-**94**. a. hexamethylene tetramine, TFA, 80°C, 2 d; b, chloromethyl methyl ether, N,N-diisopropyl ethylamine, DCM; c, $NaBH_4$, EtOH–THF (1:1); d, 2-naphthaleneboronic acid, $Pd(PPh_3)_4$, $NaHCO_3$, glyme–water (4:1); e. methanesulfonyl chloride, Et_3N, DCM; f, NaN_3, DMF; g, triethyl phosphonoacetate, NaH, THF; h, PPh_3, benzyl chloroformate, THF–water (10:1); i, OsO4, $(DHQD)_2PHAL$, benzyl N-(4-chlorobenzoyloxy)carbamate, acetonitrile–water (6:1); j. TBSCl, imidazole, DMF; k, 33% TFA/DCM; l, tert-butyl N-(2-aminoethyl)carbamate, THF; m, $Pd(OAc)_2$, Et_3N, Et_3SiH, DCM; n, pyridine-2-carboxaldehyde, $NaBH(OAc)_3$, DCE; o, 16% TFA/DCM; p, fluorophore-acid, EDC, HOBt, DMF; q, $Zn(ClO_4)_2 \cdot 6H_2O$, acetonitrile.

Synthesis of **95**: To a solution of hexamethylenetetramine (84g, 0.6 mol, 4.0 equiv.) in TFA (450 mL) was added 25.7 g of 4-bromophenol (0.15 mol, 1.0 equiv.). The mixture was stirred for 2 days at 80°C and concentrated under reduced pressure. The residue was diluted by 4 M aqueous HCl (3 L) and stirred for 6 hours, during which time yellow precipitates were formed. The solid was collected via filtration using sintered glass funnel and washed with water (2 L × 3). The solid was re-dissolved in dichloromethane (1 L) and washed with water twice. The organic layer was dried over anhydrous Na_2SO_4, filtered, and concentrated under reduced pressure. The residue (~ 22 g, ~ 0.1 mol) was dissolved in anhydrous dichloromethane (250 mL). The solution was successively treated with N,N-diisopropyl ethylamine (23 mL, 0.13 mol) and chloromethyl methyl ether (8.4 mL, 0.11 mol), and stirred for 3 hours. The solution was quenched by adding 200 mL of water, and the organic layer was successively washed with water, half-saturated $NaHCO_3$, and brine. The organic layer was dried over anhydrous $MgSO_4$ and filtered through a pad of silica gel (5 cm). The filtrate was concentrated under reduced pressure to give 22.7 g of analytically pure **95** (55% in two steps). ^1H (300 MHz, $CDCl_3$) δ 10.31 (s, 2H), 8.21 (s, 2H), 5.23 (s, 2H), 3.63 (s, 3H). ^{13}C (75 MHz, $CDCl_3$) δ 187.6, 160.9, 137.5, 132.0, 118.9, 103.1, 58.5. LRMS (MALDI-TOF) m/z: $[M+H]^+$ calcd for $C_{10}H_{10}BrO_4$ 273.0; found 273.0.

Synthesis of **96**: To a pre-chilled solution of **95** (21.8 g, 80 mmol, 1.0 equiv.) in EtOH–THF (350 mL, 1:1) at –15°C was slowly added $NaBH_4$ (756 mg, 20 mmol, 0.25 equiv.). The mixture was stirred overnight before most of the solvent was evaporated in vacuo. The residue was diluted with 0.5 M HCl (200 mL) and extracted with dichloromethane (250 mL × 3). The combined organic layer was dried over anhydrous Na_2SO_4, filtered, and evaporated. The residue was purified by

chromatography over silica gel with gradient elution of ethyl acetate in hexanes (10 to 40%) to give analytically pure **96** (17.2 g, 78%). ^{1}H (300 MHz, $CDCl_3$) δ 10.36 (s, 1H), 8.17 (s, 1H), 8.08 (m, 2H), 7.96–7.77 (m, 3H), 7.76 (d, *J* = 6.9 Hz, 1H), 7.54 (m, 2H), 5.20 (s, 2H), 4.83 (s, 2H), 3.69 (s, 3H). ^{13}C (75 MHz, $CDCl_3$) δ .190.0, 157.88, 138.2, 136.3, 134.8, 133.6, 132.8, 129.6, 128.8, 128.4, 128.3, 127.7, 126.6, 126.3, 125.9, 125.0, 10,.8, 60.5, 57.9. LRMS (MALDI-TOF) m/z: $[M+H]^+$ calcd for $C_{10}H_{12}BrO_4$ 275.0; found 275.0.

Synthesis of **97**: **96** (5.5 g, 20 mmol, 1.0 equiv.), 2-naphthaleneboronic acid (3.8g, 22 mmol, 1.1 equiv.), $NaHCO_3$ (4.2 g, 50 mmol, 2.5 equiv.), and $Pd(PPh_3)_4$ (760 mg, 0.66 mmol, 3.3 mol–%) was dissolved in glyme–water (200 mL, 4:1) and refluxed for 10 hours under inert atmosphere. Glyme was evaporated in vacuo and the aqueous layer was extracted with dichloromethane (100 mL × 3). The combined organic layer was dried over anhydrous Na_2SO_4, and filtered through a pad of silica gel (~ 3 cm). The filtrate was evaporated under reduced pressure, and the residue was chromatographed over silica gel to give analytically pure **97** (5.6 g, 87%). ^{1}H (300 MHz, $CDCl_3$) δ 10.20 (s, 1H), 7.92 (s, 1H), 7.82 (s, 1H), 5.12 (s, 2H), 4.71 (s, 2H), 3.64 (s, 3H), 2.72 (br, 1H). ^{13}C (75 MHz, $CDCl_3$) δ 188.6, 157.3, 138.3, 138.1, 132.0, 130.8, 118.5, 101.8, 59.8, 58.0. LRMS (MALDI-TOF) m/z: $[M+H]^+$ calcd for $C_{20}H_{19}O_4$ 323.1; found 323.2.

Synthesis of **98**: 5 g of **97** (15.5 mmol, 1.0 equiv.) in anhydrous dichloromethane (100 mL) was successively treated with triethylamine (4.1 mL, 29 mmol, 1.9 equiv.) and methanesulfonyl chloride (1.44 mL, 18.6 mmol, 1.2 equiv.) at 0 °C. The mixture was stirred for 3 hours at the same temperature before being quenched by addition of water (100 mL). The biphasic mixture was extracted with dichloromethane (100 mL × 2). The combined organic layer was dried over

anhydrous Na2SO4, filtered, and evaporated under reduced pressure. The residue was re-dissolved in DMF (45 mL) and treated with sodium azide (2.0 g, 31 mmol, 2.0 equiv.). The mixture was stirred for 3 hours, and quenched by addition of water (150 mL). The aqueous layer was extracted with diethyl ether (150 mL × 3). The combined organic layer was dried over anhydrous $MgSO_4$, filtered, and evaporated under reduced pressure to afford 4.1 g of pure intermediate (~83% for 2 steps). To a suspension of sodium hydride (60% in mineral oil, 680 mg, 17 mmol, 1.3 equiv.) in anhydrous THF (125 mL) was added triethyl phosphonoacetate (3.4 mL, 17 mmol, 1.3 equiv.), and stirred until no more gas evolution was observed. A solution of intermediate in THF (30 mL) was added to the phosphonate solution via cannula. The mixture was stirred for 5 hours before the removal of volatiles under reduced pressure. The residue was diluted with water and the aqueous layer was extracted with diethyl ether (150 mL × 2). The combined organic layer was dried over anhydrous $MgSO_4$, filtered, and evaporated under reduced pressure. The residue was chromatographed over silica gel by a gradient elution of ethyl acetate in hexanes (10 to 40 %) to give analytically pure **98** (5.17 g, 12.5 mmol, 80% in 3 steps). ^{1}H (300 MHz, $CDCl_3$) δ 8.05 (d, *J* = 30 Hz, 2H), 7.97–7.88 (m, 4H), 7.30 (d, *J* = 10.1 Hz, 2H), 7.55–7.52 (m, 2H), 6.59 (d, *J* = 16.1 Hz, 1H), 5.10 (s, 2H), 4.59 (s, 2H), 4.32 (q, *J* = 7.1 Hz, 2H), 3.70 (s, 3H), 1.38 (t, *J* = 7.1 Hz, 3H). ^{13}C (75 MHz, $CDCl_3$) δ 166.8, 154.7, 139.5, 138.1, 136.9, 133.6, 132.8, 130.6, 129.2, 128.7, 128.2, 127.7, 126.6, 126.3, 125.8, 125.1, 120.2, 101.3, 60.7, 58.0, 50.1, 14.3. LRMS (MALDI-TOF) m/z: $[M+H]^+$ calcd for $C_{24}H_{24}N_3O_4$ 418.2; found 418.3.

Synthesis of **99**: To a mixture of **98** (5.0 g, 12 mmol, 1.0 equiv.), CbzCl (2.0 mL, 14 mmol, 1.17 equiv.) in THF–water (70 mL, 6:1) was treated with PPh_3 (3.9 g, 15 mmol, 1.25 equiv.). After stirring the mixture for 6 hours, an aqueous solution of

NH_4Cl (100 mL) was added and stirred for additional 3 hours. The aqueous layer was extracted with dichloromethane (100 mL × 3). The combined organic layer was dried over anhydrous Na_2SO_4, filtered, and evaporated under reduced pressure. The residue was chromatographed over silica gel by a gradient elution of ethyl acetate in hexanes (30 to 60 %) to give analytically pure **99** (3.8 g, 60%). ^1H (300 MHz, $CDCl_3$) δ 8.03–7.80 (m, 6H), 7.79 (s, 1H), 7.73 (d, *J* = 4.3 Hz, 1H), 7.55–7.52 (m, 2H), 7.37–7.25 (m, 5H) 6.58 (d, *J* = 16.1 Hz, 1H), 5.67 (br, 1H), 5.16 (s, 2H), 5.08 (s, 2H), 4.55 (d, *J* = 5.8 Hz, 2H), 4.34 (q, *J* = 7.1 Hz, 2H), 3.66 (s, 3H), 1.38 (t, *J* = 7.1 Hz, 3H). ^{13}C (75 MHz, $CDCl_3$) δ 166.8, 156.6, 155.0, 139.5, 138.1, 137.0, 136.6, 133.6, 133.5, 132.7, 130.8, 128.8, 128.6, 128.5, 128.2, 128.1, 127.7, 126.5, 126.2, 126.0, 125.8, 125.2, 120.1, 101.0, 66.8, 60.7, 57.8, 40.6, 14.3. LRMS (MALDI-TOF) m/z: $[M+H]^+$ calcd for $C_{32}H_{32}NO_6$ 525.2; found 525.3.

Synthesis of **100**: To a suspension of $(DHQD)_2PHAL$ (130 mg, 0.17 mmol, 2.4 mol–%), benzyl N-(4-chlorobenzoyloxy)carbamate (3.0 g, 9.8 mmol, 1.4 equiv.) in acetonitrile (60 mL) was treated with OsO4 (4 wt% in water, 1 mL, 0.14 mmol, 2 mol–%) at 0 °C. The mixture was stirred for 30 minutes at the same temperature before the successive addition of **99** (3.7 g, 7 mmol, 1.0 equiv.) and water (9 mL). The mixture was overnight at the same temperature, during which time a white precipitate formed. The mixture was diluted with ethyl acetate (250 mL), and the organic was washed with water, half-saturated $NaHCO_3$ solution (× 2). The organic layer was dried over anhydrous Na_2SO_4, filtered, and concentrated under reduced pressure. The residue was roughly chromatographed over silica gel by a gradient elution of ethyl acetate in hexanes (60 to 100 %) to give analytically pure **100** (3.6 g, 74%). ^1H (300 MHz, Acetone-d_6) δ 8.14 (s, 1H), 7.99–7.92 (m, 4H), 7.81 (m, 2H), 7.54–7.51 (m, 2H), 7.41–7.26 (m, 10H), 7.10 (d, *J* = 10 Hz, 1H), 6.81 (br, 1H), 5.85

(d, *J* = 10 Hz, 1H), 5.28 (s, 2H), 5.15 (s, 2H), 5.09 (s, 2H), 4.61–4.50 (m, 4H), 4.23–4.18 (m, 2H), 3.74 (s, 3H), 1.21 (t, *J* = 8.5 Hz, 3H). ^{13}C (75 MHz, Acetone-d_6) δ 172.1, 156.7, 155.9, 152.5, 137.9, 137.5, 137.4, 136.8, 134.2, 133.8, 133.4, 132.7, 128.5, 128.3, 128.3, 128.1, 127.8, 127.7, 127.6, 126.9, 126.8, 126.4, 126.0, 125.3, 125.2, 100.6, 72.9, 65.9, 65.8, 61.1, 57.2, 52.4, 39.9, 13.6. LRMS (MALDI-TOF) m/z: $[M+H]^+$ calcd for $C_{40}H_{41}N_2O_9$ 693.3; found 693.3.

Synthesis of **101**: To a solution of **100** (3.6 g, 5.2 mmol, 1.0 equiv.) and imidazole (500 mg, 7.3 mmol, 1.4 equiv.) in DMF (40 mL) was added TBSCl (940 mg, 6.2 mmol, 1.2 equiv.). The mixture was stirred for 3 hours at an ambient temperature before being quenched by addition of water (150 mL). The aqueous layer was extracted with diethyl ether (100 mL × 2). The combined organic layer was dried over anhydrous $MgSO_4$, filtered, and concentrated under reduced pressure. The residue was chromatographed over silica gel by elution of ethyl acetate in hexanes (33 %) to give analytically pure **101** (3.47 g, 83%). ^{1}H (300 MHz, Acetone-d_6) δ 8.21 (s, 1H), 8.0–7.84 (m, 6H), 7.55–7.52 (m, 2H), 7.41–7.28 (m, 9H, 7.13 (d, *J* = 9.7 Hz, 1H), 6.84 (br, 1H), 5.86 (d, *J* = 9.7 Hz, 1H), 5.30 (s, 2H), 5.14 (s, 2H), 5.08 (s, 2H), 4.73 (s, 1H), 4.60 (brs, 2H), 4.20 (m, 2H), 3.76 (s, 3H), 1.21 (t, *J* = 7.3 Hz, 3H), 0.73 (s, 9H), –0.11 (s, 3H), –0.36 (s, 3H). ^{13}C (75 MHz, Acetone-d_6) δ 170.9, 156.5, 155.8, 152.5, 137.7, 137.6, 137.4, 136.6, 133.9, 133.8, 133.5, 132.7, 128.3, 128.1, 127.8, 127.7, 127.6, 127.1, 126.7, 126.3, 125.9, 125.3, 100.7, 74.2, 65.9, 65.8, 60.7, 59.7, 57.3, 53.5, 39.9, 25.1, 20.0, 17.9, 13.7, –6.2, –6.59. LRMS (MALDI-TOF) m/z: $[M+H]^+$ calcd for $C_{46}H_{55}N_2O_9Si$ 806.4; found 806.4.

Synthesis of **102**: A solution of **101** (3.23 g, 4 mmol) was dissolved in anhydrous dichloromethane (15 mL) was treated by TFA–DCM (30 mL, 1:1) at 0 °C and stirred for 2.5 hours at the same temperature. The mixture was poured into 150

mL of half-saturated $NaHCO_3$ solution, and the aqueous layer was extracted with dichloromethane (100 mL × 3). The combined organic layer was dried over anhydrous $MgSO_4$, filtered, and concentrated under reduced pressure. The residue was re-dissolved by THF (40 mL), treated with *tert*-butyl N-(2-aminoethyl)carbamate (1.6 g, 10 mmol, 2.5 equiv.), and stirred overnight. Volatiles were removed under reduced pressure, and the residue was diluted with water. The aqueous layer was extracted with dichloromethane (100 mL × 2), and the combined organic layer was dried over anhydrous Na_2SO_4, filtered, and evaporated under reduced pressure. The residue was chromatographed over silica gel by a gradient elution of ethyl acetate in hexanes (40 to 60 %) to give analytically pure **102** (1.47g, 42 %). ^{1}H (300 MHz, Acetone-d_6) δ 9.73 (br, 1H), 8.05 (s, 1H), 7.95–7.90 (m, 6H), 7.62–7.52 (m, 3H), 7.52–7.40 (m, 3H), 7.40–7.25 (m, 9H), 6.80 (d, J = 7.8 Hz, 1H), 6.20 (br s, 1H), 5.81 (d, J = 7.7 Hz, 1H), 5.20–5.10 (m, 2H), 5.10–5.04 (m, 2H) 4.78 (s, 1H), 4.79–4.44 (m, 2H), 3.49–3.10 (m, 4H), 1.44 (s, 9H), 0.79 (s, 9H), –0.12 (s, 3H), –0.44 (s, 3H). ^{13}C (75 MHz, Acetone-d_6) δ 171.2, 159.4, 156.0, 155.6, 152.6, 138.2, 137.4, 136.6, 133.9, 132.4, 131.9, 128.9, 128.8, 128.4, 128.3, 128.1, 127.9, 127.8, 127.7, 127.6, 126.7, 126.4, 126.3, 125.6, 125.1, 124.4, 78.0, 74.3, 67.0, 65.9, 54.0, 40.8, 40.6, 39.0, 25.3, 17.7, 13.7, –6.4, –6.7. LRMS (MALDI-TOF) m/z: $[M+H]^+$ calcd for $C_{49}H_{61}N_4O_9Si$ 876.4; found 876.5.

Synthesis of **103**: To a solution of **102** (877 mg, 1 mmol, 1.0 equiv.), $Pd(OAc)_2$ (22.4 mg, 0.1 mmol, 0.1 equiv.) in dichloromethane (30 mL) was successively added triethylamine (42 μL, 0.3 mmol, 0.3 equiv.) and triethylsilane (0.45 mL, 3 mmol, 3.0 equiv.). The mixture was stirred for 7 hours, at which time NMR analysis indicates the complete disappearance of benzylic proton of Cbz group. The mixture was quenched by addition of a half-saturated $NaHCO_3$ solution (30 mL), and the biphasic

mixture was stirred for 3 hours at an ambient temperature. The aqueous layer was extracted with dichloromethane (30 mL × 2). The combined organic layer was dried over anhydrous Na_2SO_4, filtered through a pad of celite (4 cm), and evaporated under reduced pressure. The residue was re-dissolved by 1,2-dichloroethane (10 mL), and treated with pyridine-2-carboxaldehyde (0.58 mL, 6.0 mmol, 6.0 equiv.) and $NaBH(OAc)_3$ (1.28 g, 7.0 mmol, 7.0 equiv.). The mixture was stirred overnight before the volatiles were removed under reduced pressure. The residue was diluted with water (50 mL), and the aqueous layer was extracted with dichloromethane (50 mL × 3). The combined organic layer was dried over anhydrous Na_2SO_4, filtered, and evaporated under reduced pressure. The residue was chromatographed over silica gel by a gradient elution of methanol in dichloromethane (0 to 7 %) to give **103** (504 mg, 52 %). LRMS (MALDI-TOF) m/z: $[M+H]^+$ calcd for $C_{57}H_{69}N_8O_5Si$ 972.5; found 972.7.

Synthesis of **104**: 200 mg of **103** (0.21 mmol) in 5 mL of dichloromethane was treated with 1 mL of TFA, and stirred for 3 hours at an ambient temperature. The mixture was poured into 12 mL of half-saturated $NaHCO_3$ solution, and the aqueous layer was extracted with dichloromethane twice. The combined organic layer was dried over anhydrous Na_2SO_4, filtered, and evaporated under reduced pressure. The residue, fluorophore-acid (0.31 mmol, 1.5 equiv. flavin-acid[146] or 2',7'-dichlorofluorescein[147]), EDC·HCl (59 mg, 0.31 mmol, 2.0 equiv.), and HOBt (27 mg, 0.2 mmol, 1.0 equiv.) was dissolved in DMF (1 mL), and the mixture was stirred overnight. Volatiles were removed in vacuo, and the residue was diluted with water (5 mL). The aqueous layer was extracted with dichloromethane (10 mL × 3). The combined organic layer was dried over anhydrous Na_2SO_4, filtered, and evaporated under reduced pressure. The residue was chromatographed over silica gel by a

gradient elution of methanol in dichloromethane (0 to 10 %) to afford pure products. **104a**: 70.4 mg. NMR is too complicate to assign completely. LRMS (MALDI-TOF) m/z: $[M+H]^+$ calcd for $C_{79}H_{89}N_{12}O_{14}Si$ 1456.6; found 1457. **104b**: 126 mg. NMR is too complicate to assign completely. LRMS (MALDI-TOF) m/z: $[M+H]^+$ calcd for $C_{72}H_{68}Cl_2N_8O_7Si$ 1254.4; found 1255.

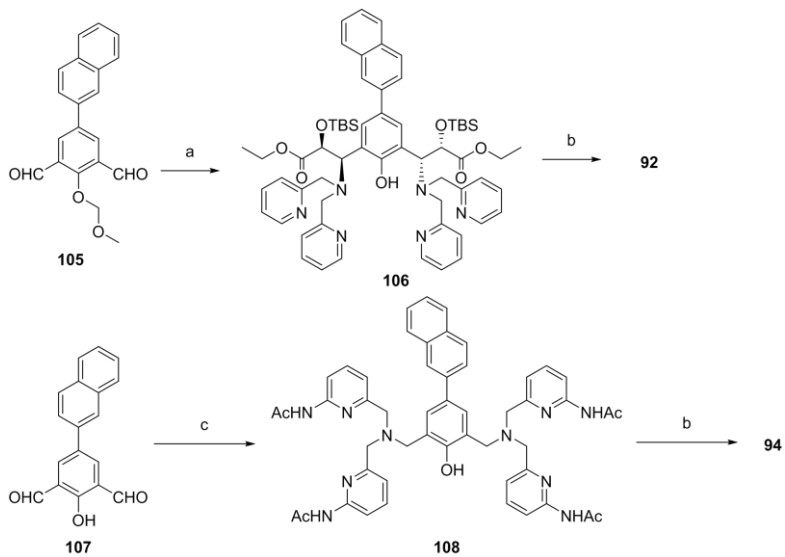

Scheme 3–5. Synthesis of probes **92** and **94**. a, analogous to Part II, Section 3; b, $Zn(ClO_4)_2 \cdot 6H_2O$, acetonitrile; c, bis(6-acetamidopyridin-2-ylmethyl)amine, $NaBH(OAc)_3$, DCE.

Synthesis of **106**: **106** was synthesized analogously to (*R*,*R*)-**80b**, using **105** instead of **75**. LRMS (MALDI-TOF) m/z: $[M+H]^+$ calcd for $C_{62}H_{79}N_6O_7Si_2$ 1075.5; found 1075.8.

Synthesis of **108**: To a solution of **107**[148] (56 mg, 0.2 mmol, 1.0 equiv.) and bis((6-acetamidopyridin-2-yl)methyl)amine (138 mg, 0.44 mmol, 2.2 equiv.) in 1,2-dichloroethane (3 mL) was treated with $NaBH(OAc)_3$ (136 mg, 0.6 mmol, 3.0 equiv.).

The mixture was stirred overnight before being concentrated under reduced pressure. The residue was taken up by water (10 mL), and the aqueous layer was extracted with dichloromethane (10 mL × 3). The combined organic layer was dried over anhydrous Na_2SO_4, filtered and evaporated under reduced pressure. The residue was chromatographed over silica gel by a gradient elution of methanol in dichloromethane (0 to 5 %) to give analytically pure **108** (123 mg, 71 %). ^{1}H (400 MHz, Acetone-d_6) δ 11.07 (s, 1H), 9.28 (s, 4H), 8.05 (d, J = 8.2 Hz, 4H), 7.99 (s, 1H), 7.96–7.85 (m, 3H), 7.74 (dd, J = 8.5, 1.8 Hz, 1H), 7.68 (t, J = 7.8 Hz, 4H), 7.60 (s, 2H), 7.54–7.39 (m, 2H), 7.26 (d, J = 6.1 Hz, 4H), 3.88 (s, 4H), 3.81 (s, 8H), 2.14 (s, 12H). LRMS (MALDI-TOF) m/z: $[M+H]^+$ calcd for $C_{50}H_{51}N_{10}O_5$ 871.4; found 871.4.

Synthesis of **90**-**94**: 5 μmol of free ligand (**104a**, **104b**, **103**, **106**, and **108** for **90**-**94**, respectively) in acetonitrile (0.1 mL) was treated with $Zn(ClO_4)_2 \cdot 6H_2O$ (3.82 mg, 10.25 μmol, 2.05 equiv.) in acetonitrile (0.1 mL). The mixture was shaken for 30 minutes and lyophilized and used without further purification.

Section 3. Molecular Probes with PeT Strategy

1. Introduction

At the beginning of this part, we discussed several requirements for a probe that is suitable for monitoring enzymatic reactions. Particularly for binding strength, a probe preferably has a moderate association constant for it to be mostly saturated in the presence of a millimolar concentration of ATP, which usually is satisfied indeed. Therefore, we can expect that there would be a negligible amount of free probe in the enzymatic reaction mixture. Thanks to the condition, we need to develop a turn-off probe for ATP, but not a turn-on probe for PPi, which widen the choice of fluorophore. For instance, BODIPY R6G dye could be a choice of fluorophore because of high susceptibility to PeT quenching in the presence of nucleotide. However, we could not select it for designing FRET–PeT probes because it is not a FRET acceptor to **HPN** in that its absorption spectra does not overlap with the emission spectra of **HPN**.

In a prior section, we have debated about what mechanisms we should give up for designing a PPi-selective turn-on probe using PeT strategy. For example, FRET mechanism using **HPN** as the FRET donor is incompatible with PeT mechanism because of the intrinsic HOMO energy levels of adenine and **HPN** moieties. Besides, amine-containing functional groups such as amide and carbamates would be the final option for a linker for their potential ability as a fluorescence

quencher. Therefore, we designed additional PeT-based probes for PPi by removing aforementioned functional groups.

2. Result and discussion

We designed new PeT-based probes **109**, **110**, and **111** (Scheme 3–6). The probes contain bis(Zn-DPA) moiety without phenol group, and fluorophores, which are connected by alkyl ether linkage. For the convenience of the synthesis, we selected amide linker for probe **126**. The probes were synthesized in several steps including S_N2, reductive amination, Staudinger reduction, and acylation of amine (see experimental section).

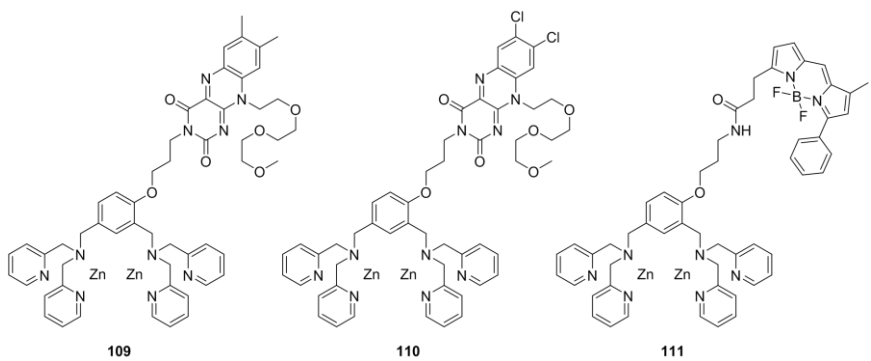

Scheme 3–6. The molecular structure of probes **109**-**111**.

We conducted titration experiments with PPi and ATP using probe **109** and **110**. As depicted in Figure 3–3, the addition of PPi and ATP both slightly increased the fluorescence of **109**. On the other hand, the fluorescence of **110** was decreased

by a small extent by the addition of either PPi or ATP, and a little bit more in the presence of GTP. Although it is intriguing that the structurally similar **109** and **110** showed an opposite behavior in a titration experiment, the reason for it is unclear. However, we believe that the fluorophores electronically interact with Zn-DPA or anisole moieties. It is also noticeable that the change in fluorescence is almost the same regardless of the added ion (Table 3–1). This clearly indicates that the changes in fluorescence are mostly attributed to the binding events that restore the inherent properties of the probes but not to the interaction between the fluorophores and adenine moiety.

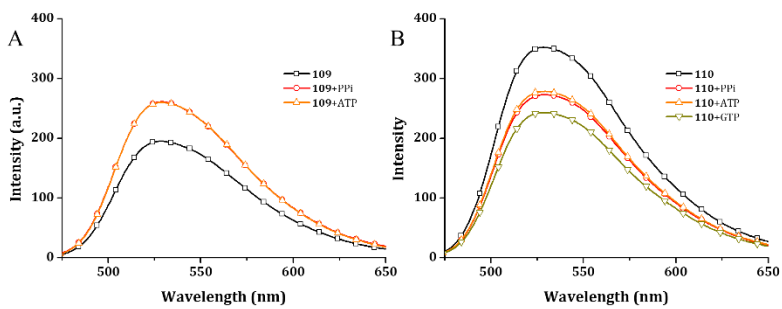

Figure 3–3. Fluorescence response of (A) **109** (10 μM) and (B) **110** (20 μM) toward 50 μM of PPi (red lines) and ATP (orange lines).

Table 3–1. The fluorescence intensity changes at λ_{max} ($\Delta F = I_f/I_0 - 1$) of probes in the presence of 5 equivalents of the guests.

	109	**110**
PPi	+35.2 %	–22.4 %
ATP	+34.9 %	–21.0 %

Probe **111** was also titrated with PPi and ATP. However, we could not observe any significant change in fluorescence intensity (Figure 3–4). Therefore, it is very likely that there would be no interaction between BODIPY R6G dye and any other functional group involved in the sensing system. Considering the typical hydrophobicity of the BODIPY dyes,[149] the molecular structures of the probes appear to force their dyes to separate from the bound adenine moiety.

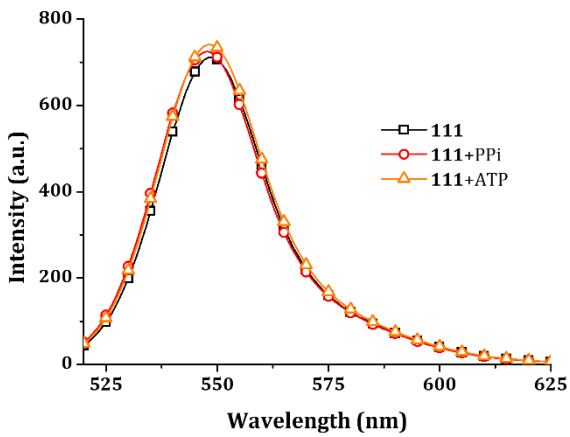

Figure 3–4. Fluorescence response of **111** (10 μM) to PPi and ATP (5 equiv.).

In order to bring fluorophore and nucleobase more closely, we designed additional molecular probe **112** using monosubstituted DPA derivative (Figure 3–5). Although probes **112** and **111** are consisted of virtually identical functional groups, they exhibited completely different response to anions. The fluorescence of **112** was greatly diminished in the presence of GTP and PPi concomitant with slight hypsochromic shift (550 nm to 548 nm), while ATP barely quenched the fluorescence of **112** (Figure 3–5). Considering the fluorescence quenching ability of PPi, the nucleobases are surely affecting the fluorescence quantum yield of the

fluorophores through certain kind of interactions. Especially in this case, adenine and guanine acted like fluorescence enhancer and quencher, respectively. We also calculated apparent association constant (K_a) between anions and **112** using the fluorescence intensity change at maximum under assumption of 1:1 binding. The strongest binding of **112** was observed for GTP (2.05×10^6 M^{-1}) followed by ATP (1.92×10^6 M^{-1}), and PPi exhibited weakest binding to **112** (1.03×10^6 M^{-1}), which also suggest the physical interaction between nucleobase and fluorophore giving additional driving force for binding.

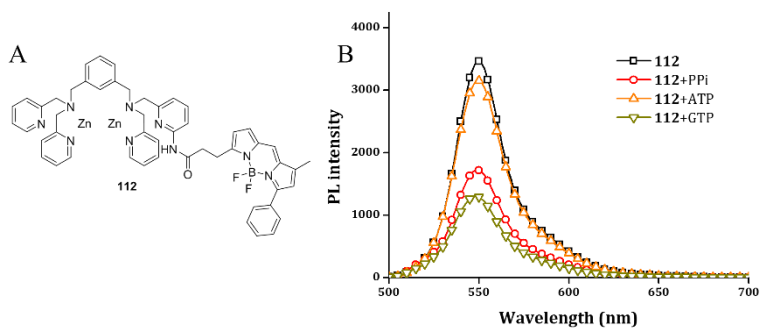

Figure 3–5. (A) Molecular structure and (B) the fluorescence response of **112** (10 μM) toward various PPi-containing anions (50 μM each) in HEPES buffered solution (10 mM pH 7.40, 1% DMSO)

Because BODIPY derivatives are well-known for high hydrophobicity and environmental sensitivity, we envisioned that the fluorescence response would be largely affected by the media, particularly when overall polarity was decreased. Therefore, we varied the acetonitrile content of the media from 10 to 30% and measured the fluorescence response of **112** toward anions (Figure 3–6). We found; (1) overall intensity was enhanced as the acetonitrile content was increased, which is typical for simple BODIPY dyes,[150] (2) the fluorescence enhancement ($I_{30\%CH3CN}$

– $I_{10\%CH3CN}$) for PPi (1170 a.u.) was bigger than those for ATP (543 a.u.) or GTP (601 a.u.), (3) the fluorescence intensity of **112** was consistently measured in order of ATP-bound > free > GTP-bound state, (4) the fluorescence intensity of **112**+PPi and **112**+ATP were almost identical in the media containing 30% acetonitrile, possibly due to negligible interaction between adenine moiety and fluorophore. Therefore, the fluorescence modulation seemed to be ascribed to the conformational change depending on the solvent composition,[151] and the binding preference to aromatic surface, which is greater for guanine than adenine moiety.[152]

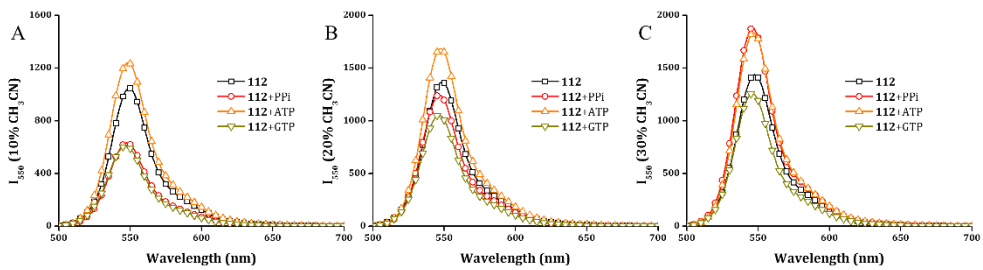

Figure 3–6. Fluorescence response of **112** (10 μM) toward various PPi-containing anions (50 μM each) in HEPES buffered solution (10 mM pH 7.40, 1% DMSO) containing (A) 10%, (B) 20%, and (C) 30% of acetonitrile.

3. Conclusion

A number of probes were designed for selective fluorescence turn-off response toward nucleotides. Fluorophores having low-lying HOMO energy level for efficient PeT from nucleobase were connected to bis(Zn-DPA) moiety through moderately flexible linkers (2-3 carbon units). We successfully demonstrated the importance of the choice of fluorophore and spatial arrangement for enabling the nucleotide-

selective quenching effect by comparing the probes **109**-**112**. The fluorescence of **109** was enhanced by the presence of anionic guests while **110** exhibited only guanine-specific quenching effect, which is presumably due to extraordinary quenching ability of guanine. Contrary to the completely silent behavior of **111** to binding, **112** exhibited guanine-specific quenching and adenine-specific enhancing properties. We expect solvent polarity-depending response of **112** would be utilized in monitoring turnover of ATP and GTP to PPi selectively by using corresponding media.

4. Experimental section

4.1. General information

All chemicals were purchased from either Sigma–Aldrich or Tokyo Chemical Industry (TCI) and were used as received except anhydrous solvents. Solvents were purchased from Samchun Chemical Corporation. Thin layer chromatography was performed over Merck silica gel 60 F254 on aluminum foil. Silicycle 60 was used for the stationary phase in chromatographic separation or silica pad filtration. Celite® 545 was used for celite filtration. All ^{1}H and ^{13}C NMR spectra were obtained from Bruker DRX 300 NMR spectrometer or Agilent 400MHz DD2MR400 spectrometer. Fluorescence emission spectra were recorded on a JASCO FP-8300 spectrophotometer. LRMS were taken by MALDI-TOF mass analyzer (Bruker Instrument Inc.).

4.2. Synthesis of the probes

Dichloromethane and tetrahydrofuran were distilled over calcium hydride and sodium/benzophenone ketyl, respectively. NMR samples were prepared by dissolving in $CDCl_3$ or acetone-d_6. Multiplicities: s, singlet; d, doublet; t, triplet; m, multiplet; br, broad.

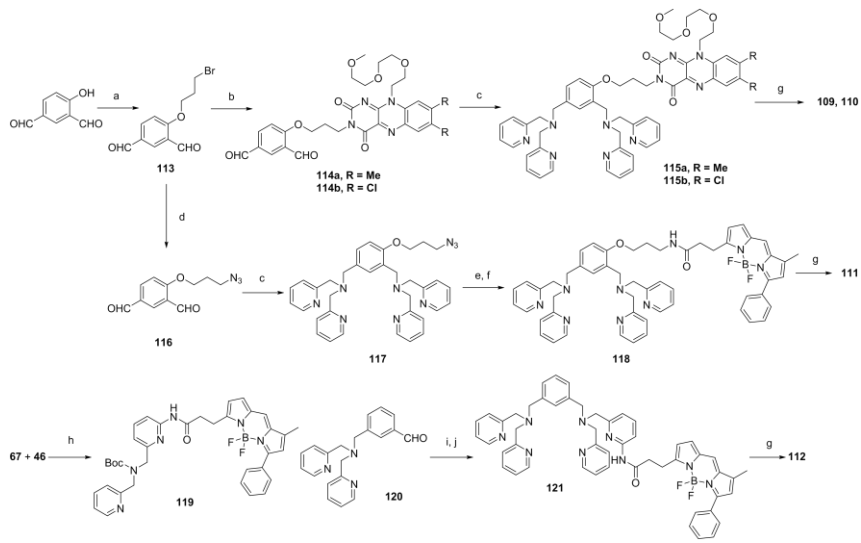

Scheme 3–7. Synthetic procedures for probes **109**-**112**. a, 1,3-dibromopropane, K_2CO_3, acetone; b, flavins, K_2CO_3, DMF; c, bis(2-pyridylmethyl)amine, NaBH(OAc)3, DCE; d, NaN_3, DMF; e, PPh_3, THF–water (9:1); f, **46**, EDC·HCl, DMF; g, $Zn(ClO_4)_2·6H_2O$, acetonitrile; h, EDC·HCl, DMF; i, 20% TFA in DCM; j, $NaBH(OAc)_3$, 1,2-DCE.

Synthesis of **113**: To a stirred solution of 4-hydroxyisophthalaldehyde (1.5 g, 10 mmol, 1.0 equiv.) in acetone (50 mL) was treated with K_2CO_3 (2.7 g, 20 mmol, 2.0 equiv.) and 1,3-dibromopropane (2.04 mL, 20 mmol, 2.0 equiv.). The mixture was gently heated for 6 hours. Most of the acetone was removed under reduced pressure, and the residue was dissolved in water (40 mL). The aqueous layer was extracted with dichloromethane (50 mL × 3), and the combined organic layer was

dried over anhydrous $MgSO_4$, filtered, and concentrated. The residue was chromatographed over silica gel by a gradient elution of ethyl ether in hexanes (10 to 20 %) to give analytically pure **127** (4.4 g, 81 %). ^{1}H NMR (300 MHz, $CDCl_3$) δ 10.51 (s, 1H), 9.98 (s, 1H), 8.36 (d, *J* = 2.2 Hz, 1H), 8.15 (dd, *J* = 8.7, 2.2 Hz, 1H), 7.20 (d, *J* = 8.7 Hz, 1H), 4.39 (t, *J* = 5.9 Hz, 2H), 3.66 (t, *J* = 6.2 Hz, 2H), 2.57–2.30 (m, 2H).

Synthesis of **114**: **113** (0.54 g, 2.0 mmol, 1.0 equiv.), K_2CO_3 (0.55 g, 4 mmol, 2.0 equiv.) and flavin derivatives[59] (2.2 mmol, 1.1 equiv.) were dissolved in DMF (20 mL). The mixture was gently heated for 4 hours. Volatiles were removed in vacuo, and the residue was diluted with water (50 mL). The aqueous layer was extracted with chloroform (40 mL × 3), and the combined organic layer was dried over anhydrous $MgSO_4$, filtered, and evaporated under reduced pressure. The residue was chromatographed over silica gel by a gradient elution of methanol in EtOAc–DMC mixture (0 to 3%, 4:6) to give analytically pure products (607 mg for **114a**, 622 mg for **114b**).

114a: ^{1}H NMR (300 MHz, $CDCl_3$) δ10.36 (s, 1H), 9.84 (s, 1H), 8.16 (s, 1H), 8.01 (d, *J* = 8.5 Hz, 1H), 7.93 (s, 1H), 7.72 (s, 1H), 7.09 (d, *J* = 8.6 Hz, 1H), 4.86 (t, *J* = 4.9 Hz, 2H), 4.31 (q, *J* = 5.9 Hz, 4H), 3.95 (t, *J* = 4.9 Hz, 2H), 3.58–3.37 (m, 8H), 3.27 (s, 3H), 2.50 (s, 3H), 2.39 (s, 3H), 2.37–2.25 (m, 2H). ^{13}C NMR (75 MHz, $CDCl_3$) δ 207.19, 190.13, 188.44, 165.16, 160.09, 155.45, 148.71, 147.70, 136.75, 135.78, 135.17, 135.01, 132.13, 132.00, 131.33, 129.43, 124.70, 116.92, 113.16, 71.76, 70.80, 70.44, 68.01, 67.58, 58.92, 45.37, 39.05, 30.10, 27.62, 21.38, 19.43. LRMS (MALDI-TOF) m/z: $[M+H]^+$ Calcd for $C_{30}H_{35}N_4O_8$ 579.2; Found 579.3.

114b: ^{1}H NMR (300 MHz, $CDCl_3$) δ 10.38 (s, 1H), 9.91 (s, 1H), 8.32 (s, 1H), 8.23 (d, *J* = 2.4 Hz, 2H), 8.08 (dd, *J* = 8.7, 2.0 Hz, 1H), 7.13 (d, *J* = 8.7 Hz, 1H),

4.97–4.76 (m, 2H), 4.37 (dd, *J* = 13.7, 6.3 Hz, 4H), 4.01 (t, *J* = 4.5 Hz, 2H), 3.68–3.40 (m, 8H), 3.32 (s, 3H), 2.51–2.28 (m, 2H). ^{13}C NMR (75 MHz, $CDCl_3$) δ 190.12, 188.48, 165.02, 159.21, 155.00, 148.89, 140.19, 137.53, 135.83, 134.55, 133.08, 132.59, 131.76, 131.02, 129.59, 124.76, 119.20, 113.08, 71.82, 70.97, 70.57, 70.49, 68.31, 67.59, 59.00, 46.41, 39.52, 27.54. LRMS (MALDI-TOF) m/z: $[M+H]^+$ Calcd for $C_{28}H_{29}Cl_2N_4O_8$ 619.1; Found 619.1.

Synthesis of **115**: To a solution of **114** (0.3 mmol, 1.0 equiv.) and bis(2-pyridylmethyl)amine (0.12 mL, 0.66 mmol, 2.2 equiv.) in 1,2-dichloroethane (5 mL) was treated with $NaBH(OAc)_3$ (190 mg, 0.9 mmol, 3.0 equiv.). The mixture was stirred overnight. Volatiles were removed under reduced pressure, and the residue was diluted with water (20 mL). The aqueous layer was extracted with dichloromethane (20 mL × 3). The combined organic layer was dried over anhydrous $MgSO_4$, filtered, and evaporated. The residue was chromatographed over silica gel by a gradient elution of methanol in dichloromethane (0 to 10 %) to give analytically pure **115** (134 mg for **115a**, 111 mg for **115b**).

115a: ^{1}H NMR (300 MHz, Acetone-d_6) δ (d, *J* = 4.2 Hz, 4H), 7.89 (s, 1H), 7.82 (s, 1H), 7.78 (s, 1H), 7.77–7.54 (m, 8H), 7.20 (dd, *J* = 8.5, 4.6 Hz, 5H), 6.88 (d, *J* = 8.3 Hz, 1H), 4.88 (d, *J* = 4.9 Hz, 2H), 4.23 (t, *J* = 6.5 Hz, 2H), 4.09 (t, *J* = 6.0 Hz, 2H), 3.95 (t, *J* = 5.0 Hz, 2H), 3.77 (dd, *J* = 19.8, 10.9 Hz, 8H), 3.65–3.52 (m, 4H), 3.49–3.38 (m, 4H), 3.38–3.28 (m, 2H), 3.22 (s, 3H), 2.53 (s, 3H), 2.42 (s, 3H), 2.20 (dd, *J* = 12.8, 6.5 Hz, 2H). LRMS (MALDI-TOF) m/z: $[M+H]^+$ Calcd for $C_{54}H_{61}N_{10}O_6$ 945.5; Found 945.4.

115b: ^{1}H NMR (300 MHz, Acetone-d_6) δ 8.48 (t, *J* = 4.9 Hz, 4H), 8.38 (s, 1H), 8.28 (s, 1H), 7.79 (s, 1H), 7.76–7.61 (m, 8H), 7.21 (dd, *J* = 10.2, 6.4 Hz, 5H), 6.88 (d, *J* = 8.3 Hz, 1H), 4.91 (s, 2H), 4.24 (t, *J* = 6.7 Hz, 2H), 4.10 (t, *J* = 6.1 Hz, 2H),

3.98 (t, *J* = 4.7 Hz, 2H), 3.91–3.69 (m, 10H), 3.61 (s, 2H), 3.53 (d, *J* = 4.9 Hz, 2H), 3.46 (dd, *J* = 6.2, 3.5 Hz, 2H), 3.42 (d, *J* = 6.5 Hz, 2H), 3.35 (dd, *J* = 10.5, 5.4 Hz, 2H), 3.22 (s, 3H), 2.29–2.13 (m, 2H). LRMS (MALDI-TOF) m/z: $[M+H]^+$ Calcd for $C_{52}H_{55}Cl_2N_{10}O_6$ 945.5; Found 945.4.

Synthesis of **116**: To a solution of **113** (1.14 g, 4.21 mmol, 1.0 equiv.) in DMF (10 mL) was added 2 mL of aqueous NaN_3 (550 mg, 8.4 mmol, 2.0 equiv.). The mixture was stirred for 4 hours, and the volatiles was removed in vacuo. The residue was diluted with water (30 mL) and extracted with dichloromethane (30 mL × 2). The combined organic layer was dried over anhydrous Na_2SO_4, filtered, and evaporated. The residue was chromatographed over silica gel by a gradient elution of ethyl ether in hexane (10 to 30 %) to give analytically pure **116** (814 mg, 83 %).

Synthesis of **117**: To a solution of **116** (0.8 g, 3.4 mmol, 1.0 equiv.) and bis(2-pyridylmethyl)amine (1.36 mL, 7.6 mmol, 2.2 equiv.) in 1,2-dichloroethane (20 mL) was treated with $NaBH(OAc)_3$ (2.18 g, 10.3 mmol, 3.0 equiv.). The mixture was stirred overnight. Volatiles were removed under reduced pressure, and the residue was diluted with water (100 mL). The aqueous layer was extracted with dichloromethane (100 mL × 3). The combined organic layer was dried over anhydrous $MgSO_4$, filtered, and evaporated. The residue was chromatographed over silica gel by a gradient elution of methanol in dichloromethane (0 to 10 %) to give analytically pure **117** (1.32 g, 64 %).

Synthesis of **118**: To a solution of **117** (300 mg, 0.5 mmol, 1.0 equiv.) in THF–water (10 mL, 9:1) was added PPh_3 (197 mg, 0.75 mmol, 1.5 equiv.). The mixture was vigorously stirred for 6 hours, and diluted with water (30 mL). The aqueous layer was extracted with dichloromethane (30 mL × 3). The combined organic layer was dried over anhydrous Na_2SO_4, filtered, and evaporated. The residue, **46** (212 mg,

0.6 mmol, 1.2 equiv.), EDC·HCl (114 mg, 0.6 mmol, 1.2 equiv.) was dissolved in DMF (3 mL). The mixture was stirred overnight and diluted with water (30 mL). The aqueous layer was extracted with dichloromethane (40 mL × 3). The combined organic layer was dried over anhydrous Na_2SO_4, filtered, and evaporated under reduced pressure. The residue was chromatographed over silica gel by a gradient elution of methanol in dichloromethane (0 to 12 %) to give analytically pure **118** (211 mg, 46 %).

Synthesis of **119**: To a solution of **67** (157 mg, 0.5 mmol, 1.0 equiv.), 46 (177 mg, 0.5 mmol, 1.0 equiv.) in anhydrous DMF (5 mL) was treated with EDC·HCl (114 mg, 0.6 mmol, 1.2 equiv.). The mixture was stirred overnight and diluted with water (30 mL). Aqueous layer was extracted with dichloromethane (40 mL × 3). The combined organic layer was dried over anhydrous Na_2SO_4, filtered, and evaporated under reduced pressure. The residue was chromatographed over silica gel by an elution of ethyl acetate to give analytically pure **119** (214 mg, 66% yield). ^{1}H NMR (300 MHz, $CDCl_3$) δ 9.55 (d, *J* = 5.5 Hz, 1H), 8.51 (d, *J* = 4.2 Hz, 1H), 8.13 (d, *J* = 8.2 Hz, 1H), 8.04–7.97 (m, 2H), 7.82–7.71 (m, 2H), 7.69 (s, 1H), 7.55–7.40 (m, 3H), 7.39–7.28 (m, 1H), 7.24 (dd, *J* = 7.1, 5.3 Hz, 1H), 7.18 (d, *J* = 4.0 Hz, 1H), 7.03 (dd, *J* = 14.7, 7.4 Hz, 1H), 6.65 (s, 1H), 6.53 (d, *J* = 4.0 Hz, 1H), 4.55 (t, *J* = 30.7 Hz, 4H), 3.36 (t, *J* = 7.6 Hz, 2H), 2.97 (t, *J* = 7.6 Hz, 2H), 2.39 (s, 3H), 1.39 (s, *J* = 10.2 Hz, 9H). LRMS (MALDI-TOF) m/z: $[M+H]^+$ Calcd for $C_{36}H_{38}BF_2N_6O_3$ 651.3; Found 651.3.

Synthesis of **121**: A pre-chilled solution of 119 (160 mg, 0.25 mmol) in dichloromethane (2 mL) at 0°C was treated with TFA-DCM mixture (33%, 3 mL). The mixture was stirred for 3 h before being quenched by addition of half-saturated $NaHCO_3$ solution (20 mL). Aqueous layer was extracted with dichloromethane three

times. Combined organic layer was dried over anhydrous Na_2SO_4, filtered, and concentrated under reduced pressure. The residue was redissolved in 1,2-dichloroethane (4 mL) and successively added **120**[153] (73 mg, 0.23 mmol), and $NaBH(OAc)_3$ (84.8 mg, 0.4 mmol). The mixture was stirred overnight and concentrated under reduced pressure before being quenched by addition of 1M HCl (10 mL). Aqueous layer was basified by addition of solid Na_2CO_3 until pH 9 and extracted with dichloromethane three times. Combined organic layer was dried over anhydrous $MgSO_4$, filtered, and concentrated under reduced pressure. The residue was chromatographed over silica gel by gradient elution of methanol in dichloromethane (0 to 6%) to afford analytically pure **121** (86 mg, 44%). ^{1}H NMR (300 MHz, Acetone-d_6) δ 9.96 (s, 1H), 8.50 (d, J = 4.5 Hz, 3H), 8.08 (d, J = 8.3 Hz, 1H), 7.78–7.61 (m, 8H), 7.55 (dd, J = 6.4, 5.3 Hz, 2H), 7.37 (d, J = 7.4 Hz, 1H), 7.24 (ddd, J = 13.2, 10.1, 3.2 Hz, 8H), 7.06 (t, J = 7.3 Hz, 1H), 6.28 (d, J = 2.6 Hz, 1H), 5.75–5.67 (m, 1H), 5.67–5.57 (m, 1H), 3.85–3.65 (m, 12H), 2.89 (t, J = 6.9 Hz, 2H), 2.78 (d, J = 6.9 Hz, 2H), 1.98 (s, 3H). LRMS (MALDI-TOF) m/z: $[M+H]^+$ Calcd for $C_{51}H_{49}BF_2N_9O$ 852.4; Found 852.4.

Synthesis of **109**-**112**: 5 µmol of free ligand (**115a**, **115b**, **118**, and **121** for **109**-**112**, respectively) in acetonitrile (0.1 mL) was treated with $Zn(ClO_4)_2 \cdot 6H_2O$ (3.82 mg, 10.25 µmol, 2.05 equiv.) in acetonitrile (0.1 mL). The mixture was shaken for 30 minutes and lyophilized and used without further purification.

Section 4. Solvent Effect on the Pyrophosphate Sensing

A part of this section was published in *Bulletin of the Korean Chemical Society*.[154]

1. Introduction

Measuring the concentration of PPi precisely in a complex mixture is highly beneficial for analyzing activities of some enzyme such as DNA polymerase,[132,141] aminoacyl-tRNA synthetases,[155] and adenylyl cyclase because they commonly consume ATP and produce PPi.

It is well-known that many enzymes require specific conditions such as temperature, salt concentration and acidity (pH) to show optimal reactivity. However, we often perform preliminary tests of a molecular receptor or probe, such as **10** (Scheme 3–8), in fundamental media (e.g. 10 mM HEPES pH 7.4 without any additional salt), which is far from that for enzyme assay. Since the solvent system is different for each case, necessary is to understand an effect of solvent compositions in order to maintain consistency in preliminary test and actual application. Therefore, studying effects of media is a crucial step for developing a highly selective and sensitive probe for pyrophosphate that is suitable for the real-time monitoring. In that regard, it is worth noting that Jolliffe's macrocyclic host molecules (e.g. **122**,[156] Scheme 3–8) showed higher selectivity for PPi in the biologically relevant Krebs buffer system than in low ionic strength buffers.[50,156,157] Nevertheless, the underlying principles for such high selectivity is still unclear. Therefore, we investigated how

the buffer compositions affect the association between **10** and PPi. Therefore, we investigated how the buffer composition affected molecular recognition of PPi and ATP.

Normal Krebs buffer (pH 7.4) contains a number of ions such as sodium (Na^+, 137 mM), potassium (K^+, 5 mM), magnesium (Mg^{2+}, 1.2 mM), calcium (Ca^{2+}, 2.8 mM), chloride (Cl^-, 150 mM), sulfate (SO_4^{2-}, 1 mM), and phosphate (PO_4^{3-}, 1 mM) as well as nonionic glucose (10 mM). Because aforementioned glucose and anions would have insignificant effects on the molecular recognition of PPi, it is without a doubt that cations (especially Mg^{2+} and Ca^{2+}) play critical roles in modulating association constants.

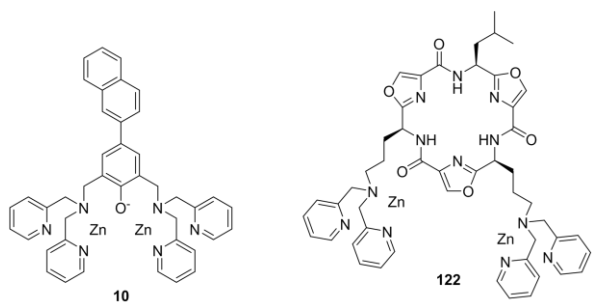

Scheme 3–8. The molecular structure of **10** and **122**.

2. Result and discussion

We conducted a series of titration experiments in several media containing individual cations. Since probe **10** showed considerable signal enhancement in the presence of either PPi or ATP as depicted in Figure 3–7, **10** is a suitable probe for determining association constants. Table 3–2 summarized the results obtained by fitting the

fluorescence intensity at 470 nm (I_{470}) against the analyte concentrations. It is noticeable that log $K_{a,PPi}$ – log $K_{a,ATP}$ (difference of two individual log K_a's) and log K_{PPi}/K_{ATP} (obtained by competition experiment) did not fully agree with each other (Table 3–2, column 4 and 5, respectively). However, we believe that the latter one is more significant because it directly reflects the ability to detect PPi in the presence of large amounts of ATP.

Addition of 100 mM NaCl slightly reduced the association constant between **10** and analytes, which supports the fact that intermolecular forces predominantly rely on ion-ion interactions.[158] However, there is only a little change in association constants, indicating that sodium and chloride ions would have negligible effects on binding of **10** to PPi and ATP.

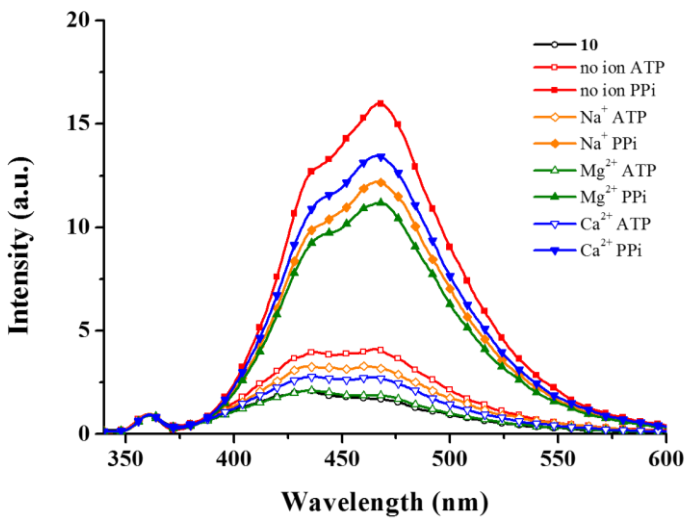

Figure 3–7. Fluorescence responses of **10** (8 μM) to analytes (5 equiv.) in various media: No ion, 50 mM HEPES; Na^+, 50 mM HEPES, 100 mM NaCl; Mg^{2+}, 50 mM HEPES, 5 mM $MgCl_2$; Ca^{2+}, 50 mM HEPES, 5 mM $CaCl_2$. All HEPES buffers were set at a pH of 7.4.

Table 3–2. Apparent association constant (log K_a) between **10** and analytes in 50 mM HEPES buffered media (pH 7.41) with various ionic concentrations.

Add ion	PPi[a]	ATP[a]	log $K_{a,PPi}$ – log $K_{a,ATP}$[a]	log K_{PPi}/K_{ATP}[b]
none	8.4 ± 0.3	6.6 ± 0.2	1.8 ± 0.3	1.3 ± 0.05
100 mM NaCl	8.1 ± 0.2	6.2 ± 0.2	1.9 ± 0.2	1.5 ± 0.05
5 mM $MgCl_2$	6.0 ± 0.05	4.9 ± 0.5	1.1 ± 0.5	0.8 ± 0.05
5 mM $CaCl_2$	6.3 ± 0.1	5.2 ± 0.2	1.1 ± 0.2	1.6 ± 0.05

[a]According to 1:1 binding algorithm. [b]According to the competitive binding algorithm.

Surprisingly, alkaline earth metal ions efficiently suppressed the association between **10** and analytes without inducing a substantial change in association constant ratio (log $K_{a,PPi}/K_{a,ATP}$). This phenomenon is clearly different from that of Jollife's peptoid hosts since many of them showed enhanced selectivity in Krebs buffer system.[41] Therefore, we thought that the selectivity difference between ours and Jolliffe's would be attributed to not only the action of divalent cations but also the molecular structure of host molecules.

In order to understand how the alkaline earth metal ions modulate the association constant, we calculated association constant between **10** and analytes in another way, by assuming that the divalent cations and **10** competitively bind to analytes, and the result was summarized in Table 3–3. The new association constants agreed with previous ones within error range for those obtained from the solution containing Mg^{2+}. However, those from the Ca^{2+} solution were either one order of magnitude smaller (PPi, 7.2 ± 0.1) than or one-third (ATP, 6.1 ± 0.2) to those

determined previously (8.4 ± 0.3 and 6.6 ± 0.2, respectively). Therefore, it is highly likely that Ca^{2+} ions participate in complexation with the diphosphate unit of PPi and ATP in a different way when compared to the binding mode of Mg^{2+} ions (*vide infra*).

Table 3–3. Calculated association constants (log *K*) between **10** and analytes according to competitive binding of a host and an ion to a guest.

Reference ion	PPi	ATP
none	8.4 ± 0.3	6.6 ± 0.2
Mg^{2+}	7.9 ± 0.05	6.8 ± 0.5
Ca^{2+}	7.2 ± 0.1	6.1 ± 0.2

log K_a's of MgPPi = 4.26,[159] MgATP = 4.22,[159] CaPPi = 3.17,[160] CaATP = 3.18.[160]

Many crystal structures of biomacromolecules exclusively carry a unique 6-membered ring structure composed of a Mg^{2+} and a PPi ion (MgPPi),[161-163] which is structurally analogous to the complex between PPi and **10**.[39] However, a Ca^{2+} ion sometimes forms a 4-membered ring structure with PPi in a side-on manner.[164] This is perhaps not a coincidence considering the fact that the ionic radii of Mg^{2+} (86 pm) is similar to that of Zn^{2+} (88 pm) whereas Ca^{2+} (114 pm) is about 30 % bigger.[129] Therefore, one can expect that binding of **10** and Mg^{2+} ion to PPi takes place at the same location with the same geometry (between two phosphate groups), while Ca^{2+} can bind to PPi at a different position (at the end of PPi). Consequently, Mg^{2+} ions necessarily compete with **10** for binding PPi, whereas Ca^{2+} ions can inhibit the binding between **10** and PPi both competitively and uncompetitively.

A recent study claimed that a three-point contact through three oxygen atoms of each phosphate (P_α, P_β, P_γ) is the most favorable conformation of Mg^{2+}-bound

ATP (MgATP).[165] Therefore, a MgATP complex in the most stable conformation must release two consecutive points of contact before binding to a host molecule, where Mg^{2+} ion still can be attached to ATP, preferentially at the P_{α} oxygen. Therefore, one can rationally imagine that the proximal hydroxyl group of the ribosyl moiety and water molecules can fill the empty coordinating sites of the Mg^{2+} ion, resulting in a large hydration sphere in which way ATP becomes more sterically hindered. An energy-minimized structure of the **10**–ATP complex clearly reveals that the adenosine monophosphate (AMP) unit of ATP is far away from **10** and thus can be solvated freely (Figure 3–8). However, the AMP unit of the **122**–ATP complex experiences severe steric interference with **122** (Figure 3–9). In other words, it is more likely that **122** encounters steric interactions with the AMP unit. Combining two arguments, we can expect that the sterically demanding MgATP must lose affinity to a greater extent for **122**.

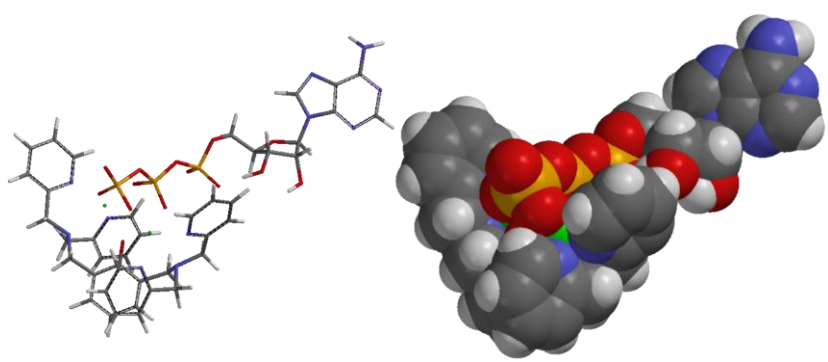

Figure 3–8. An energy-minimized structure of the complex of ATP with **10** (without a naphthyl group) shown in a stick model (left) and a space-filling model (right).

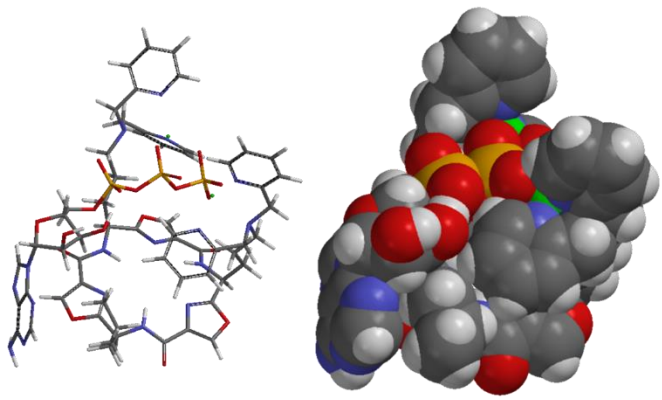

Figure 3–9. An energy-minimized structure of the complex of ATP with **122** shown in a stick model (left) and a space-filling model (right).

3. Conclusion

In conclusion, we conducted a series of titration experiments to analyze the effects of metal ions in Krebs buffer on the selectivity and sensitivity of PPi probes. The selectivity is certainly attributed to not only the action of divalent cations but also the molecular structure of the host molecules. We confirmed that divalent cations competitively bind PPi with host molecules, while Ca^{2+} participates in complexation with host molecules in an additional uncompetitive manner. Moreover, we rationalized the reason why macrocyclic host molecules have greater selectivity for PPi in Krebs buffer.

4. Experimental section

4.1. Competitive binding of a host and an ion to a guest

For a competitive binding of a host (H) and an ion (I) to a guest (G), we can define three constants K_{HG}, K_{IG}, K as Eqs. 3–1~3. In addition, three mass balance equations are given by Eqs. 3–4~6, when ions are present in large excess, so that (1) there is a negligible amount of free guest in the solution, and (2) the amount of IG complex is very small compared to the amount of ion.

$$\mathrm{H} + \mathrm{G} \overset{K_{\mathrm{HG}}}{\rightleftarrows} \mathrm{HG} : K_{\mathrm{HG}} = \frac{[\mathrm{HG}]}{[\mathrm{H}][\mathrm{G}]} \quad \text{(Eq. 3–1)}$$

$$\mathrm{H} + \mathrm{G} \overset{K_{\mathrm{IG}}}{\rightleftarrows} \mathrm{HG} : K_{\mathrm{IG}} = \frac{[\mathrm{IG}]}{[\mathrm{I}][\mathrm{G}]} \quad \text{(Eq. 3–2)}$$

$$K = \frac{K_{\mathrm{HG}}}{K_{\mathrm{IG}}} = \frac{[\mathrm{HG}][\mathrm{I}]}{[\mathrm{H}][\mathrm{IG}]} \quad \text{(Eq. 3–3)}$$

$$\mathrm{H}_0 = [\mathrm{H}] + [\mathrm{HG}] \quad \text{(Eq. 3–4)}$$

$$\mathrm{I}_0 = [\mathrm{I}] + [\mathrm{IG}] \approx [\mathrm{I}] \quad \text{(Eq. 3–5)}$$

$$\mathrm{G}_0 = [\mathrm{G}] + [\mathrm{HG}] + [\mathrm{IG}] \approx [\mathrm{HG}] + [\mathrm{IG}] \quad \text{(Eq. 3–6)}$$

Substitution of [H], [I] and [IG] of Eq. 3–3 using Eqs. 3–4~6 results in Eq. 3–7, which is a quadratic function of [HG]. Choosing an appropriate solution gives an [HG] as a function of H_0, I_0, G_0, and K (Eq. 3–8).

$$K \approx \frac{[\mathrm{HG}]\,\mathrm{I}_0}{(\mathrm{H}_0 - [\mathrm{HG}])\,(\mathrm{G}_0 - [\mathrm{HG}])} \quad \text{(Eq. 3–7)}$$

$$[\mathrm{HG}] = \frac{b - \sqrt{b^2 - 4\,K^2 \mathrm{H}_0 \mathrm{G}_0}}{2\,K - 2} \qquad \text{(Eq. 3–8)}$$

$$\text{where } b = (\mathrm{H}_0 + \mathrm{G}_0)K + \mathrm{I}_0$$

Since the fluorescence predominantly arises from H and HG complexes, the fluorescence intensity would follow Eq. 3–9 as a function of H_0, I_0, G_0, and K.

$$\mathrm{F} = \mathrm{a}\,[\mathrm{H}] + (\mathrm{b} + \mathrm{a})\,[\mathrm{HG}] = \mathrm{a} \cdot \mathrm{H}_0 + \mathrm{b} \cdot [\mathrm{HG}] \qquad \text{(Eq. 3–9)}$$

References and Notes

(1) Cram, D., *Science*, **1988**, *240*, 760-767.

(2) Berg, J. M.; Tymoczko, J. L.; Stryer, L. *Biochemistry*; 6th ed.; W. H. Freeman and Company: New York, 2006.

(3) Webb, B. A.; Forouhar, F.; Szu, F.-E.; Seetharaman, J.; Tong, L.; Barber, D. L., *Nature*, **2015**, *523*, 111-114.

(4) Cram, D. J.; Lein, G. M., *J. Am. Chem. Soc.*, **1985**, *107*, 3657-3668.

(5) Cram, D. J.; DeGrandpre, M.; Knobler, C. B.; Trueblood, K. N., *J. Am. Chem. Soc.*, **1984**, *106*, 3286-3292.

(6) Artz, S. P.; Cram, D. J., *J. Am. Chem. Soc.*, **1984**, *106*, 2160-2171.

(7) Lehn, J.-M., *Angew. Chem., Int. Ed. Engl.*, **1988**, *27*, 89-112.

(8) Ribeiro, A. A. S. T.; Ortiz, V., *Chem. Rev.*, **2016**, *116*, 6488-6502.

(9) Ikeda, M.; Takeuchi, M.; Sugasaki, A.; Robertson, A.; Imada, T.; Shinkai, S., *Supramol. Chem.*, **2000**, *12*, 321-345.

(10) Kollman, P. A.; Allen, L. C., *Chem. Rev.*, **1972**, *72*, 283-303.

(11) Laitinen, O. H.; Hytönen, V. P.; Nordlund, H. R.; Kulomaa, M. S., *Cell. Mol. Life Sci.*, **2006**, *63*, 2992-3017.

(12) Lin, K.-Y.; Matteucci, M. D., *J. Am. Chem. Soc.*, **1998**, *120*, 8531-8532.

(13) Nakagawa, O.; Ono, S.; Li, Z.; Tsujimoto, A.; Sasaki, S., *Angew. Chem., Int. Ed.*, **2007**, *46*, 4500-4503.

(14) Gilday, L. C.; Robinson, S. W.; Barendt, T. A.; Langton, M. J.; Mullaney, B. R.; Beer, P. D., *Chem. Rev.*, **2015**, *115*, 7118-7195.

(15) Cavallo, G.; Metrangolo, P.; Milani, R.; Pilati, T.; Priimagi, A.; Resnati, G.; Terraneo, G., *Chem. Rev.*, **2016**, *116*, 2478-2601.

(16) Ma, J. C.; Dougherty, D. A., *Chem. Rev.*, **1997**, *97*, 1303-1324.

(17) Zhao, Y.; Cotelle, Y.; Sakai, N.; Matile, S., *J. Am. Chem. Soc.*, **2016**, *138*, 4270-4277.

(18) Giese, M.; Albrecht, M.; Rissanen, K., *Chem. Rev.*, **2015**, *115*, 8867-8895.

(19) Satow, Y.; Cohen, G. H.; Padlan, E. A.; Davies, D. R., *J. Mol. Biol.*, **1986**, *190*, 593-604.

(20) Dougherty, D.; Stauffer, D., *Science*, **1990**, *250*, 1558-1560.

(21) Wagner, J. P.; Schreiner, P. R., *Angew. Chem., Int. Ed.*, **2015**, *54*, 12274-12296.

(22) Dion, M.; Rydberg, H.; Schröder, E.; Langreth, D. C.; Lundqvist, B. I., *Phys. Rev. Lett.*, **2004**, *92*, 246401.

(23) McNaught, A. D. *Compendium of chemical terminology*; Blackwell Science Oxford, 1997.

(24) de Silva, A. P.; Gunaratne, H. Q. N.; Gunnlaugsson, T.; Huxley, A. J. M.; McCoy, C. P.; Rademacher, J. T.; Rice, T. E., *Chem. Rev.*, **1997**, *97*, 1515-1566.

(25) Martínez-Máñez, R.; Sancenón, F., *Chem. Rev.*, **2003**, *103*, 4419-4476.

(26) Basabe-Desmonts, L.; Reinhoudt, D. N.; Crego-Calama, M., *Chem. Soc. Rev.*, **2007**, *36*, 993-1017.

(27) Vendrell, M.; Zhai, D.; Er, J. C.; Chang, Y.-T., *Chem. Rev.*, **2012**, *112*, 4391-4420.

(28) Wu, J.; Kwon, B.; Liu, W.; Anslyn, E. V.; Wang, P.; Kim, J. S., *Chem. Rev.*, **2015**, *115*, 7893-7943.

(29) Walkup, G. K.; Burdette, S. C.; Lippard, S. J.; Tsien, R. Y., *J. Am. Chem. Soc.*, **2000**, *122*, 5644-5645.

(30) Lee, D. H.; Lee, K. H.; Hong, J.-I., *Org. Lett.*, **2001**, *3*, 5-8.

(31) Zhao, J.; Ji, S.; Chen, Y.; Guo, H.; Yang, P., *Phys. Chem. Chem. Phys.*, **2012**, *14*, 8803-8817.

(32) Henary, M. M.; Wu, Y.; Fahrni, C. J., *Chem. – Eur. J.*, **2004**, *10*, 3015-3025.

(33) Schröder, H. C.; Müller, W. E. G. *Inorganic Polyphosphates: Biochemistry, Biology, Biotechnology*; Springer: Berlin, Heidelberg, 1999, pp 127-150.

(34) Doherty, M., *Ann. Rheum. Dis.*, **1983**, *42 Suppl 1*, 38-44.

(35) McCarty, D. J., *Arthritis Rheum.*, **1976**, *19 Suppl 3*, 275-285.

(36) Kim, S. K.; Lee, D. H.; Hong, J.-I.; Yoon, J., *Acc. Chem. Res.*, **2009**, *42*, 23-31.

(37) Lee, S.; Yuen, K. K. Y.; Jolliffe, K. A.; Yoon, J., *Chem. Soc. Rev.*, **2015**, *44*, 1749-1762.

(38) Vance, D. H.; Czarnik, A. W., *J. Am. Chem. Soc.*, **1994**, *116*, 9397-9398.

(39) Lee, D. H.; Im, J. H.; Son, S. U.; Chung, Y. K.; Hong, J.-I., *J. Am. Chem. Soc.*, **2003**, *125*, 7752-7753.

(40) Lee, D. H.; Kim, S. Y.; Hong, J.-I., *Angew. Chem., Int. Ed.*, **2004**, *43*, 4777-4780.

(41) Jolliffe, K. A., *Acc. Chem. Res.*, **2017**, *50*, 2254-2263.

(42) Kim, H. J.; Lee, J. H.; Hong, J.-I., *Tetrahedron Lett.*, **2011**, *52*, 4944-4946.

(43) Yang, S.; Feng, G.; Williams, N. H., *Org. Biomol. Chem.*, **2012**, *10*, 5606-5612.

(44) Lee, D.-N.; Jo, A.; Park, S. B.; Hong, J.-I., *Tetrahedron Lett.*, **2012**, *53*, 5528-5530.

(45) Chao, D.; Ni, S., *Sci. Rep.*, **2016**, *6*, 26477.

(46) Nishizawa, S.; Kato, Y.; Teramae, N., *J. Am. Chem. Soc.*, **1999**, *121*, 9463-9464.

(47) Cho, H. K.; Lee, D. H.; Hong, J.-I., *Chem. Commun.*, **2005**, 1690-1692.

(48) Lee, H. N.; Xu, Z.; Kim, S. K.; Swamy, K. M. K.; Kim, Y.; Kim, S.-J.; Yoon, J., *J. Am. Chem. Soc.*, **2007**, *129*, 3828-3829.

(49) Chen, W.-H.; Xing, Y.; Pang, Y., *Org. Lett.*, **2011**, *13*, 1362-1365.

(50) Yuen, K. K. Y.; Jolliffe, K. A., *Chem. Commun.*, **2013**, *49*, 4824-4826.

(51) Oh, J.; Rhee, H.-W.; Hong, J.-I. *Synthetic Receptors for Biomolecules: Design Principles and Applications*; The Royal Society of Chemistry: 2015, pp 204-252.

(52) Ojida, A.; Takashima, I.; Kohira, T.; Nonaka, H.; Hamachi, I., *J. Am. Chem. Soc.*, **2008**, *130*, 12095-12101.

(53) Kurishita, Y.; Kohira, T.; Ojida, A.; Hamachi, I., *J. Am. Chem. Soc.*, **2010**, *132*, 13290-13299.

(54) Kwon, T. H.; Kim, H. J.; Hong, J.-I., *Chem. – Eur. J.*, **2008**, *14*, 9613-9619.

(55) Zeng, Z. H.; Spiccia, L., *Chem. – Eur. J.*, **2009**, *15*, 12941-12944.

(56) Rhee, H. W.; Lee, C. R.; Cho, S. H.; Song, M. R.; Cashel, M.; Choy, H. E.; Seok, Y. J.; Hong, J.-I., *J. Am. Chem. Soc.*, **2008**, *130*, 784-785.

(57) Rhee, H. W.; Choi, S. J.; Yoo, S. H.; Jang, Y. O.; Park, H. H.; Pinto, R. M.; Cameselle, J. C.; Sandova, F. J.; Roje, S.; Han, K.; Chung, D. S.; Suh, J.; Hong, J.-I., *J. Am. Chem. Soc.*, **2009**, *131*, 10107-10112.

(58) Fenniri, H.; Hosseini, M. W.; Lehn, J. M., *Helv. Chim. Acta*, **1997**, *80*, 786-803.

(59) Oh, J.; Hong, J.-I., *Org. Lett.*, **2013**, *15*, 1210-1213.

(60) Bruice, T. C., *Acc. Chem. Res.*, **1980**, *13*, 256-262.

(61) Walsh, C., *Acc. Chem. Res.*, **1980**, *13*, 148-155.

(62) Massey, V., *Biochem. Soc. Trans.*, **2000**, *28*, 283.

(63) Soga, T.; Igarashi, K.; Ito, C.; Mizobuchi, K.; Zimmermann, H.-P.; Tomita, M., *Anal. Chem.*, **2009**, *81*, 6165-6174.

(64) Britz-McKibbin, P.; Markuszewski, M. J.; Iyanagi, T.; Matsuda, K.; Nishioka, T.; Terabe, S., *Anal. Biochem.*, **2003**, *313*, 89-96.

(65) Sarma, R. H.; Dannies, P.; Kaplan, N. O., *Biochemistry*, **1968**, *7*, 4359-4367.

(66) Siders, P.; Marcus, R. A., *J. Am. Chem. Soc.*, **1981**, *103*, 748-752.

(67) Kool, E. T., *Chem. Rev.*, **1997**, *97*, 1473-1488.

(68) Jenal, U.; Reinders, A.; Lori, C., *Nat. Rev. Microbiol.*, **2017**, *15*, 271.

(69) Christen, M.; Kulasekara, H. D.; Christen, B.; Kulasekara, B. R.; Hoffman, L. R.; Miller, S. I., *Science*, **2010**, *328*, 1295-1297.

(70) Chan, C.; Paul, R.; Samoray, D.; Amiot, N. C.; Giese, B.; Jenal, U.; Schirmer, T., *Proc. Natl. Acad. Sci. U. S. A.*, **2004**, *101*, 17084-17089.

(71) Yan, H.; Chen, W., *Chem. Soc. Rev.*, **2010**, *39*, 2914-2924.

(72) Zhang, Z.; Kim, S.; Gaffney, B. L.; Jones, R. A., *J. Am. Chem. Soc.*, **2006**, *128*, 7015-7024.

(73) Shanahan, C. A.; Gaffney, B. L.; Jones, R. A.; Strobel, S. A., *J. Am. Chem. Soc.*, **2011**, *133*, 15578-15592.

(74) Smith, K. D.; Shanahan, C. A.; Moore, E. L.; Simon, A. C.; Strobel, S. A., *Proc. Natl. Acad. Sci. U. S. A.*, **2011**, *108*, 7757.

(75) Che, X.; Zhang, J.; Zhu, Y.; Yang, L.; Quan, H.; Gao, Y. Q., *J. Phys. Chem. B*, **2016**, *120*, 2670-2680.

(76) Grzesiek, S.; Bax, A., *J. Am. Chem. Soc.*, **1993**, *115*, 12593-12594.

(77) Grzesiek, S.; Bax, A., *J. Biomol. NMR*, **1993**, *3*, 627-638.

(78) Du, W.; Zhao, M.-N.; Ren, Z.-H.; Wang, Y.-Y.; Guan, Z.-H., *Chem. Commun.*, **2014**, *50*, 7437-7439.

(79) Kerstin, G.; Helmut, G.; Daniela, G.; Thomas, S.; Clemens, R., *Eur. J. Org. Chem.*, **2010**, *2010*, 3611-3620.

(80) Anslyn, E. V.; Dougherty, D. A. *Modern physical organic chemistry*; University Science Books: Sausalito, CA, 2006.

(81) Krug, R. R.; Hunter, W. G.; Grieger, R. A., *J. Phys. Chem.*, **1976**, *80*, 2335-2341.

(82) Dunitz, J. D., *Chem. Biol.*, **1995**, *2*, 709-712.

(83) Starikov, E. B.; Nordén, B., *J. Phys. Chem. B*, **2007**, *111*, 14431-14435.

(84) Exner, O., *Chem. Commun.*, **2000**, 1655-1656.

(85) Linert, W.; Jameson, R. F., *Chem. Soc. Rev.*, **1989**, *18*, 477-505.

(86) Liu, L.; Guo, Q.-X., *Chem. Rev.*, **2001**, *101*, 673-696.

(87) Boots, H. M. J.; De Bokx, P. K., *J. Phys. Chem.*, **1989**, *93*, 8240-8243.

(88) Grunwald, E.; Steel, C., *J. Am. Chem. Soc.*, **1995**, *117*, 5687-5692.

(89) Sharp, K., *Protein Sci.*, **2001**, *10*, 661-667.

(90) Tidemand, K. D.; Schönbeck, C.; Holm, R.; Westh, P.; Peters, G. H., *J. Phys. Chem. B*, **2014**, *118*, 10889-10897.

(91) Pan, A.; Biswas, T.; Rakshit, A. K.; Moulik, S. P., *J. Phys. Chem. B*, **2015**, *119*, 15876-15884.

(92) Inoue, Y.; Hakushi, T.; Liu, Y.; Tong, L.; Hu, J.; Zhao, G.; Huang, S.; Tian, B., *J. Phys. Chem.*, **1988**, *92*, 2371-2374.

(93) Inoue, Y.; Amano, F.; Okada, N.; Inada, H.; Ouchi, M.; Tai, A.; Hakushi, T.; Liu, Y.; Tong, L.-H., *J. Chem. Soc., Perkin Trans. 2*, **1990**, 1239-1246.

(94) Inoue, Y.; Hakushi, T.; Liu, Y.; Tong, L.; Shen, B.; Jin, D., *J. Am. Chem. Soc.*, **1993**, *115*, 475-481.

(95) Rekharsky, M.; Inoue, Y., *J. Am. Chem. Soc.*, **2000**, *122*, 4418-4435.

(96) Leung, D. H.; Bergman, R. G.; Raymond, K. N., *J. Am. Chem. Soc.*, **2008**, *130*, 2798-2805.

(97) Gilli, P.; Ferretti, V.; Gilli, G.; Borea, P. A., *J. Phys. Chem.*, **1994**, *98*, 1515-1518.

(98) Fisicaro, E.; Compari, C.; Braibanti, A., *Phys. Chem. Chem. Phys.*, **2004**, *6*, 4156-4166.

(99) Krishnamurthy, V. M.; Bohall, B. R.; Semetey, V.; Whitesides, G. M., *J. Am. Chem. Soc.*, **2006**, *128*, 5802-5812.

(100) Kocherbitov, V.; Arnebrant, T., *Langmuir*, **2010**, *26*, 3918-3922.

(101) Ward, J. M.; Gorenstein, N. M.; Tian, J.; Martin, S. F.; Post, C. B., *J. Am. Chem. Soc.*, **2010**, *132*, 11058-11070.

(102) Santamaría, J.; Martín, T.; Hilmersson, G.; Craig, S. L.; Rebek, J., *Proc. Natl. Acad. Sci. U. S. A.*, **1999**, *96*, 8344-8347.

(103) Freire, E.; Mayorga, O. L.; Straume, M., *Anal. Chem.*, **1990**, *62*, 950A-959A.

(104) Velázquez-Campoy, A.; Ohtaka, H.; Nezami, A.; Muzammil, S.; Freire, E. *Current Protocols in Cell Biology*; John Wiley & Sons, Inc.: 2001.

(105) Kwon, J. E.; Lee, S.; You, Y.; Baek, K.-H.; Ohkubo, K.; Cho, J.; Fukuzumi, S.; Shin, I.; Park, S. Y.; Nam, W., *Inorg. Chem.*, **2012**, *51*, 8760-8774.

(106) Emami Khansari, M.; Johnson, C. R.; Basaran, I.; Nafis, A.; Wang, J.; Leszczynski, J.; Hossain, M. A., *RSC Adv.*, **2015**, *5*, 17606-17614.

(107) Oh, J.; Hong, J.-I., *J. Org. Chem.*, **2019**, *84*, 15797-15804.

(108) Lee, J. H.; Park, J.; Lah, M. S.; Chin, J.; Hong, J. I., *Org. Lett.*, **2007**, *9*, 3729-3731.

(109) Wagner, J. P.; Schreiner, P. R., *Angew. Chem. Int. Ed.*, **2015**, *54*, 12274-12296.

(110) Liu, X.; Ngo, H. T.; Ge, Z.; Butler, S. J.; Jolliffe, K. A., *Chem. Sci.*, **2013**, *4*, 1680-1686.

(111) Yang, J.; Dong, C.-C.; Chen, X.-L.; Sun, X.; Wei, J.-Y.; Xiang, J.-F.; Sessler, J. L.; Gong, H.-Y., *J. Am. Chem. Soc.*, **2019**, *141*, 4597-4612.

(112) Kuchelmeister, H. Y.; Schmuck, C., *Chem. – Eur. J.*, **2011**, *17*, 5311-5318.

(113) Peng, X.; Wu, Y.; Fan, J.; Tian, M.; Han, K., *J. Org. Chem.*, **2005**, *70*, 10524-10531.

(114) Kim, S. K.; Lynch, V. M.; Young, N. J.; Hay, B. P.; Lee, C.-H.; Kim, J. S.; Moyer, B. A.; Sessler, J. L., *J. Am. Chem. Soc.*, **2012**, *134*, 20837-20843.

(115) Cram, D. J., *Angew. Chem., Int. Ed. Engl.*, **1988**, *27*, 1009-1020.

(116) Mareque-Rivas, J. C.; Prabaharan, R.; Martín de Rosales, R. T., *Chem. Commun.*, **2004**, 76-77.

(117) Grootenhuis, P. D. J.; Uiterwijk, J. W. H. M.; Reinhoudt, D. N.; Van Staveren, C. J.; Sudholter, E. J. R.; Bos, M.; Van Eerden, J.; Klooster, W. T.; Kruise, L.; Harkema, S., *J. Am. Chem. Soc.*, **1986**, *108*, 780-788.

(118) Bartsch, R. A.; Heo, G. S.; Kang, S. I.; Liu, Y.; Strzelbicki, J., *J. Org. Chem.*, **1982**, *47*, 457-460.

(119) Nobuhiro, K.; Yuya, T.; Hiroaki, K.; Toshikazu, T., *Chem. Lett.*, **2000**, *29*, 506-507.

(120) Inokuchi, Y.; Ebata, T.; Rizzo, T. R.; Boyarkin, O. V., *J. Am. Chem. Soc.*, **2014**, *136*, 1815-1824.

(121) Berger, M.; Schmidtchen, F. P., *Angew. Chem., Int. Ed.*, **1998**, *37*, 2694-2696.

(122) Ong, W. Q.; Zhao, H.; Du, Z.; Yeh, J. Z. Y.; Ren, C.; Tan, L. Z. W.; Zhang, K.; Zeng, H., *Chem. Commun.*, **2011**, *47*, 6416-6418.

(123) Hryniewicka, A.; Morzycki, J. W.; Witkowski, S., *J. Organomet. Chem.*, **2010**, *695*, 1265-1270.

(124) Kumar, M.; George, S. J., *Chem. Sci.*, **2014**, *5*, 3025-3030.

(125) Harris, L.; Mee, S. P. H.; Furneaux, R. H.; Gainsford, G. J.; Luxenburger, A., *J. Org. Chem.*, **2011**, *76*, 358-372.

(126) Yadav, J. S.; Pandurangam, T.; Reddy, V. V. B.; Reddy, B. V. S., *Synthesis*, **2010**, *2010*, 4300-4306.

(127) Wagner, J. P.; Schreiner Peter, R., *Angew. Chem., Int. Ed.*, **2015**, *54*, 12274-12296.

(128) Gorla, F.; Togni, A.; Venanzi, L. M.; Albinati, A.; Lianza, F., *Organometallics*, **1994**, *13*, 1607-1616.

(129) Shannon, R. D., *Acta Crystallogr., Sect. A*, **1976**, *32*, 751-767.

(130) Duma, T. W.; Marsicano, F.; Hancock, R. D., *J. Coord. Chem.*, **1991**, *23*, 221-232.

(131) Meares, C. F.; Wensel, T. G., *Acc. Chem. Res.*, **1984**, *17*, 202-209.

(132) Lee, D. H.; Hong, J. I., *Bull. Korean Chem. Soc.*, **2008**, *29*, 497-498.

(133) Han, Jung M.; Jeong, Seung J.; Park, Min C.; Kim, G.; Kwon, Nam H.; Kim, Hoi K.; Ha, Sang H.; Ryu, Sung H.; Kim, S., *Cell*, **2012**, *149*, 410-424.

(134) Seidel, C. A. M.; Schulz, A.; Sauer, M. H. M., *J. Phys. Chem.*, **1996**, *100*, 5541-5553.

(135) Torimura, M.; Kurata, S.; Yamada, K.; Yokomaku, T.; Kamagata, Y.; Kanagawa, T.; Kurane, R., *Anal. Sci.*, **2001**, *17*, 155-160.

(136) Heinlein, T.; Knemeyer, J.-P.; Piestert, O.; Sauer, M., *J. Phys. Chem. B*, **2003**, *107*, 7957-7964.

(137) Weber, G., *Biochem. J.*, **1950**, *47*, 114-121.

(138) Li, G.; Glusac, K. D., *J. Phys. Chem. B*, **2009**, *113*, 9059-9061.

(139) Ravikumar, I.; Ghosh, P., *Inorg. Chem.*, **2011**, *50*, 4229-4231.

(140) Lin, J.-R.; Chu, C.-J.; Venkatesan, P.; Wu, S.-P., *Sens. Actuators, B*, **2015**, *207*, 563-570.

(141) Lee, J. H.; Jeong, A. R.; Jung, J.-H.; Park, C.-M.; Hong, J.-I., *J. Org. Chem.*, **2011**, *76*, 417-423.

(142) Goldenberg, L.; Neilands, O., *J. Electroanal. Chem.*, **1999**, *463*, 212-217.

(143) Legrand, Y.-M.; Gray, M.; Cooke, G.; Rotello, V. M., *J. Am. Chem. Soc.*, **2003**, *125*, 15789-15795.

(144) Shin, I.-S.; Bae, S. W.; Kim, H.; Hong, J.-I., *Anal. Chem.*, **2010**, *82*, 8259-8265.

(145) Grabowski, Z. R.; Rotkiewicz, K.; Rettig, W., *Chem. Rev.*, **2003**, *103*, 3899-4032.

(146) Banekovich, C.; Matuszczak, B., *Tetrahedron Lett.*, **2005**, *46*, 5053-5056.

(147) Pomorski, A.; Adamczyk, J.; Bishop, A. C.; Krezel, A., *Org. Biomol. Chem.*, **2015**, *13*, 1395-1403.

(148) Małgorzata, P.; Agnieszka, J.; J., B. L.; Marcin, K., *Eur. J. Org. Chem.*, **2018**, *2018*, 1916-1923.

(149) Kowada, T.; Maeda, H.; Kikuchi, K., *Chem. Soc. Rev.*, **2015**, *44*, 4953-4972.

(150) Loudet, A.; Burgess, K., *Chem. Rev.*, **2007**, *107*, 4891-4932.

(151) Bao, D.; Upadhyayula, S.; Larsen, J. M.; Xia, B.; Georgieva, B.; Nuñez, V.; Espinoza, E. M.; Hartman, J. D.; Wurch, M.; Chang, A.; Lin, C.-K.; Larkin, J.; Vasquez, K.; Beran, G. J. O.; Vullev, V. I., *J. Am. Chem. Soc.*, **2014**, *136*, 12966-12973.

(152) Nobeli, I.; Laskowski, R. A.; Valdar, W. S. J.; Thornton, J. M., *Nucleic Acids Res.*, **2001**, *29*, 4294-4309.

(153) Drewry, J. A.; Fletcher, S.; Hassan, H.; Gunning, P. T., *Org. Biomol. Chem.*, **2009**, *7*, 5074-5077.

(154) Oh, J.; Hong, J.-I., *Bull. Korean Chem. Soc.*, **2018**, *39*, 899-901.

(155) Park, S. G.; Schimmel, P.; Kim, S., *Proc. Natl. Acad. Sci. U. S. A.*, **2008**, *105*, 11043-11049.

(156) Butler, S. J.; Jolliffe, K. A., *Chem. – Asian J.*, **2012**, *7*, 2621-2628.

(157) Liu, X.; Ngo, H. T.; Ge, Z.; Butler, S. J.; Jolliffe, K. A., *Chem. Sci.*, **2013**, *4*, 1680-1686.

(158) Record, M. T.; Lohman, T. M.; Haseth, P. d., *J. Mol. Biol.*, **1976**, *107*, 145-158.

(159) Airas, R. K., *Biophys. Chem.*, **2007**, *131*, 29-35.

(160) Wilson, J. E.; Chin, A., *Anal. Biochem.*, **1991**, *193*, 16-19.

(161) Tesmer, J. J. G.; Dessauer, C. W.; Sunahara, R. K.; Murray, L. D.; Johnson, R. A.; Gilman, A. G.; Sprang, S. R., *Biochemistry*, **2000**, *39*, 14464-14471.

(162) Wang, L. K.; Das, U.; Smith, P.; Shuman, S., *RNA*, **2012**, *18*, 2277-2286.

(163) Oksanen, E.; Ahonen, A.-K.; Tuominen, H.; Tuominen, V.; Lahti, R.; Goldman, A.; Heikinheimo, P., *Biochemistry*, **2007**, *46*, 1228-1239.

(164) Mou, T.-C.; Masada, N.; Cooper, D. M. F.; Sprang, S. R., *Biochemistry*, **2009**, *48*, 3387-3397.

(165) Dudev, T.; Grauffel, C.; Lim, C., *Sci. Rep.*, **2017**, *7*, 42377.

END.

국문초록

최근 수십 년간 음이온 분자의 인식 분야에서 매우 많은 연구들이 진행되어 왔습니다. 특히 불소(F^-), 청산(CN^-), 황산(SO_4^{2-}), 인산(Pi, PO_4^{3-}), 이인산(PPi, $P_2O_7^{4-}$) 이온 등과 같이 생물학적으로 중요한 음이온들을 주요 표적 물질로 하여 괄목할만한 연구 성과를 이루어 내었습니다. 그중에서도 이인산 이온은 DNA 중합효소, 아미노아실-tRNA 합성효소, cAMP 합성효소 등과 같이 생명 유지 및 세포 내 신호 전달에 결정적인 역할을 하는 수많은 효소들의 독특한 부산물로 생성되는 것으로 알려져 있습니다. 따라서 복잡한 시스템에서 이인산을 정확하게 검출하는 연구는 생리현상 연구 및 질병 진단 등에 매우 중요한 역할을 할 것이라 기대하고 있습니다. 이인산 이온이 bis(Zn-DPA)의 공동에 잘 들어맞는다는 사실이 알려진 이후로 수많은 이인산 검출용 탐침 분자(probes) 들이 bis(Zn-DPA) 구조를 기초로 제작되었으나, 효소 활성을 정밀하게 측정하는 데 사용될 수 있는 것은 매우 드물게 알려져 있습니다.

1 부는 bis(Zn-DPA) 구조를 기반으로 삼아 이인산 뿐만 아니라 인산기를 포함하는 여러 생분자들의 검출에 적용한 사례를 다룹니다. 하나의 탐침 분자만을 이용하여 생체 내의 산화 환원과 관련된 네 개의 생화학 분자들인 NAD^+, $NADP^+$, FAD, FMN 를 모두 구분하는 방법을 제시하였습니다. 또한, 엑시머-모노머 간 전환 또는 생체 모방의 두 가지 서로 다른 전략을 통해 설계된 탐침 분

자 및 수용체 분자를 이용하여 박테리아의 신호전달 물질인 cyclic-di-GMP 분자를 인식하고 검출하였습니다.

2 부는 bis(Zn-DPA)를 가지는 수용체 분자의 PPi 선택성을 증가시키기 위한 연구입니다. Bis(Zn-DPA)를 기반으로 하여 확장된 형태의 수용체, 키랄성 수용체, 그리고 이종이핵 수용체 등을 합성하여 그 성능을 각각 비교하였습니다. 치환기의 형태와 개수를 바꿔줌으로써 선택성 뿐만 아니라 교환 반응 속도를 효과적으로 조절할 수 있었습니다. 특히 고리형 수용체 분자는 향상된 선택성을 바탕으로 고농도의 ATP 존재 하에서 이인산 분자를 빠르고 선택적으로 검출할 수 있다는 사실을 확인하였습니다. 또한, 서로 다른 크기의 입체장애를 가지는 일련의 키랄성 유도체에서 *'부분 입체 선택성-민감도 보상'* 이라고 명명한 관계를 새로이 발견하였습니다. 아연 이온 대신 인듐 이온을 킬레이트화함으로써 공동(cavity)의 물리적 성질을 조절할 수 있었고, 그에 따라 수용체의 결합비 및 선택성에 변화를 줄 수 있었습니다.

3 부는 새로운 PPi 검출용 탐침 분자의 개발 과정을 담고 있습니다. 기존 연구 결과에 착안하여 푀스터 공명 에너지 전달(FRET) 및 광유발 전자전달 (PeT) 메커니즘을 기반으로 하는 탐침 분자들을 개발하였습니다. 이 과정에서 PPi 탐침 분자를 개발할 때 형광체의 선택 방법과 적용하는 메커니즘에 따른 거리 조절에 대한 기준을 제시하였습니다. 나아가 PeT 메커니즘만을 이용하여 GTP, ATP 에 대해 각각 형광 소광, 상승효과를 보이는 탐침 분자를 합성하였습니다. 특히 이

탐침 분자의 형광 세기는 ATP 나 GTP 와 결합하였을 경우에 비해 이인산 분자와 결합하였을 때 용매의 극성에 크게 좌우되므로 적절한 용매를 취함으로써 ATP 나 GTP 의 소모를 효과적으로 검출할 수 있을 것으로 기대됩니다. 마지막으로 생리 완충용액에서 자주 사용되는 나트륨, 마그네슘, 칼슘 이온이 형광 탐침 분자의 선택성 및 민감도에 미치는 영향을 정량적으로 분석하였습니다.

주요어 : 분자 인식, 이인산, bis(Zn-DPA), 열역학, 화학 반응 속도론, 지시약 교체 분석, 보상관계

학번 : 2010-20284